ENHANCEMENT IN LUMINESCENT PROPERTIES OF RARE EARTH IONS DOPED BARIUM STRONTIUM ALUMINO BOROSILICATE GLASSES FOR PHOTONIC APPLICATIONS

Thesis submitted by

SANDEEP SHARMA

Reg. Number: 2K18/Ph.D./AP/516

In Partial Fulfillment of the Requirements for the Degree of

DOCTOR OF PHILOSOPHY

Under the Supervision of

PROF. A. S. RAO

&

DR. KAMAL KISHOR

Department of Applied Physics
Delhi Technological University (DTU)
Bawana Road, Delhi-110042, India

MARCH-2024

Dedicated to my father and mother.

Delhi Technological University

(Govt. of National Capital Territory of Delhi)
Bawana Road, Delhi-110042

CERTIFICATE

This is to certify that the thesis titled "***Enhancement in Luminescent Properties of Rare Earth Ions Doped Barium Strontium Alumino Borosilicate Glasses for Photonic Applications***" is being submitted by ***Mr. Sandeep Sharma*** with registration number ***2K18/Ph.D./AP/516*** to the Delhi Technological University for the award of the degree of Doctor of Philosophy in Applied Physics. The work embodied in this thesis is a record of bonafide research work carried out by me in the Microelectronics Research Lab, Applied Physics Department, Delhi Technological University (Formerly Delhi College of Engineering), New Delhi under the guidance of ***Prof. A. S. Rao*** and ***Dr. Kamal Kishor***. It is further certified that this work is original and has not been submitted in part or fully to any other University or Institute for the award of any degree or diploma.

Mr. Sandeep Sharma
Candidate
Roll No. 2K18/Ph.D./AP/516

This is to certify that the above statement made by the candidate is correct to the best of our knowledge.

Prof. A. S. Rao
Supervisor (Professor) and Head
Department of Applied Physics
Delhi Technological University
Delhi, India

Dr. Kamal Kishor
Jt. Supervisor (Assistant Professor)
Department of Applied Physics
Delhi Technological University
Delhi, India

ACKNOWLEDGEMENTS

My study journey has been made possible by the invaluable assistance of numerous individuals. I feel sincerely grateful to acknowledge all those folks who have supported me either directly or indirectly through the finalization of my study effort. The fact that I can now thank each one of them is a pleasant feature. First and foremost, I want to express my gratitude to the goddess Saraswati, who has given me courage, guidance, and inspiration as I have traveled towards the research.

Firstly, I would like to express my sincere gratitude and respect to my supervisor, ***Professor A. S. Rao,*** *Head of the Department of Applied Physics, Delhi Technological University, Delhi. Professor Rao helped me develop the research skills I needed to pursue a successful career in science. It has been an honor to work for outstanding, vivacious, and accomplished supervisors. His unwavering support, on-going assistance, and careful oversight during my studies allowed me to reach yet another academic milestone. Throughout the writing of this thesis, his vast topic knowledge, analytical vision, foresight, and perseverance served as a steady source of inspiration.*

I am also grateful to Dr. Kamal Kishor my joint supervisor for providing his valuable supervision and support throughout my PhD journey.

I express my gratitude to Dr. M. Jayasimhadri of the Department of Applied Physics at DTU for providing the lab facilities necessary for the research. I express my gratitude to the chairman of the DRC, the members of the DRC, the SRC, and the other teaching and non-teaching personnel of the Applied Physics department.

I would like to thank my fellow researchers ***Dr. Ravita, Dr. Mukesh K. Sahu, Mr. Rajat Bajaj, Dr. Pooja Rohilla, Ms. Shristy, Ms. Anu, Ms. Sheetal, Dr. Vishal Singh, Mr. Sunil Bishnoi and Dr. Anshu Dahiya*** *for their assistance whenever needed.*

I want to thank my family once again for their encouragement and support throughout my entire research period. My mother, ***Mrs. Om Wati*** *and father,* ***Mr. Daya Kishan Sharma,*** *have given me unwavering love and support throughout my life, and for that I am truly grateful. For their unwavering encouragement, support, nurturing, love, and belief in me throughout my life. I would like to express my gratitude to them for their unwavering support.*

I express my gratitude to everyone who assisted me in completing the thesis and realizing it successfully.

Thank you all!!!

(Sandeep Sharma)

New Delhi,

MARCH-2024

ABSTRACT

A variety of multipurpose and industrial applications can benefit from the usage of glasses, glass ceramics, and ceramics, three significant classes of engineering materials. Glasses and glass ceramics have garnered significant interest because of their benefits. Within the special class of amorphous solid-state materials, inorganic glasses are typically formed over a broad range of glass-former concentrations and are thermally stable. A significant amount of research has been done on rare earth (RE) doped glasses for near-IR lasers, broadband optical amplifiers, up-conversion luminescence temperature sensors, and solid-state lighting (SSL) applications since Snitzer's 1961 initial demonstration of the laser action of Nd^{3+} ions in barium crown glass. Additionally, a number of precursor glasses were used to create optical fibers that released infrared radiation.

Recent advances in the lighting industry have benefited greatly and practically from advances based on solid-state lighting (SSL). SSL devices used relatively little energy and were compact, strong, and eco-friendly. The SSL based white light emitting diodes (w-LEDs) are better to other convectional light sources including incandescent lamps, electric bulbs, and fluorescent tubes because they are smaller, more ecologically friendly, have excellent color rendering, require less energy, and have a longer lifespan. The development of better white w-LED lighting sources has become essential for reducing artificial lighting's global energy usage. YAG: Ce^{3+} phosphor and blue LED are now the building blocks of commercial w-LED production. The current generation of w-LEDs has a number of shortcomings, such as a halo effect, an inaccurate color temperature, and a low color rendering index. To get around the restrictions, RE activated glass can be used in place of phosphors. In addition, glass has some

special properties, such as strong chemical and thermal stability, high RE ion solubility, and an easy-to-produce approach. Given this, efficient RE activated glass could be advantageous for a variety of photonic devices, such as w-LEDs.

One can adjust specific spectrum qualities by choosing the appropriate host glass composition or varying the concentration of RE ions in a glass. Referred to specific uses such as SSL as well as solid-state lasers, RE-doped glasses display unique optical properties in a range of host glasses such as chalcogenides, phosphate, borate, silicate, and telluride. The lasing features of glass hosts can be enhanced by using a good former, intermediates, and network modifier. Selecting the host glass with the right combination of RE ions for best lasing and optical properties is still a difficult task. Host glass, which has a relatively low phonon energy and raises the stimulated emission cross-section and quantum efficiency, is a dependable material for the development of lighting materials.

On the basis of the aforementioned advantages, multipurpose and industrial applications of the RE doped glasses were selected of the current thesis work. The aim of research works is to enhance the luminescent properties of RE ions doped glasses for photonic applications. The goals of the research are being met by the several chapters. Every chapter is written such that it can be read on its own.

Chapter 1: A clearer introduction, the reason for the problem, the motivation for the research, and a review of recent literature are all included in the first chapter. Based on the characteristics required for glass host, BaO-SrO-Al_2O_3-B_2O_3-SiO_2 (BaSrAlBSi) glass composition selected to synthesize, transparent, thermally and mechanically stable glass with exceptional photonic properties, which can directly be applicable in optical devices.

This approach has involved a thorough exploration of the properties of the many chemical components present in the host glass. The usefulness of RE ions doped in glasses for use in

photonic devices has been studied further. It has been discussed how the Inokuti-Hirayama (I-H) model is used to study the mechanics of luminescence degradation and energy transfer. The process of determining the CIE chromaticity color coefficients (x, y) from the luminescence spectra in order to evaluate the white light tunability has also been thoroughly explained. The examination of temperature-dependent emission indicates the value of thermal stability in the applications of produced glasses W-LEDs.

Chapter 2: The experimental process used for producing RE-doped glasses and the methods for evaluating the glasses' luminous properties are the main topics of the second chapter. There is also a detailed discussion of the melt-quench process, which is used to create the as-prepared glasses. This chapter describes the use of many sophisticated experimental techniques, such as X-ray diffraction (XRD), UV-VIS spectrophotometer, Fourier-transform infrared spectroscopy (FT-IR), and fluorescence, to study various properties, including thermal, structural, photoluminescent, and colorimetric properties.

Chapter 3: Transparent, Sm^{3+} doped and Sm^{3+}/Eu^{3+} co-doped alkaline earth alumino borosilicate (AEAlBS) glasses have been synthesized by employing melt quenching process and explored their down-shifting luminescent properties for utility in visible red photonic devices applications. The non-crystalline nature of the as prepared glass was analyzed with help of XRD pattern, containing broad peak. Photoluminescence (PL) properties demonstrate the glasses were proficiently excited by near-UV with dominant peak centered at 402 nm. The emission spectra exhibit four emission peaks with an intense peak placed at 599 nm under 402 nm excitation. The optimum emission intensity was obtained for 0.5 mol% Sm^{3+} ions doped in AEAlBS glasses. Sm^{3+} ion works as effective sensitizer for Eu^{3+} activator ion in AEAlBS glasses and part of energy transfer (ET) from sensitizer (Sm^{3+}) to activator (Eu^{3+}) ions. The PL intensity of Sm^{3+} ion peaks were demises and enhance the Eu^{3+} ion peaks with Eu^{3+} ion co-

doping in AEAlBS glasses under λ_{ex} = 402 nm. The efficient ET from sensitizer to activator ions proved to be dipole-dipole in nature via employing Dexter's formula with Reisfeld's approximation. The experimental lifetime values calculated from the PL decay profiles are decreasing with surge in Eu^{3+} ion concentration in the as prepared glasses. I-H model applied to the PL decay profiles confirm the ET process responsible for decrease in experimental lifetimes as dipole-dipole in nature. The outcome of I-H model is in consonance with the result given by Dexter theory. The CIE coordinates for single Sm^{3+} doped glasses are falling in orange region, and gradually surge into red region by co-doping with Eu^{3+} ions in AEAlBS glasses. The temperature-dependent photoluminescence (TD-PL) emission analysis reveals that the PL intensity at 150°C and 200°C perseveres up to 94.34 and 91.30 % of the PL intensity at environmental temperature, respectively. All the obtained results contemplate the superiority of the multifunctional Sm^{3+}/Eu^{3+} co-doped AEAlBS glasses for near UV triggered photonic device applications. Part of this work has been published in an international journal ***Journal of Non-Crystalline Solids 580 (2022) 121392 (Impact Factor: 3.20).***

Chapter 4: A series of Tb^{3+} activated transparent BaSrAlBSi glasses were prepared via melt quenching routes and detailed studied their optical characteristics for advanced laser and lighting appliances applications. The diffraction pattern defined the amorphous nature of the prepared transparent BaSrAlBSi glass. The UV visible spectrum shows the various absorption in n-UV visible and NIR range owing to Tb^{3+} ions. BSi:Tb glasses were proficiently near-UV excited, which emits blue, green, yellow and red light corresponding peaks situated at 487, 543, 587 and 623 nm, respectively. The maximum photoluminescence (PL) emission intensity was observed for 1.0 mol% Tb^{3+} doped BaSrAlBSi glass. Beyond the 1.0 mol% concentration of Tb^{3+} ions, quenching mechanism was recognized via applying the Dexter theory. The PL lifetimes were showing a decrease in decay time with upsurge in Tb^{3+} content. I-H model was

used to identify the type of non-radiative energy mechanism, which is found to be dipole-dipole in nature. TD-PL characteristics demonstrate the very less effect of temperature dependency on PL intensity and shows the good thermal stability of BaSrAlBSi glass with 1 mol% of Tb^{3+} ions (BSi:1.0Tb) glass. The observed results anticipate that the direct utility of the as prepared transparent Tb^{3+} doped BaSrAlBSi glasses as n-UV pumped with green emitting constituent for photonic device applications. Part of this work has been communicated to an international journal ***Optical Materials (2024) (Impact Factor: 3.80).***

Chapter 5: A number of Tb^{3+} and Tb^{3+}, Sm^{3+} incorporated BaSrAlBSi glasses were prepared, and their optical properties were carefully examined for use in high-tech lighting and laser applications. The transparent BaSrAlBSi glass's amorphous nature was established by the XRD pattern. The absorption profile demonstrates the various peaks from n-UV to NIR range caused by the Tb^{3+} as well Sm^{3+} ions in BaSrAlBSi glass. BaSrAlBSi glass with 1 mol% of Tb^{3+} ions (BSi:Tb1.0) glasses gives emission in blue, green, yellow and red light owing to the transition from $^5D_4$ to various $^7F_{(J = 6, 5, 4 \& 3)}$ under λ_{ex}=379 nm. BSi:Sm1.0 glasses exhibits the emission spectra green to red region, caused by the transitions from $^4G_{5/2}$ to $^6H_{5/2}$, $^6H_{7/2}$, $^6H_{9/2}$, and $^6H_{11/2}$ of the Sm^{3+} ions. The Tb^{3+}/Sm^{3+} co-doped BaSrAlBS glasses exhibit a mixture of blue, green, and orange-red light when excited at 379 nm, whereas they red-orange light when excited at 402 nm. The PL lifetimes demonstrated a reduction in decay time as Sm^{3+} concentration increased in Tb^{3+} doped BaSrAlBSi glass. The sort of non-radiative energy process was determined using the I-H model, and it turns out to be a dipole-dipole in the environment. CIE coordinates show the green emission was tuned towards warm white region via co-doping of Sm^{3+} in Tb^{3+} doped BaSrAlBSi glasses. The strong thermal stability of 1 mol% of Tb and Sm doped BaSrAlBSi glass (BSi:TbSm1.0) glass is confirmed via temperature dependent emission profile, which reveals that temperature dependence on PL intensity has a very small impact.

The observed results indicate that the transparent BSi:TbSm1.0 glasses as made will be directly useful for photonic device applications as n-UV pumped with the green warm white and orange emitting component. Part of this work has been published in an international Journal ***Optical Materials 145 (2023) 114446 (Impact Factor: 3.80).***

Chapter 6: A overview of the overall study effort and the conclusions drawn from the data are presented in sixth chapter of this dissertation. This chapter also looks at future directions for this study and how it could be used to inform future research directions.

LIST OF FIGURES

LIST OF TABLES

LIST OF PUBLICATIONS

- **"Energy transfer dynamics in thermally stable Sm^{3+}/Eu^{3+} co-doped AEALBS glasses for near UV triggered photonic device applications" Sandeep Sharma**, A.S. Rao, Kamal Kishore, ***Journal of Non-Crystalline Solids, 580 (2022) 121392 (Impact Factor = 3.5)***

- **"Thermally stable illuminating characteristics of Tb^{3+}/Sm^{3+} ions activated BaO-SrO-Al_2O_3-B_2O_3-SiO_2 glasses for Photonic applications" Sandeep Sharma,** Sumandeep Kaur, A.S. Rao, Kamal Kishor, ***Optical Materials 145 (2023) 114446 (Impact Factor = 3.9)***

- **Intense green-emitting, thermally stable optical characteristics of Tb^{3+} ions incorporated BaO-SrO -Al_2O_3-B_2O_3-SiO_2 glasses for photonic devices Sandeep Sharma,** A.S. Rao, Kamal Kishor, ***Communicated in Luminescence (Impact Factor = 2.9)***

TABLE OF CONTENTS

Page No.

CHAPTER 1

Introduction to Luminescent Glasses and goal of the research work

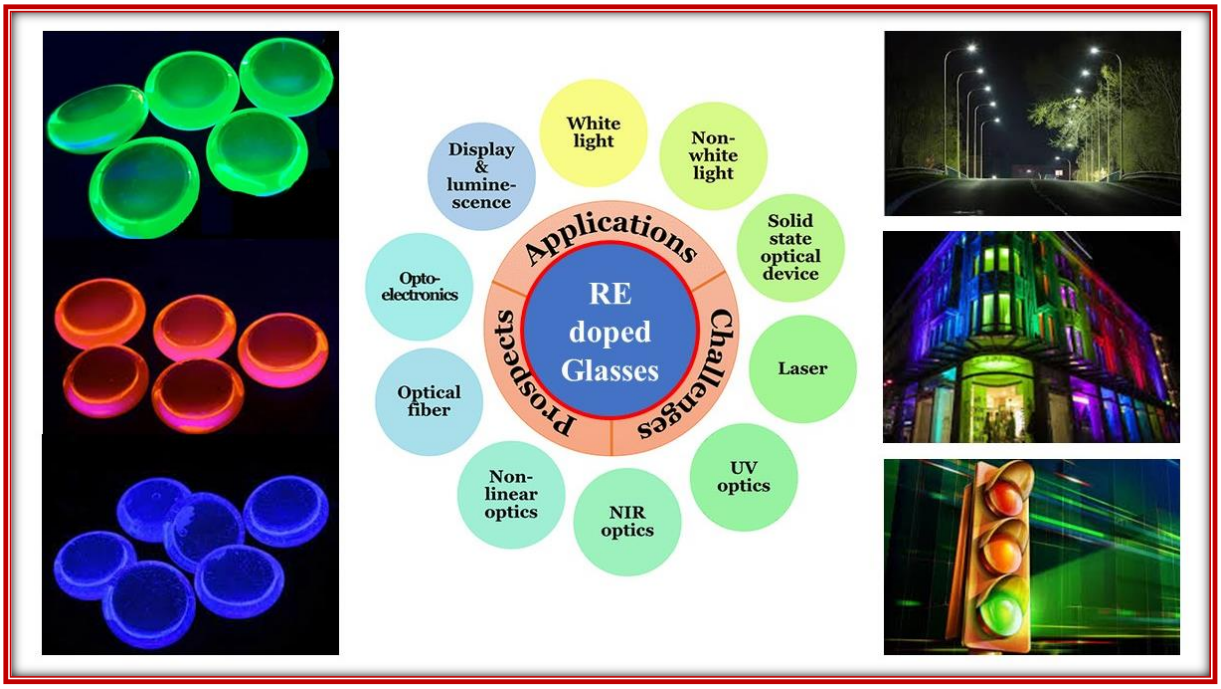

A clearer introduction, history of glasses, the reason for the problem, the motivation for the research, and a review of recent literature are all included in the first chapter. Based on the characteristics required for glass host, BaO-SrO-Al_2O_3-B_2O_3-SiO_2 (BaSrAlBSi) glass composition selected to synthesize transparent, thermally & mechanically stable glass with exceptional photonic properties, which can directly be applicable in optical devices. This approach has involved a thorough exploration of the properties of the many chemical components present in the host glass. The usefulness of RE ions doped in glasses for use in photonic devices has been studied further. It has been discussed how the Inokuti-Hirayama (I-

H) model is used to study the mechanics of luminescence degradation and energy transfer. The process of determining the CIE chromaticity color coefficients (x, y) from the luminescence spectra to evaluate the white light tunability has also been thoroughly explained. The examination of temperature-dependent emission indicates the value of thermal stability in the applications of produced glasses W-LEDs.

1.1. Introductions

An inorganic material can be classified as crystalline or amorphous based on its atomic arrangement or translational periodicity. Amorphous materials are defined as non-periodic in three-dimensional space materials exhibiting short-range order; examples of such materials include polymers, gels, thin films, and glass. Crystalline materials are defined as all solid materials whose constituents (i.e., atoms, molecules, or ions) exhibit long-range order and have periodicity in three-dimensional space [1,2]. Glass is regarded as one type of amorphous material with a solid-liquid transition. A variety of multipurpose and industrial applications can benefit from the usage of glasses, glass ceramics, and ceramics, three significant classes of engineering materials. Ultimately, amorphous materials are important for many technological applications and have special qualities that set them apart from crystalline liquids and solids. They have applications in materials science, engineering, and other domains due to their adaptability and adjustable qualities [3,4].

1.1.1. Glass and their brief History

A substance that is translucent and glossy is referred to as "glass," and another word for glassy substances is "vitreous." Glass is a uniform, amorphous, inert solid that has no biological activity. In 1997, Shelby described glass as, "*an amorphous solid completely lacking in long range order, periodic atomic structure and exhibiting a region of glass transformation*

behavior. Any material, organic, inorganic or metallic formed by any of the stated processes which shows glass transition character can be categorized as glass". Their durability, transparency, and luster make them useful in a variety of contemporary applications. Among all the disordered structures found in nature, glass is the most remarkable substances. The Indo-European root that gave rise to the word "glass" denotes anything bright. It is thought that the earliest glass object ever produced by humans was discovered in 7000 B.C. in Mesopotamia and Egypt. Greece and Macedonia also became major glass-making hubs around 400 B.C. By this time, methods for creating glass tableware, such as bowls, had been invented, along with the use of lathes and vivid colors for decorating. The mosaic-forming process helped to create amazing color effects. The Italian glassmaking techniques were developed during the Roman Empire's expansion in the second century B.C. The invention of the glass blowing process in the first century B.C. marked a significant advancement in glass technology and increased the practical uses of glasses. The invention of cameo spectacles is one of the best ideas to come out of this age. The process of grinding glass surfaces was invented in Persia in the eleventh century A.D. Other significant innovations during this time were the widespread use of enamels and the construction of gilded inscriptions. Europe saw two important advancements in glassmaking in the fourteenth century A.D. The first is the process of creating crystalline glasses. The second method involves melting glass along the edge of an iron pipe, dropping it under freezing water for a brief period, and then gusting the water, creating the appearance of an expanded web of microscopic fractures on the outside. The materials seemed frosted because of the above process. By the end of the sixteenth century, English laborers developed a method for producing sandglass [5]. Additionally, Germany invented a novel method for creating various sets of glasses for intaglio work by employing a water-power mill and cutting wheel. A tougher material than crystallo-glass, potash lime glass was created specifically to fit the needs of

engraving wheels. The lead that was used for deep cutting was used to create a new pair of spectacles known as utility glasses. Machines were used to create these spectacles during this time. In the latter half of the 19th century, the contemporary techniques for making glasses were introduced to China, India, Europe, America, and other countries. In the US, several glittering effects were created that caused glasses to heat up and change color.

With the arrival of the 20th century, more advancements were made possible by the invention of new methods for producing glass sheets in any thickness. To create glasses that could be used in lasers, machinery was developed to dope them with rare-earth ions. Additionally, the glasses are designed to be used as telescope lenses to view astronomical objects. In the twenty-first century, glass that is produced by enterprises for a variety of uses is a component of increased economic growth in practically every nation [5,6].

1.1.2. Motivation of the research work

On account of the numerous applications of rare earth (RE) doped glasses in a variety of fields, including solid-state lasers, mid-infrared lasers, optical fibers, photovoltaics, telecommunications, modern lighting technology, and displays, RE-doped glassy and crystalline materials have garnered a lot of attention over the past few decades. Glasses activated with RE ions have amazing qualities like high emission efficiency, memory, and photoconducting capabilities [1,7]. Furthermore, glasses are better than crystalline materials because they are less expensive and have a higher doping capacity for RE ions. Furthermore, glasses are simply produced and molded. Their fascinating qualities make them a good fit for the creation of luminous glass products. It is commonly recognized that, in comparison to other glassy systems, oxide glasses are the most stable. It is desired to investigate the relationship between the local structure and fluorescence properties of oxide glasses that include RE ions in

order to build new glassy phosphors and laser glasses. The ligand field concerning the RE ions and the phonon energy of the host glass are the two variables that determine the optical characteristics of RE ions. Low phonon energy host glasses are selected because they provide excellent quantum efficiency. Researchers are currently looking at a variety of chemical compositions as glass hosts for RE ions in different labs across the globe to create a glassy system that is appropriate, mechanically strong, transparent optically, and chemically inert. Therefore, the primary goal of this work is to create and evaluate RE-doped glasses that are appropriate for the creation of optoelectronic devices. In addition, the host matrix's structure has a significant impact on the intensity, effective bandwidths, and quantum efficiency of emission transitions. Consequently, choosing a good host matrix with a comparatively greater luminescence efficiency is crucial to produce a high-quality photonic device [8–10].

The advantages of rare-earth ion-doped glasses over PC W-LEDs include ease of sculpting any shape, lower production costs, improved thermal stability, and most importantly a manufacturing process that doesn't require epoxy resin. Additionally, RE-doped glasses are used as an active medium in several important technical fields, such as optical amplifiers, optical detectors, and fibers. Materials that emit light can be used in many ways [11–13]. Because glasses may exhibit interesting properties including large inhomogeneous bandwidths, wavelength adjustment, and substantial doping capabilities, they are considered the finest hosts [14,15]. RE-doped glasses are better than phosphors because of their special qualities, which also include their easy to make, affordable, and very stable thermal features. To predict innovative luminous materials for usage in research and business, we need an in-depth knowledge of the wavelength absorption and luminescence properties of RE-doped glasses. Glasses may easily be molded and shaped into bigger sizes, making them suitable as hosts for different types of activator ions. The composition, structure, thermo-mechanical quality,

optical properties, and chemical resistance of glasses can all have an impact on their optical performance. Among the many excellent advantages of glasses are. The ability to choose from a wide range of glass compositions with flexibility [16–18].

1.1.3. Glass components

The components of glass influence its properties and use primarily. Glass components, such as glass or network formers, network modifiers, and intermediates, were divided into three groups based on their varying bond strengths.

Glass or network formers: As glass or network formers, oxides with bond strengths more than 80 kcal/mol are typically effective. Notable and often utilized glass formers included SiO_2, P_2O_5, PO_4, B_2O_3, V_2O_5, GeO_2, As_2O_5, and Sb_2O_5. A tetrahedral structure is formed by the majority of the four cations-oxygen coordination number [1].

Network modifiers: Modifiers are oxides with bond strengths between 10 and 40 kcal/mol that do not integrate into the glass network former. The network modifiers' primary task is to alter the characteristics of glass. Alkali oxides make up most glass modifiers. On the other hand, additional oxide materials can also be employed as network modifiers. Key network modifiers include MgO, Li_2O, BaO, SrO, ZnO, CaO, and Na_2O. the appropriate selection of a cation-oxide modifier, which has a wide range of recent applications including optoelectronic devices, conducting glasses, bioactive materials, and sensors [2,19].

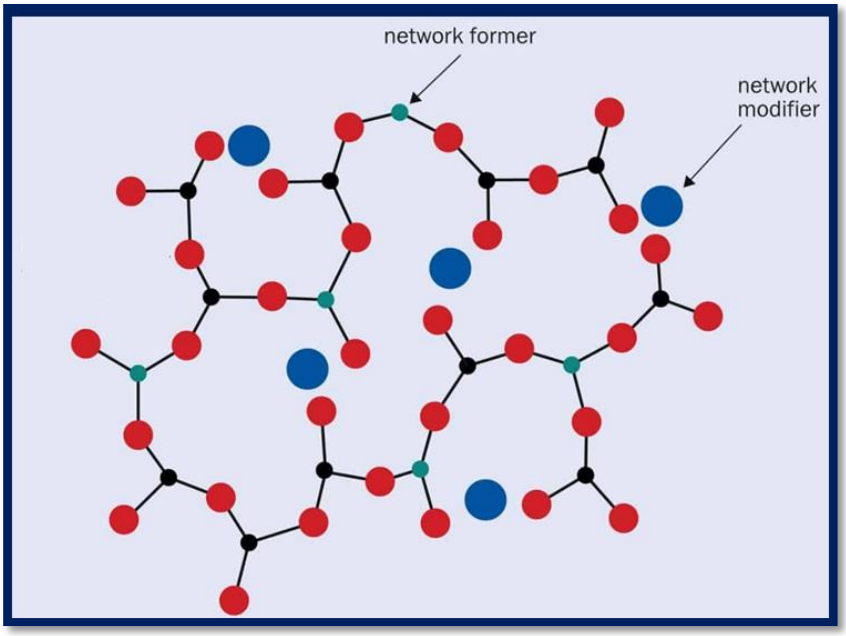

Fig. 1.1: *Glass compositions include glass formers, glass network modifier.*

Intermediates: Among the glass formers and the modifiers, there is a space where intermediates reside. TiO_2, ZnO, CdO, PbO, BeO, and Al_2O_3 are a few significant intermediates. When describing the function of individual oxides in multi-component glasses, the phrases glass formers, modifiers, and intermediates are commonly employed. In certain cases, intermediate oxides can participate in the glass's network and function as network modifiers, based on the chemical composition of the material [20–22].

1.1.4. Preparation mechanism of Glass

All chemical types of materials, including covalent, ionic, molecular, metallic, and hydrogen-bonded compounds, can produce glass. Elements, simple chemical compounds, complex organic molecules, salt combinations, and alloys have all been used to create glasses. Grouping glass forming materials in a particularly beneficial fashion does not exist. By rapidly chilling, nearly any substance can be made into an amorphous solid, avoiding the crystallization process and enabling the production of glass. Every material cool [23,24]at a different rate,

producing a unique glass. Glass is produced when a material is rapidly cooled from a supercooled liquid. To become an amorphous solid, the substance is cooled below the temperature commonly referred to as the glass-transition temperature. After that, the atoms begin to move more slowly in a molecular pattern, causing the substance to begin to transform into glass. The newly formed amorphous structure is less ordered than a crystal, but it is still more ordered than a liquid [25].

To comprehend the glass transition process, the behavior of amorphous materials as they change from the supercooled condition to glass must be plotted on a V-T diagram, as shown in Fig. 1.2. In the volume and enthalpy of the material, the y-axis in the V-T diagram represents the temperature, and the x-axis the temperature. The temperatures of the glass transition and melting point are represented by the letters Tg and Tm, respectively [26].

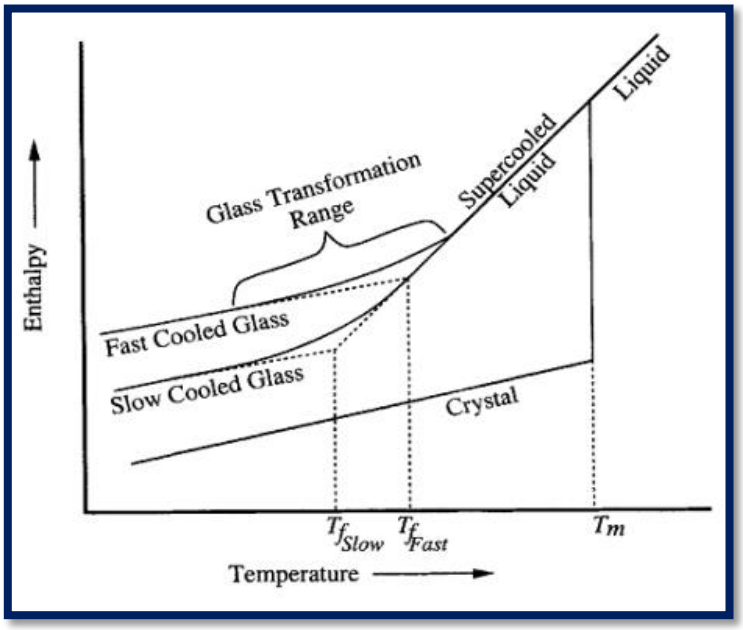

Fig.1.2: *V-T diagram*

A supercooled liquid does not abruptly discontinue in volume as it freezes into an amorphous solid at or around the glass transition temperature. At this point, the glass transition

takes place [[4]]. The Tg of the crystalline material state is found to be less than the Tm. A liquid may cool in one of two ways.

- Crystallization at T_m
- Converted to super cooled below T_m

The fluid thickens and crystallizes into glass when the temperature drops even lower. The glass transition is only caused by an increase in viscosity if the chemical composition remains unchanged, and Tg is dependent on the rate of glass cooling [2]. The following are the key ideas behind glass transition:

- There is more free energy in glasses, as seen by the V-T image.
- Viscosity increases with decreasing temperature.
- The glass is in a metastable state.
- When creating glass, the cooling rate is accelerated to thwart crystal nucleation and development.

1.2. Luminescence

A material or substance that emits light due to a variety of processes, including chemical reactions, electrical energy, or radiation exposure, is said to exhibit luminescence. It is the process via which light is emitted after being absorbed by a substance. When energy is absorbed and then released as light, a situation involving cold body radiation is referred to as luminescence. Luminescent materials are those that can convert absorbed (invisible) energy into visible light, such as ultraviolet, x-rays, β, α, and so on [[27,28]]. Luminescent materials include crystalline substances like phosphor, but amorphous materials are typically used to make luminescent glass[29].

When stimulated by the right sources, some chemicals, known as activators, can release energy right away. A distinct class of impurities known as sensitizers can be added when activator ions show insufficient absorption of energy. After the energy is absorbed by sensitizers, it is transferred to activators. This process involves the transfer of energy by luminous materials. Fig. 1.3 (a, b, c & d) depicts the functions of the sensitizer and activator in the luminescence process. A purposeful introduction of dopant ions and/or other flaws to an inert imperfect host lattice is the fundamental component of luminous materials. In different host lattices, the dopants have different roles according to their electrical configuration, solubility, and host lattice structure [30].

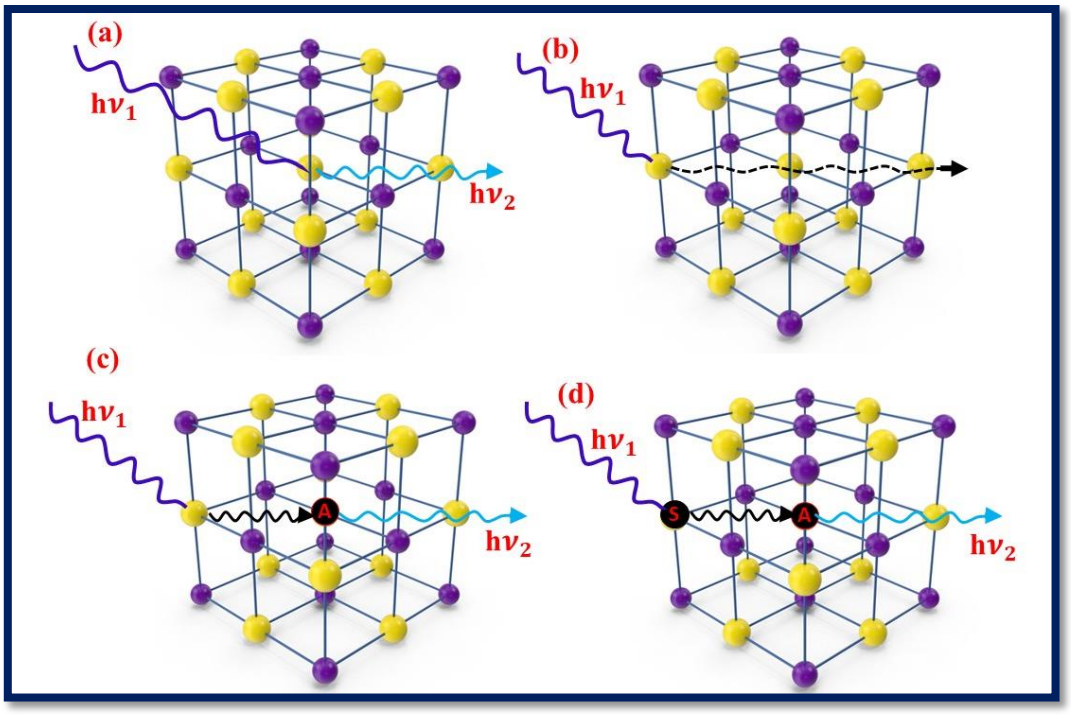

Fig.1.3: *Mechanism of Luminescence involving activator and sensitizer*

Activator: An activator (A) also known as a luminous center is a dopant ion electron that, upon receiving excitation energy, leaps to the excited state and, when returning to the ground state, releases the energy as radiation[29].

Sensitizer: In Fig. 1.3 (d), two dopants are shown; one is called an activator (A) and the other a sensitizer (S) when they are present in a crystal lattice. Before the energy is delivered to the "A" for emission, the "S" absorbs most of the energy[28].

As will be covered below, there are various forms of luminescence depending on the source of excitation, including photoluminescence:

Electroluminescence: Electroluminescence is the process by which a substance generates light when an electric current passes through it. A few examples of devices that take advantage of this phenomenon are electroluminescent displays, LEDs, and organic light-emitting diodes (OLEDs) [31].

Bioluminescence: The term "bioluminescence" refers to a kind of luminescence that spontaneously transpires in living organisms. The phenomenon occurs when specific organisms, like bacteria, deep-sea creatures, and fireflies, release light as a consequence of internal chemical reactions [32].

Chemiluminescence: In this technique, light is released by a chemical reaction—typically an oxidation—without the need for an outside light source. Common examples are glow sticks and the light released during certain chemical reactions, like when luminol and hydrogen peroxide combine [32].

Luminescence is used in many different industries, such as displays, forensics, medical diagnostics, environmental monitoring, lighting, and materials research. The ability to control and harness luminescence has proven beneficial for LED lighting, scientific research imaging techniques, and fluorescence microscopy [33].

1.2.1. Photoluminescence (PL)

The phenomenon where light emerges from atoms or molecules after they soak up rays is known as photoluminescence. Due to photoexcitation, the material's electrons move into

permitted excited states. When such electrons approach the lowest energy or the ground states, they release the excess energy as a phonon, a non-radiative process, or as visible light, a radiative process as demonstrated in Fig. 1.4 [27,34]. The amounts of energy at which the two-electron states are involved in the mechanism of transitioning across the more energetic excited state and the equilibrium (a lower energy) state are at distinct energy levels that affect the amount of energy of light that is emitted (photoluminescence). PL can be divided into two groups according to the emission or decay time.

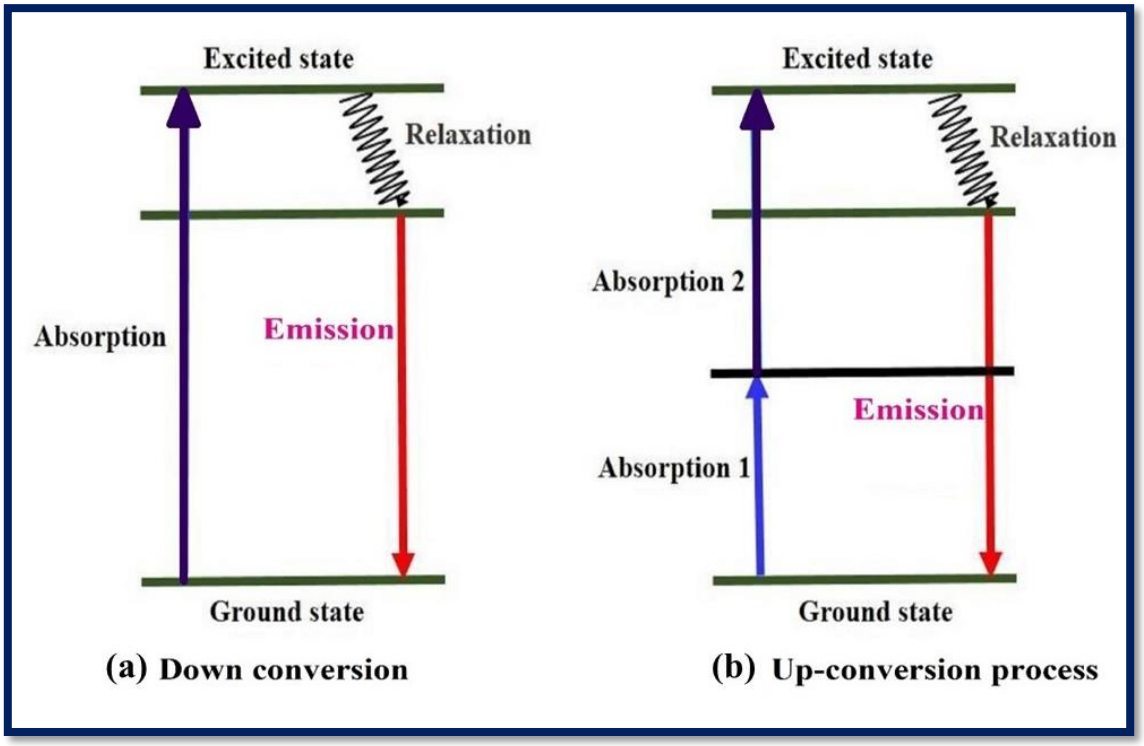

Fig.1.4. *Schematic representation of* ***(a)*** *down-conversion and* ***(b)*** *up-conversion PL process*

When a photon is emitted with less energy than it was when it was incident, this is known as the Stokes emission, or down-conversion, and it results in energy loss throughout the photoluminescence process. The Stokes shift is the energy difference between the energy of the excited and emission photons. A material may also have the additional possibility of absorbing two or more photons simultaneously, which would encourage the production of a higher energy

photon. Anti-Stokes emissions are the result of this process, which is known as an up-conversion process [28,35]. Fig.1.3 (a) and (b) provide clarification on the down-conversion and up-conversion PL procedures.

1.3. Rare earth (RE) elements

The essential features of 4f–4f electronic transitions make rare earth elements activated luminous and photonic materials highly sought after in a variety of applications, including solid-state lasers, lighting, optical fiber amplifiers, and small microchip lasers. Because they were only sporadically found in nature, the lanthanide group elements of the periodic table are known as rare earth elements. Because of their distinctive quality, they draw the attention of researchers and are important to the investigation. The fifteen elements in the RE element group, which range in atomic number from Z = 57 to Z = 71, are lanthanum through lutetium [27,36]. Because of their comparable properties, yttrium and scandium elements are likewise categorized as rare earth elements. In practically every field of research and technology, rare earth elements are used extensively. Rare earth elements are primarily found as trivalent state (RE^{3+}) RE_2O_3 oxide, while a very small number can also be found in the divalent state (RE^{2+}). Electronically, RE elements are configured as $[Xe]4f^n$ (n = 0–14), where [Xe] is the xenon configuration. Fig.1.5 displays the electrical arrangement of RE components with respect to their ground state and various excited states. From these configurations, several energy levels can be obtained, which are defined by the spectral expression ($^{2S+1}L_J$), where the three quantum numbers L, S, and J resulted from the spin-orbit coupling. Dieke's energy level diagram for trivalent rare-earth ions, shown in Fig. 1.5, provides a clear definition of these energy levels, which have specified energies [27,28].

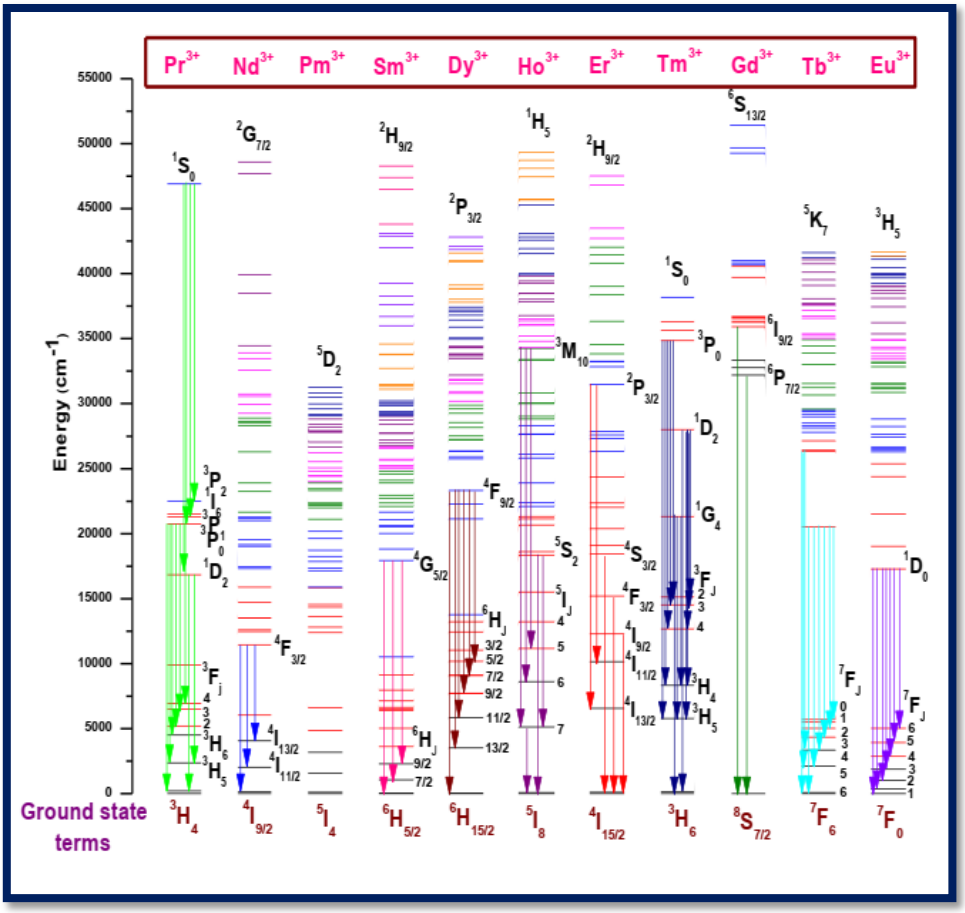

Fig.1.5: *Dieke's energy level diagram for* RE^{3+} *ions.*

1.3.1. Transitions in RE ions

Three types of optical transitions are generally used to classify the interaction between the various levels of RE ions. These transitions include charge transfer transitions, transitions between multiple 4f levels, and characteristic transitions between multiple $4f^{n-1}5d^1$ -$4f^n5d^0$ levels. These transitions are explained below[37,38]:

Discrete $4f^n$– $4f^n$ transitions: Discrete Transitions between electronic states within the f orbitals of lanthanides or rare-earth elements are referred to as $4f^n$–$4f^n$ transitions. After absorbing or releasing photons, the partially filled *f* orbitals of these elements can change in energy. Lanthanide ion 4f electronic energy levels are not significantly affected by their surroundings because the outer $5s^2$ and $5p^6$ electrons shield the *4f* electrons from external electric fields. It is

strictly forbidden to transition within 4f shells since Laporte's criteria is not met by parity. The RE ion's interaction with the crystal field or the lattice vibrations, which can combine states of different parities into *4f* states, is what causes the observed forbidden transitions. Conversely, when spin-orbit contact occurs, such transitions are allowed. The luminous lifetime resulting from *4f -4f* transitions is usually in the millisecond range because the luminescence transition is prohibited [38,39]. There are three ways to understand the proper interpretation of *4f -4f* transitions.

- An electric quadrupole occurs when a charge exhibits quadrupole behavior or a zero-dipole moment. Electric quadrupole transitions are weaker than induced ED and MD transitions, and even parity follows them. Quadrupole transitions in RE ions have not yet been experimentally verified. The quadrupole transitions' selection principles apply to some transitions, referred to as hypersensitive transitions [40].
- The incoming source electromagnetic radiation's electric field vector component interacts with the activator (RE) ions to produce induced electric dipole transitions. In RE ions, the induced electric dipole type transitions account for most of the transitions, according to the literature review. Essentially, the electric dipole (ED) transition is caused by linearly moving charges. Odd parity exists in the ED transition because of the odd transformation that comes after it and relates to the inversion center [37,41].
- When activator (RE) ions interact with the magnetic dipole caused by the electromagnetic radiation, an induced magnetic dipole (MD) transition occurs. A charge forms a magnetic dipole when it travels along a curved path. The MD transition is believed to have a low intensity rotating displacement of charge in comparison to the ED transition [42].

1.3.2. Energy Transfer in RE ions

This section will provide a comprehensive analysis of the energy transfer (ET) in RE ions. Luminescent glasses are mostly composed of inorganic glass compositions that have been doped with RE or transition metal ions, or weakly activated. The electromagnetic radiation is absorbed by either the sensitizer or the glass host lattice. However, only in the vicinity of the activator ions does radiation emission occur. Consequently, the sensitizer has been sensitizing the activator by providing electromagnetic energy, which ideally creates light in the visible range[10,43]. Very rarely, a small amount of the excitation energy can be transferred from one activator to another. The following distributions of excited state energy and electron transit from the bright center to excited states are frequently observed: Via phonon emission or other energy transfer from the sensitizer to the activator, the activator can be directly excited to produce a photon of visible light, as shown in Fig. 1.6 (a), or indirectly stimulated to emit a photon of visible light (ii), as shown in Fig. 1.6 (b).

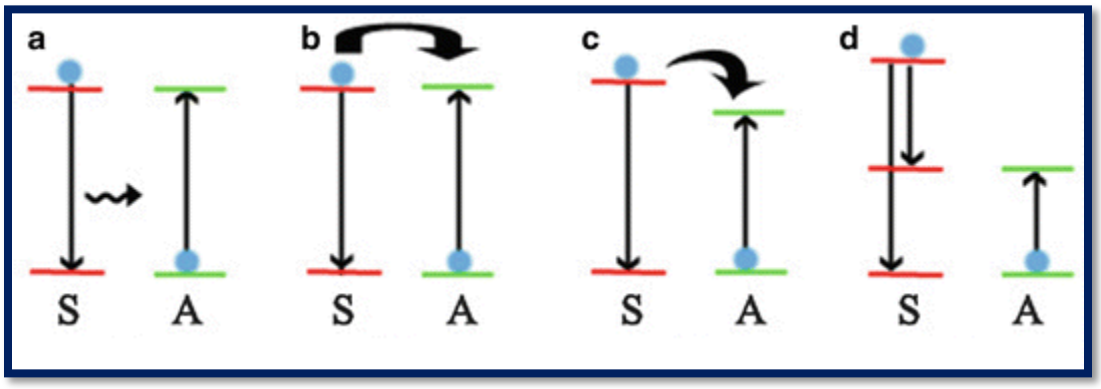

Fig.1.6: *ET processes in RE ions.*

It is possible to compute radiative ET efficiency based on the sensitizer emission's ability to activate the activator, as seen in Fig. 1.6(a). There should be a noticeable overlap between the activator's and sensitizer's excitation spectra in their emission spectra. The activator

concentration has no effect on the lifetime of the sensitizer fluorescence if radiative energy transfer takes place primarily. With an increase in activator concentration, Figure 1.6(b) illustrates a non-radiative energy transfer with a significant reduction in the sensitizer fluorescence decay period. The excited states of the sensitizer and activator have an energy differential of the same magnitude, which drives the energy transfer process[44,45]. It is possible for a phonon to aid in non-resonant ET if there is a significant distance between the ground and excited states of the sensitizer and activator. The ET process in luminous materials is largely dependent on the potential contacts, characteristic transitions, and energy differential between the sensitizer and activator. For phonon-assisted non-radiative transitions (Fig. 1.6(c)), where the two ions are in different excited states, there is little chance of energy transfer. The term "cross-relaxation" refers to any kind of down conversion energy transfer between ions or similar luminous centers that are adjacent to one another. When the first ion, which is originally excited—trades energy with the second ion, which is initially in the ground state cross-relaxation, a straightforward potential energy level scheme takes place. As a result, inside the energy between the two beginning states, both ions lie in some state of intermediary concurrently[46].

1.3.3. Concentration quenching mechanism

When materials are doped with RE ions, the intensity of luminescence grows to a specific point and then declines. We refer to this process as quenching concentration. Increases in absorption efficiency generate an increase in luminescence intensity, which is greatest at a specific doping ion concentration known as the critical concentration [47,48]. In any RE ions doped phosphor host lattice, concentration quenching is mostly caused by energy transfer between activator ions. Concentration quenching occurs when the distance between the donor

and acceptor atoms gets smaller to such an extent that the energy exchange between them is induced. Two explanations exist for the concentration quenching process [49].

i. In the first kind of mechanism, dominant energy transfer allows the excitation energy to be spread into several luminescent centers prior to emission. Multi-phonon relaxation returns these excited luminous centers to their ground state. These centers have the potential to function as energy sinks in the transfer chain, leading to the quenching of emission intensity [50,51].

ii. The second type of mechanism uses a cross-relaxation process to utilize the excitation energy from the emitted state. This process is caused by resonant energy transfer between the two neighboring activator ions [52,53].

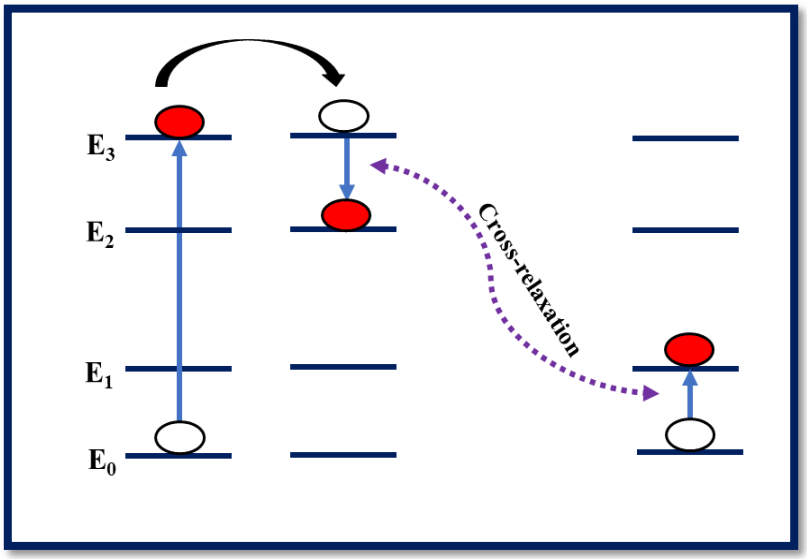

Fig. 1.7: *Cross-relaxation between pairs of centers.*

Fig. 1.7 shows the energy level diagram with cross-relaxation. Resonant energy transfer occurs when the energy difference (E_0-E_1) of one nearby center (acceptor) and the energy difference (E_3-E_2) of another luminous center (donor) are equal. This largely depends on the type of energy

level. The excited electron moves from E_3 to E_2, acting as a donor center, and releases energy that was absorbed by another electron at E_0, moving from E_0 to E_1 levels, acting as an acceptor, in a process known as cross-relaxation. The emission intensity is quenched because of the non-radiative energy transfer between the closest activator ions.

1.4. Decay time process of RE Ions

The process of excitation and de-excitation is initiated by the intra $4f - 4f$ electronic transition of the RE ion, provided that the required energy is present. In Fig. 1.7, a time-resolved intensity spectrum shows the excitation and de-excitation process. Through radiative transition, energy exchange between nearby RE ions, cross relaxation channels, or other mechanisms, the excited RE ion can return to its ground state. At low RE ion concentrations, RE ions are not able to interact with one another, hence a single exponential function fits the intensity decay curve against time. The PL intensity can be expressed using the following equation [54,55].

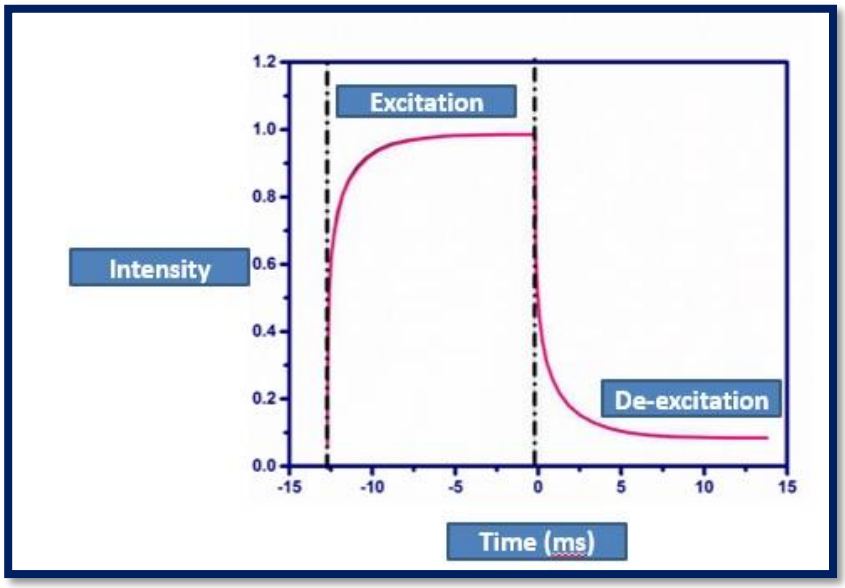

Fig. 1.8: *Excitation and de-excitation Process of RE ions.*

$$I_t = I_0 + A_1 \exp\left(-\frac{t}{\tau}\right) \tag{1.1}$$

In this instance, the PL intensity at time zero is denoted by I_0. The logarithmic plot of intensity against time can be used to determine the excited RE ion's lifespan, represented by τ. The excited state's intensity steadily decreases with time as 1/e, as seen in Fig. 1.8. The experimental lifetime of an excited RE ion can be predicted using the following formula[56].

$$\tau_{exp} = \frac{\int tI(t)dt}{\int I(t)dt} \tag{1.2}$$

However, at higher concentrations of RE ions, the decay profiles suit the bi-exponential function quite well. For a bi-exponential fit, the PL intensity can be represented by an equation[57,58].

$$I_t = I_0 + A_1 \exp\left(-\frac{t}{\tau_1}\right) + A_2 \exp\left(-\frac{t}{\tau_2}\right) \tag{1.3}$$

To find the average lifespan (τ_{avg}) in this case, apply the following formula[59].

$$\tau_{avg} = \frac{A_1\tau_1^2 + A_1\tau_2^2}{A_1\tau_1 + A_2\tau_2} \tag{1.4}$$

In this case, the lifespan components τ_1, τ_2 are exponential, and A_1, A_2 are fitting constants.

Inokuti-Hirayama (I-H) model: It is well known that there are two distinct ways by which an ion can relax from an excited state to a lower energy state. In the first process, the donor ions may transfer the energy among themselves before it reaches the unexcited acceptor ions. Direct energy transfer from the donor ions to the acceptor ions is made possible by the second mechanism. The quick decay is caused by the energy transfer that took place between the donor and acceptor ions when they are equally distributed throughout the host matrix and there is little energy movement between the donor ions. In these situations, the I-H model is a useful tool for understanding the primary energy transfer mechanism. The luminescence intensity in this case is established by [60,61]:

$$I_t = I_0 \exp\left\{-\frac{t}{\tau_0} - Q\left(\frac{t}{\tau_0}\right)^{\frac{3}{S}}\right\} \quad (1.5)$$

"τ_0" indicates the donors' intrinsic decay duration in the absence of acceptors, and "t" is the elapsed time after stimulation. To get "Q," the energy transfer parameter, use the equation below [62,63]:

$$Q = \frac{4\pi}{3}\Gamma\left(1 - \frac{3}{S}\right) N_0 {R_0}^3 \quad (1.6)$$

The acceptor ion concentration (N_0) and the required energy transfer distance (R_0) are given in the above relation. Based on the values of S and gamma function (x), the interactions that comprise the mechanism can be classified as dipole-quadrupole (S=8, Γ(x)=1.43), quadrupole-quadrupole (S=10, Γ(x)=1.43), and dipole-dipole (S=6, Γ(x)=1.77). The following formulas are used to compute the donor-acceptor interaction parameter C_{DA} and the energy transfer probability W_{ET}.[64,65]

$$C_{DA} = {R_0}^{(S)} {\tau_0}^{-1} \text{ and } W_{ET} = C_{DA} {R_0}^{(S)} \quad (1.7)$$

1.5. Present glass host composition

Specifically, glasses doped with RE ions have several intriguing characteristics, including high concentrations of RE ions that can be accepted, wide inhomogeneous bandwidths, inexpensive production costs, and simple manufacturing processes. A network of borosilicate glass with essential advantageous properties including strong mechanical strength, low melting point, high thermal stability, and corrosion resistance is formed among a variety of host glass matrixes by a suitable combination of borate (B_2O_3) and silicate (SiO_2). For a variety of optical applications, borosilicate glass systems have proven suitable and valuable due to these advantageous characteristics. Because network-forming oxides stretch when they vibrate, borosilicate glasses contain relatively high phonon energy, which accounts for non-radiative

losses. A network of borosilicate glass with essential advantageous properties including strong mechanical strength, low melting point, high thermal stability, Heavy metal oxides (HMOs) can be effectively added to the glass host matrix to minimize such high phonon energy. To do this, researchers typically decide to incorporate HMOs with relatively high phonon energies, such as bismuth (Bi_2O_3) and lead oxides (PbO), into the host glass matrix. Because of its high atomic number and density, HMOs can serve as a useful shielding material against radioactive radiation [8, 26–28]. The network of borosilicate glasses is altered by low PbO concentration because of the lead structural unit [PbO_4]. As PbO concentration rises, lead functions somewhat as a glass former. Lead oxides, then, have a dual function and can enhance the radiative emission characteristics of host glass. However, lead's harmful effects on the environment and human health result in several problems. A network of borosilicate glass with essential advantageous properties including strong mechanical strength, low melting point, high thermal stability. Furthermore, by increasing the critical distance between the doping ions in the glass host, Al_2O_3 can be added to increase the emission properties of borosilicate glass. Al_2O_3 can also function as a network modifier and improve the host glass's mechanical, thermal, and chemical stability [66–68]. Alkaline earth oxides have the potential to function as a suitable network modifier in various glass formers. They can enhance the structure and chemical stability of the glass, reduce the molar heat of dissolution, and significantly compact the glass network, making them acceptable for photonic applications. The aforementioned numerous distinctive qualities provided by substances like B_2O_3, Al_2O_3, SiO_2, SrO and BaO motivated us to prepare a host glass in this thesis with the following chemical composition (in mol%).

$$50B_2O_3\text{-}20SiO_2 - 10Al_2O_3 - 10\ SrO - 10\ BaO$$

1.6. The current research work's objectives

- To optimize the process parameters of a high-quality optical glass activated with certain RE ions for numerous photonic applications.
- To optimize the effective glasses composition, doped with RE ions and examines absorption, excitation, and emission spectrum features studied to comprehend the concentration of RE ion dependency as well as the glass host.
- Comprehensive physical evaluation of glasses through measurements of their density, refractive index, and other characteristics. Techniques like XRD and FT-IR are used in the structural examinations.
- For improved luminescence efficiency, optimize the concentration of RE ions and co-dope the produced glassy systems with appropriate RE ions.

CHAPTER 2

Experimental and Instrumentation

Expertise in experimental techniques is essential for the development of high-quality glassy materials. This chapter provides a detailed discussion of the traditional melt quenching process used to prepare RE doped glass materials. The structural and optical characteristics of the as prepared luminescent glasses have been described. X-ray diffraction (XRD), Fourier transforms infrared (FT-IR), UV-VIS-NIR spectroscopy, spectrofluorophotometer, and other analytical techniques have all been used to investigate the characteristics of RE doped glasses. This chapter describes the instrumentation and working concept of the characterization approaches that are used.

2.1. RE doped glasses preparation

A rare earth-doped glass study's experimental and instrumentation section covers the techniques and tools used to investigate the optical and spectroscopic characteristics of the glass substance. The luminescent properties of glass is enhanced optically by the addition of rare earth dopants, which makes it suitable for a variety of uses, including amplifiers, sensors, and lasers [69]. Here's an outline of the experimental and instrumentation aspects:

- Melt quenching.
- Sol-gel method
- Electrochemical methods
- Solid state methods
- Vapor quenching Sputtering.
- Pyrolysis

Among all listed techniques, melt quenching is the oldest and easiest technique for preparing amorphous material. This technique is widely used commercially also.

2.1.1 Melt quenching process

Melt quenching is the process of rapidly cooling precursor material molten form to create amorphous materials into the appropriate shape. The melt quenching process is unique in that the uniformly melted material is continuously hardened, resulting in the formation of amorphous solids. The necessary cooling rate to produce glassy states differs depending on the host glass system. After removing the melt from the temperature-controlled electric furnace, it can be quickly quenched before being poured across warmed conductive materials such as brass or copper plates. This will achieve essential cooling.[70].

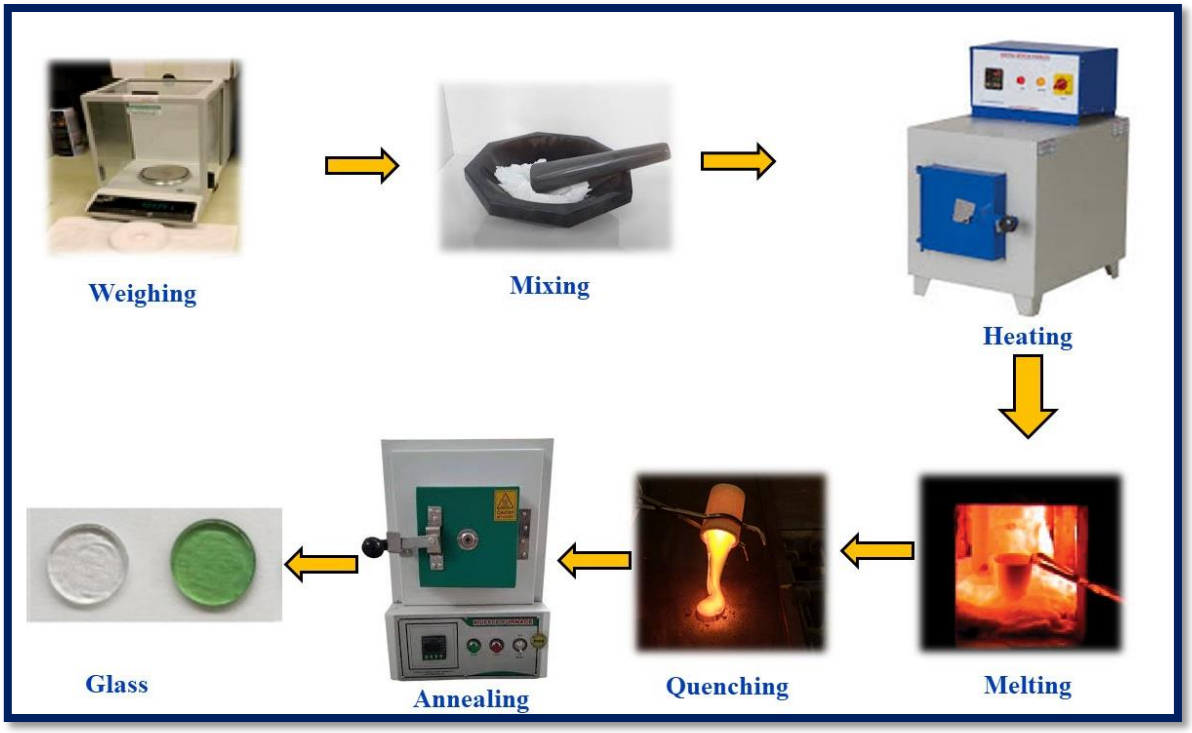

Fig. 2.1: *Melt Quench procedure used for the preparation of the glasses.*

Fig. 2.1 shows the process for producing the glass host matrix using the melt quenching technique. To get rid of various imperfections like air bubbles, thermal shocks, and cracks in the manufactured glasses, the acquired glasses were annealed for three to four hours in a muffle furnace, below the glass transition temperature. Finally, glasses with the right thickness and transparency, free of air bubbles have been produced. The produced glasses are subjected to additional characterization techniques, including XRD, PL, Absorption, temperature-dependent photoluminescence spectral analysis, optical absorption, FT-IR, PL excitation, PL emission, and PL decay measurements.

2.2. Glass composition calculations and preparation

2.2.1. Precursor Materials

The oxide raw materials H_3BO_3, SiO_2, Al_2O_3, $SrCO_3$, $BaCO_3$ and dopant RE^{3+} ions, have been purchased from several companies together with high A. R. quality (≥ 99.90%). The

chemical composition of single RE^{3+} ions doped glasses synthesized via melt quenching method as follows:

$$50B_2O_3\text{-}20SiO_2 - (10\text{-}x)\ Al_2O_3 - 10\ SrO - 10\ BaO: x\ RE$$

where RE^{3+} ions concentration varies through x = 0.1, 0.5, 1.0, 1.5 and 2.0 mol%. The chemical composition for RE ions co-doped AEAlBS glasses as follows:

$$50B_2O_3\text{-}20SiO_2 - (10\text{-}x\text{-}y)\ Al_2O_3 - 10\ SrO - 10\ BaO: x\ RE1 - y\ RE2$$

where the RE1 and RE2 are two different rare earth ions. Weighing the above specified raw materials according to the proper proportion at room temperature was done using a computerized balance (Shimadzu modal: ATX244). Up until a smooth and uniform mixture is achieved, roughly 6 grams of raw materials are combined and mixed in an agate mortar with acetone acting as a wetting agent.

2.2.2. Glass preparation process

The highly pure H_3BO_3**,** SiO_2**,** Al_2O_3**,** $SrCO_3$, $BaCO_3$, RE oxides precursor materials were used to prepare single Sm^{3+} doped and co-doped AEAlBS glasses as shown in table 1. Above-mentioned precursors were weighed in stoichiometric amounts and ground in liquid (acetone) mixing medium using agate mortar. The grounded mixer was taken in alumina crucible and heated at around 1250°C for 30 min in an electric furnace to get uniform melt. At a temperature >650 °C, $SrCO_3$ &, $BaCO_3$, release CO_2 and only SrO & BaO remain in the final melted glass composition. The melted precursors were quickly quenched with the help of two pre-heated brass plates. Further the as prepared AEAlBS glasses were annealed at 350°C for 3.5 hrs, to eliminate air bubbles and cracks produced inside due to sudden quenching.

2.3. Characterization techniques

A wide range of approaches are included in glass characterization techniques, which are used to examine and comprehend the characteristics and behavior of materials at different scales, ranging from the atomic to the macroscopic. In numerous disciplines, such as materials science, nanotechnology, chemistry, physics, engineering, and biology, these methods are crucial for research, development, and quality control. Several methods were used to study different characterizations of the as-prepared rare earth ions doped barium strontium alumino borosilicate glasses, including optical, photoluminescent, structural and physical. The manifestations of the various characterization tools used in the present work are explained as follows.

2.3.1. X-ray Diffraction (XRD)

A strong method for determining a material's phase composition, crystallite size, and crystallographic structure is the most essential non-destructive procedure is X-ray diffraction (XRD). It is possible to identify structural features including contraction, lattice points, and preferred orientation. X-rays are short wavelength electromagnetic waves that fluctuate within a few angstroms; this wavelength range is comparable to the materials' atoms' interplanar spacing. When a CuS crystal was subjected to an x-ray beam and the findings were recorded on photographic plates, the XRD technique was first discovered in 1912. The first crystal structure was solved by Bragg and his son, who also described the diffraction pattern's guiding principle [71,72]. Although it can also be used to analyze amorphous or non-crystalline materials, this technique works best with crystalline or partially crystalline materials.

Bragg's Law: The basis for X-ray diffraction by crystalline materials, as articulated by Bragg's Law, is X-ray diffraction. Upon incoming monochromatic X-rays on a crystalline

sample, the interatomic spacing inside the crystal lattice determines the exact angles at which the radiation is diffracted. Bragg's Law equation[73]:

$$n\lambda = 2d\ Sin\theta \qquad (2.1)$$

- n is the order of the diffraction peak,
- λ is the wavelength of the incident X-rays.
- d is the interplanar spacing of crystal lattice planes,
- θ is the diffraction angle,

Detector: A detector calculates the diffraction angle-dependent intensity of diffracted X-rays. Analyzing the Data: The diffraction pattern that is produced tells us about the orientation, phase composition, and crystal structure of the material. It is usually a plot of intensity against diffraction angle.

Figure 2.2 shows a schematic illustration of an X-ray diffractometer that is furnished with a rotating X-ray line detector, a moving X-ray tube, several slit kinds, a sample holder, and a goniometer.

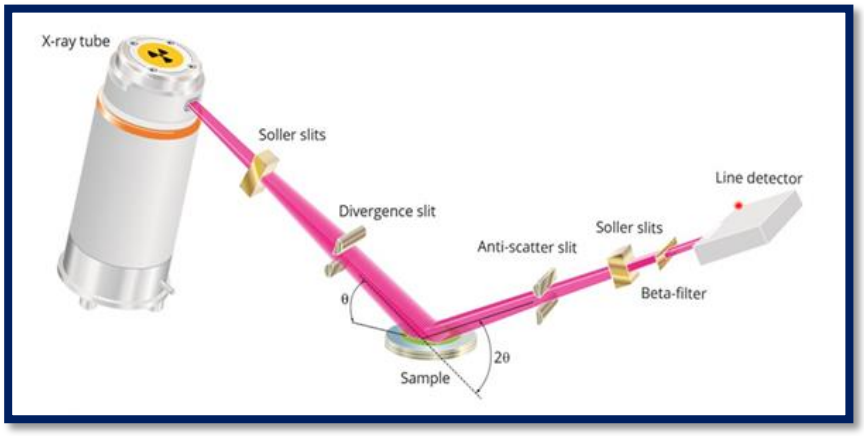

Fig. 2.2: *Schematic illustration of XRD.*

The steps in the X-ray radiation detection process (XRD) begin with the generation of X-rays, which are then followed by striking a sample and detector detection of diffracted X-rays. High-intensity electrons impact a rotating metal anode target (Cu), which emits a variety of radiation, including X-rays, and this process generates X-rays. Using Be windows, which offer a transparent environment for generated X-rays, X-rays exit the tube. Nickel-based thin metal foil is typically used to select and filter out other lines, leaving only the K_α line visible. X-ray incident on the sample, which is positioned and rotates at an angle θ concerning the X-ray beam's path. Both the detector and the sample's rotational angle can be controlled by the goniometer. Constructive interference occurs when an X-ray incident strikes the sample's surface and meets Bragg's equation requirements [73]. To detect the incident diffracted X-ray beam and convert the signal to count rate, the detector rotates at an angle of 2θ with regard to the path of the incident X-ray beam. Ultimately, the counts of detected X-rays were supplied directly into a computer, which plotted the counts against angle 2θ and saved the data for later processing. The produced crystalline powder samples' XRD profiles were recorded using a Bruker D8 advanced X-ray diffractometer, as seen in Fig. 2.3.

Fig.2.3: *Bruker D8 Advance X-ray diffraction machine.*

2.3.2. Fourier transform infrared spectroscopy (FT-IR)

The technique of far-infrared to near-infrared spectroscopy is used to identify absorption bands. One of the most sophisticated spectroscopic techniques, FT-IR spectroscopic analysis concurrently gathers data at all wavelengths. Vibrational and bonding groups in both organic and inorganic materials are often identified using this technique. It may be able to classify the atomic conformations of glass-forming network structures. There are two different kinds of vibrations in molecules: bending and stretching. During stretching, the distance between two

successive atoms changes, but the angle between them doesn't. However, with respect to the bond axis, the atoms' bending positions vary. A given frequency's vibration amplitude has increased in proportion to the amount of infrared radiation that strikes the molecule. Consequently, one method of locating the functional groups that are present with the molecules—such as OH, NH2, C=O, and NO2—is to use infrared (IR) spectroscopy. Typically, the Michelson Interferometer technique is used by FT-IR instruments. [74]. The two mirrors used in the interferometer technique are positioned via the beam splitter at right angles to one another. The output beam is the result of the interference of the reflected beam from both mirrors, one of which is moving to a specific distance while the other is fixed. The sample creates an interference pattern when the beam passes by it; this interference pattern can be used to obtain the material's infrared spectrum by using the Fourier transform method [75].

An FT-IR device typically consists of an IR source, an interferometer, a sample holder, and a detector. All of these components are connected and controlled by software on a separate computer. Fig. 2.4 represent the FT-IR spectrometer, which was used for characterization.

Fig. 2.4. Schematic representation of FT-IR Spectrometer (Perkin Elmer).

2.3.3. UV-VIS-NIR Spectroscopy

Ultraviolet-Visible-Near Infrared spectroscopy, or UV-VIS-NIR spectroscopy, is a potenttial analytical method used to examine how molecules in the ultraviolet, visible, and near-infrared portions of the electromagnetic spectrum absorb, reflect, and transmit light. In UV-VIS-NIR spectroscopy, the sample is exposed to light in the UV to NIR range, and the light that is absorbed, reflected, and transmitted is detected at the other end of the sample. Since the radiation changes after encountering the test sample, the information about the test sample is provided by the radiation through the sample of fixed thickness. Fast analysis, non-destructive nature, and low sample preparation requirements are several benefits of UV-VIS-NIR spectroscopy. It is extensively used for qualitative and quantitative analysis, compound identification, and chemical reaction monitoring in a variety of domains, including biochemistry, materials science, environmental research, and pharmaceuticals [76].

UV-VIS-NIR Spectroscopy employs the Beer-Lambert law, which states that the rate at which the intensity of radiation decreases with the thickness of an absorbing solution is directly proportional to the concentration of the solution and the radiation incident. This law applies to monochromatic light beams passing through absorbing materials. The following is the expression for absorbance (A).

[77,78]:

$$A = log_{10}\left(\frac{I_t}{I_0}\right) \qquad (2.2)$$

The transmitted light intensity I_t and the incident light intensity I_0 are indicated in the above expression, respectively. T stands for transmittance, which is defined as $T=I/I_0$. The thickness of the sample affects the transmitted light's intensity when monochromatic light travels through

it. The following relationship can be used to determine the absorbance (A) value from the transmittance spectra:

$$A = log_{10}\left(\frac{I}{I_0}\right) = log_{10}\left(\frac{1}{T}\right) \qquad (2.3)$$

In this instance, the absorption coefficient α(ϑ) under investigation has been approximated using the absorption data using the subsequent equation [79]:

$$\alpha(\vartheta) = \frac{1}{d} ln\left(\frac{I_t}{I_0}\right) \qquad (2.4)$$

In this case, d is the test sample thickness, α(ϑ) is the absorption coefficient, and factor $ln\left(\frac{I_t}{I_0}\right)$ indicates the absorbance [80]. The Jasco-770 spectrophotometer, which has a 0.2 nm spectral resolution, was used in the current work to measure the optical absorption spectrum as demonstrated in Fig 2.5. This device has a deuterium lamp for the UV spectral region and a tungsten lamp for the VIS to NIR range. The percentage of electromagnetic energy that is absorbed or transmitted in the UV, VIS, and NIR spectra is determined using a spectrophotometer.

Fig.2.5. UV-VIS Spectrometer Jasco V-770 instrument.

2.3.4. Photoluminescence (PL) spectroscopy

An analytical tool for examining a material's luminescence characteristics is a PL spectrometer. When a substance emits light, it is referred to as luminescence. This can happen through a variety of processes, including photoluminescence, phosphorescence, and fluorescence. In order to examine the luminous properties of both solid or liquid samples, PL spectroscopy provides a versatile, non-destructive, and potent analytical technique. Emission spectra, PL decay time measurements, and confocal pictures are parameters that define the research of luminescent-based materials. Any material that is monitored with the right excitation can spontaneously emit light, as explained by PL spectroscopy [81]. To describe the electronic structure of the materials used, this considerable contactless method is employed. A certain wavelength of input light is focused on the test sample and absorbed there; as a result, the electrons are stimulated above their ground state. Upon returning to ground state, these electrons release energy in two ways: either as heat, which is known as the non-radiative process, or as light, which is known as the radiative process. Fig. 2.6 shows the schematic diagram connected to the spectrometer's arrangement.

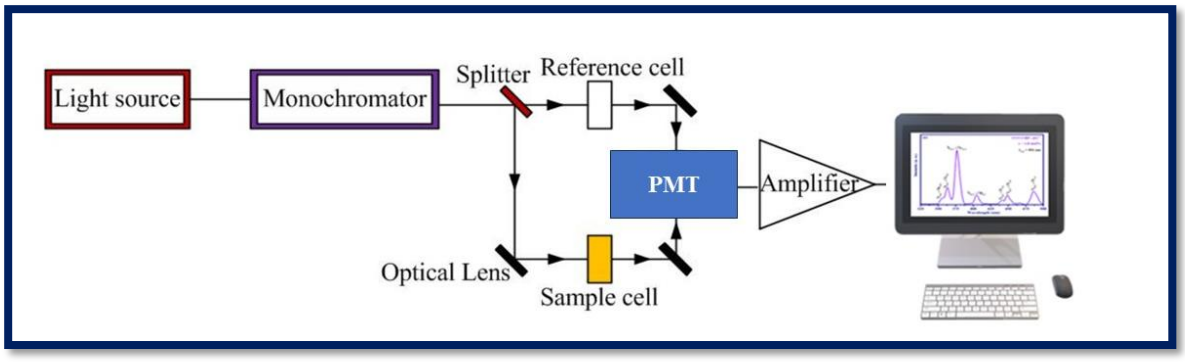

***Fig.2.6**: Schematic diagram of a spectrofluorometer.*

(i) Method and equipment: The three primary components of the PL spectrophotometer are the sample holder, the detector, and the excitation source. A continuous spectrum within the

line spectrum must be produced by the used excitation source. Because it can produce a relatively continuous, bright light output with a wavelength longer than 220 nm, Xenon (Xe) lamped is typically utilized as an excitation source. An assembly that only allows light at the desired wavelength is connected to the monochromator. To increase the spectrofluorometer's sensitivity, the excitation monochromator uses diffraction gratings with larger aperture values to collect the most luminous excitation light. As a light beam from the excitation monochromator flashes through the specimen holder, samples made of glass or phosphor are placed within. A photodetector functions as a photomultiplier tube (PMT) in the specimen, allowing the emission monochromator to selectively combine fluorescent light and measure fluorescence intensity. With a substantial spectrum response, the PMT is regarded as a reliable current source. Increased noise and signal distortion result from Xe-lamps' volatile light production and irregularities in the radiation spectrum of their light. A light-source compensation plan is being used to avoid this problem. In addition to the excitation monochromator, a PMT and reference cells have been installed to monitor and adjust that portion of the excitation light and provide the resulting signal return to the detector. [78,82]. By selecting the proper wavelength scanning mode at low, medium, and high scanning speeds, using a high-voltage PMT setup, and using an excitation and emission slit width of 0.1 nm, the PL excitation and PL emission spectra have been observed at room temperature. Time scanning mode is used to perform the PL decay analysis. Pulsed excitation source is utilized for time-resolved PL (TR-PL) measurements. Temperature-dependent PL (TD-PL) involves heating the sample to a higher temperature using a handmade heating apparatus, followed by multiple higher temperature PL spectral observations.

(ii) Data analysis: In the case of the luminous materials, stimulation of charged carriers has occurred if the energy of the incident photon corresponds to or greater than the energy bandgap.

Radiation of photons occurs when these stimulated carriers relax radiatively. The PL spectrum therefore provides details about the optical shifts of states of electrons and recombination processes involving radiative and non-radiative transitioning inside the light-emitting materials. It can be amassed and assessed in this way. The stimulation power, pressure, temperature, and external perturbation, such as an electric or magnetic field, can all be changed while doing PL spectral observations. Therefore, we may have further information on the bands and electronic states**.**

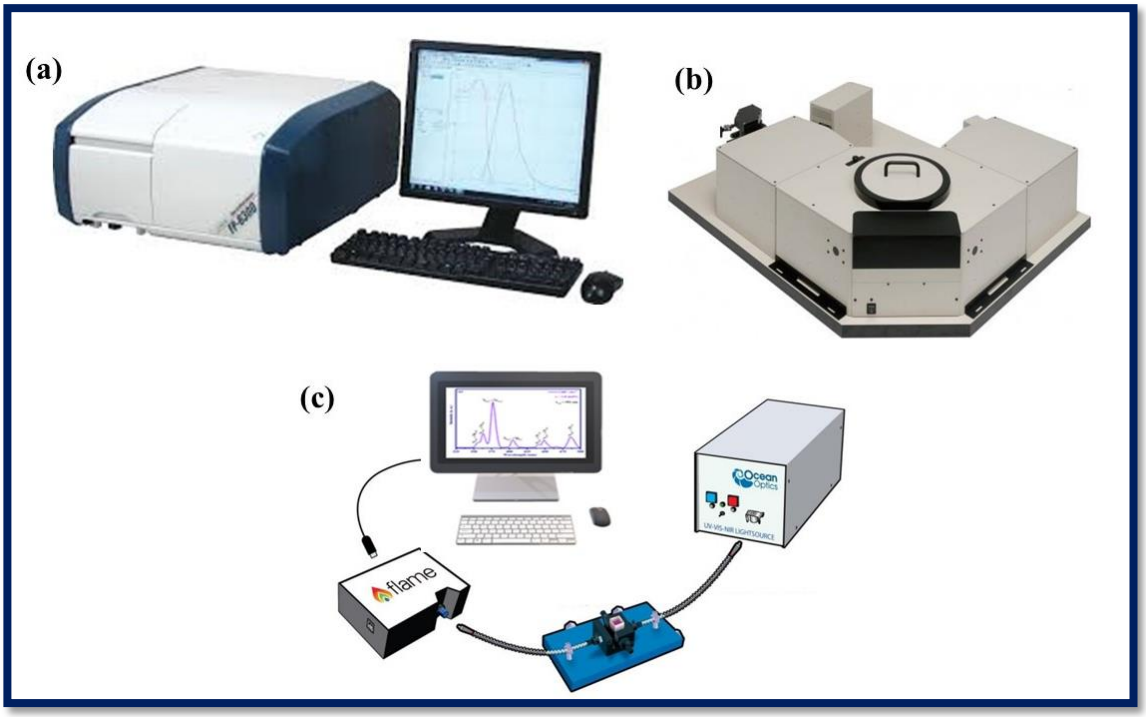

Fig.2.7: *(a) JASCO FP 8300 Spectrofluorophotometer (b) Edinburgh FLSP920 TRPL and (c) Ocean Optics FLAME- Spectrometer.*

We will be able to comprehend certain specific details about the non-radiative relaxations by fitting the TR-PL data using single, bi-, or tri-exponential equations. As a result, TR-PL is a very effective instrument for studying luminous materials' non-radiative processes. For illumination applications, the luminous materials must be thermally stable, which can be determined by evaluating PL spectra at a higher temperature [83]. The configuration is therefore

denoted as Temperature-dependent PL (TD-PL). In general, it was not anticipated that the PL profile would change at higher temperatures; but thermal quenching events could cause its intensity to decrease. The minimal thermal quenching required for improved luminous materials is intended to reflect their increased thermal resilience at higher temperatures. As shown in Fig. 2.7 (a-c), the luminous properties of the as prepared RE doped glasses were characterized via utilizing various Spectrofluorophotometer.

CHAPTER 3

Energy Transfer Dynamics in Thermally Stable Sm^{3+}/Eu^{3+} Co-Doped AEAlBS Glasses for Near UV Triggered Photonic Device Applications

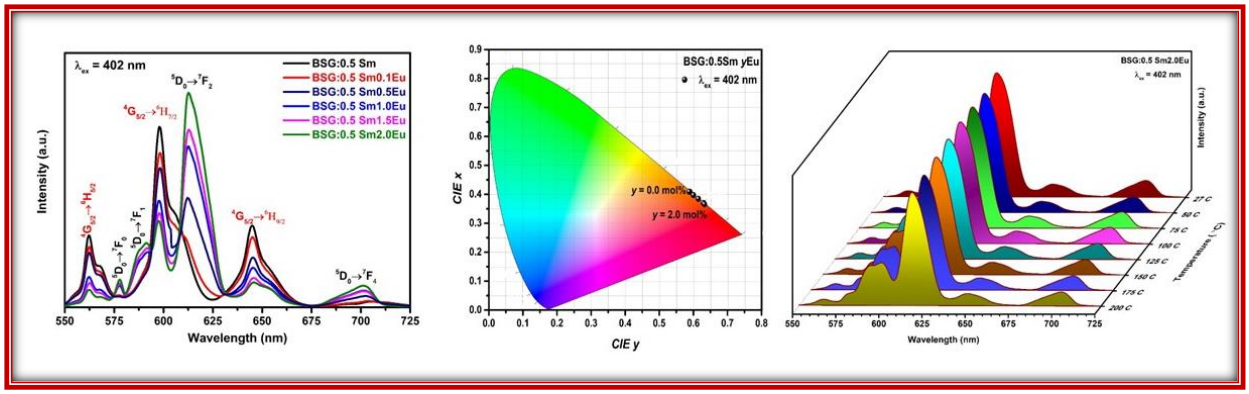

Part of this work has been published in Journal of Non-Crystalline Solids 580 (2022) 121392 (Impact Factor: 3.5)

Transparent, Sm^{3+} doped and Sm^{3+}/Eu^{3+} co-doped alkaline earth alumino borosilicate (AEAlBS) glasses have been synthesized by employing melt quenching process and explored their down-shifting luminescent properties for utility in visible red photonic devices applications. The amorphous (non-crystalline) nature of the as prepared glass was analyzed with help of X-ray powder diffraction (XRD) pattern, containing broad peak. The PL properties demonstrate the glasses were proficiently excited by near-UV with dominant peak centered at 402 nm. The emission spectra exhibit four emission peaks with an intense peak placed at 599 nm under 402 nm excitation. The optimum emission intensity was obtained for 0.5 mol% Sm^{3+}

ions doped in AEAlBS glasses. Sm^{3+} ion work as effective sensitizer for Eu^{3+} activator ion in AEAlBS glasses and part of energy transfer (ET) from sensitizer (Sm^{3+}) to activator (Eu^{3+}) ions. The PL intensity of Sm^{3+} ion peaks were demises and enhance the Eu^{3+} ion peaks with Eu^{3+} ion co-doping in AEAlBS glasses at λ_{ex} = 402 nm. The efficient ET from sensitizer to activator ions proved to be dipole-dipole in nature via employing Dexter's formula with Reisfeld's approximation. The experimental lifetime values calculated from the PL decay profiles are decreasing with surge in Eu^{3+} ion concentration in the as prepared glasses. Inokuti Hirayama (I-H) model applied to the PL decay profiles confirm the ET process responsible for decrease in experimental lifetimes as dipole-dipole in nature. The outcome of I-H model is in consonance with the result given by Dexter theory. The CIE coordinates for single Sm^{3+} doped glasses are falling in orange region, and gradually surge into red region by co-doping with Eu^{3+} ions in AEAlBS glasses. The temperature-dependent emission analysis reveals that, the PL intensity at 150°C and 200°C perseveres up to 94.34 and 91.30 % of the PL intensity at environmental temperature, respectively. All the obtained results contemplate the superiority of the multifunctional Sm^{3+}/Eu^{3+} co-doped AEAlBS glasses for near UV triggered photonic device applications.

3.1. Introduction

In recent several years, crystalline and amorphous luminescent materials doped with trivalent/divalent lanthanides have recognized abundant consideration among the scientific community ascribed to its expanded applications in the area of advance photonic devices [43,84,85]. In addition, luminescent based phosphor coated white light emitting diodes (w-LEDs) are crucial illuminating devices, which can save huge amounts of power and used as an advanced lighting source. The w-LEDs emended with phosphor is one of most prominent

lighting sources and mostly substitute the long lasting incandescent and fluorescent illuminating sources [86]. Presently, w-LEDs are fabricated by the combination of yellow phosphor coated resin on blue LED chip [87,88]. But this approaches having numerous downsides for instance lesser thermal stability, high correlated color temperature (7750 K), lesser color rendering index (70-80) owing to the non-appearance of red color constituent [89,90]. Also, the phosphor was mixed with organic compound, which further degrades the quality and performance of lighting devices. To fulfill these limitations, w-LEDs are prepared by coating an epoxy resin with a combination of primary color emitting (red, green & blue) phosphors energized by near-UV LED chip. However, this methodology has shown some improvements like better CRI value but undergoes low efficacy owed to the re-absorption of blue radiation by red or green emanating phosphors and surge the production cost [86,91]. In the above mentioned both approaches, an organic epoxy resin is very much need as mixing medium for phosphors. The thermal stability of organic epoxy is very less and as a consequent there will be a degradation of color quality and lifetime of the w-LEDs [59]. The mentioned deficiencies can be overcome by using inorganic glasses. Also, lanthanides or transition metal ions doped glasses functioned as wavelength converters as well as encapsulants.

Lanthanide ions in glasses, can act as both sensitizers along with an activator and upsurge the excitation along with emission wavelength region of glasses [92,93]. One of the suitable lanthanides is Sm^{3+} ions, which can act as a sensitizer as well as activator in many inorganic glasses under the n-UV and blue light excited. Sm^{3+} ions can act as sensitized for many lanthanides ions and more appropriate sensitizer for Eu^{3+} ion due to closed energy level, which can perform as an activator [63,94]. Hence, the lanthanides ions in co-doped glasses cover the huge portion of near-UV LED chip emission wavelength owing to extended excitation range as

well as energy transfer (ET) from effective sensitizer to appropriate activator, which improves the excitation as well as emission characteristics along with performance of the glasses [95]. Inorganic glass doped with lanthanides ion have remarkable physical characteristics like less preparation cost, simple preparation procedure, prepared in any size with desired shape, excellent optical properties, which can be direct applied in numerous photonic applications [9,96]. In several inorganic oxides glass forming hosts, the combination of B_2O_3 and SiO_2 materials can produces an important inorganic glass network as borosilicate glasses and possess high thermal stability, minor thermal expansion coefficient, high softening temperature, melting at low temperatures with high corrosive resistant [67,97]. These remarkable properties of borosilicate glasses can be useful in diversified areas such as lighting, automation, photovoltaic cells, displays and lasers, etc. Additionally, the emission properties of borosilicate glass can be improved by adding the Al_2O_3 in glass host, which can enhance the critical distance among the doping ions. In addition, Al_2O_3 boost the chemical, thermal and mechanical stability of the host glass and can act as a network modifier [17,49]. The alkaline earth oxides can work as an appropriate network modifier in many glass formers, improving glass structure, enhancing glass chemical stability, decreasing the molar heat of dissolution and significant compaction of the glass network, which can be suitable for photonic applications [68].

The prime aim of the present work is to synthesize AEAlBS glass doped with single Sm^{3+} and co-doped with Sm^{3+} & Eu^{3+} ions glasses employing the melt quenching process and to examine their structural, energy transfer and down-shifting photoluminescent properties in deatiled. ET transfer mechanism was studed via employing Dexter's ET formula Reisfeld's approximation and I-H model. Furthermore, temperature dependent emission, CIE coordinates and lifetime curve analysis enhance the quality of luminescence characteristics Sm^{3+} & Eu^{3+} co-doped AEAlBS glasses for the utility of glass in w-LEDs and numerous photonic device applications.

3.2. Experimental

3.2.1. Synthesis of single Sm^{3+} ions doped and Sm^{3+} & Eu^{3+} ions co-doped AEAlBS glasses

The chemical composition of single Sm^{3+} ions doped AEAlBS glasses synthesized via melt quenching method as follows:

$$50B_2O_3\text{-}20SiO_2 - (10\text{-}x)\ Al_2O_3 - 10\ SrO - 10\ BaO: x\ Sm_2O_3$$

$$50B_2O_3\text{-}20SiO_2 - (10\text{-}x)\ Al_2O_3 - 10\ SrO - 10\ BaO: y\ Eu_2O_3$$

where Sm^{3+} ions concentration varies through x = 0.1, 0.5, 1.0, 1.5 and 2.0 mol% and the synthesized glasses are abbreviated as BSG:0.1Sm, BSG0.5Sm, BSG:1.0Sm, BSG:1.5Sm & BSG:2.0Sm respectively. Eu^{3+} ions doping concentration was y = 0.5 mol% and abbreviated as BSG0.5Eu. The chemical composition for Sm^{3+}/Eu^{3+} ions co-doped AEAlBS glasses as follows:

$$50B_2O_3\text{-}20SiO_2 - (10\text{-}x\text{-}y)\ Al_2O_3 - 10\ SrO - 10\ BaO: x\ Sm_2O_3 - y\ Eu_2O_3$$

where the Sm^{3+} ions concentration was fixed at x = 0.5 mol% and Eu^{3+} concentration varies through y = 0.1, 0.5, 1.0, 1.5 & 2.0 mol%, and the prepared glasses are titled as BSG:0.5Sm0.1Eu, BSG:0.5Sm0.5Eu, BSG:0.5Sm1.0Eu, BSG:0.5Sm1.5Eu and BSG:0.5Sm2.0Eu, respectively. The highly pure H_3BO_3, SiO_2, Al_2O_3, $SrCO_3$, $BaCO_3$, Sm_2O_3 and Eu_2O_3 precursor materials were used to prepare single Sm^{3+} doped and Sm^{3+}/ Eu^{3+} co-doped AEAlBS glasses as shown in table 1. Above-mentioned precursors were weighed in stoichiometric amounts and ground in liquid (acetone) mixing medium using agate mortar. The grounded mixer was taken in alumina crucible and heated at 1250°C for 30 min in an electric furnace to get uniform melt. At a temperature >650 °C, $SrCO_3$ &, $BaCO_3$, release CO_2 and only SrO & BaO remain in the final melted glass composition. The melted precursors were quickly

quenched with the help of two pre-heated brass plates. Further the as prepared AEAlBS glasses were annealed at 350°C for 3.5 hrs, to eliminate air bubbles and cracks produced inside due to sudden quenching.

3.2.2. Characterizations of single Sm^{3+} doped and Sm^{3+}/Eu^{3+} co-doped AEAlBS glasses

The amorphous or non-crystalline nature of the AEAlBS glass has been examined by diffraction data obtained from XRD (Bruker, D8 advance attached with $CuK\alpha$ radiation and Ni filter) over the $10° \leq 2\theta \geq 60°$ range. PL excitation as well PL emission spectra were recorded by using a Jasco made (FP-8300) Spectrofluorophotometer. The Pl decay curves were recorded by employing an Edinburgh made (FLS920) spectrofluorophotometer with UV flash lamp as a source of excitation. Temperature dependent PL spectra were recorded using Ocean optics spectrometer equipped with Xenon flash lamp as an excitation source and a heating assembly.

3.3. Results and discussion

3.3.1. AEAlBS glass structural study

The structural investigation of an undoped Ba AEAlBS glass was scrutinized by diffraction patterns. Fig. 3.1 signifies the diffraction pattern for AEAlBS glass, which shows a broad hump lacking of sharp crystalline patterns. The absence of sharp crystalline peaks with a broad hump evidences the amorphous characteristics of the as prepared AEAlBS glass.

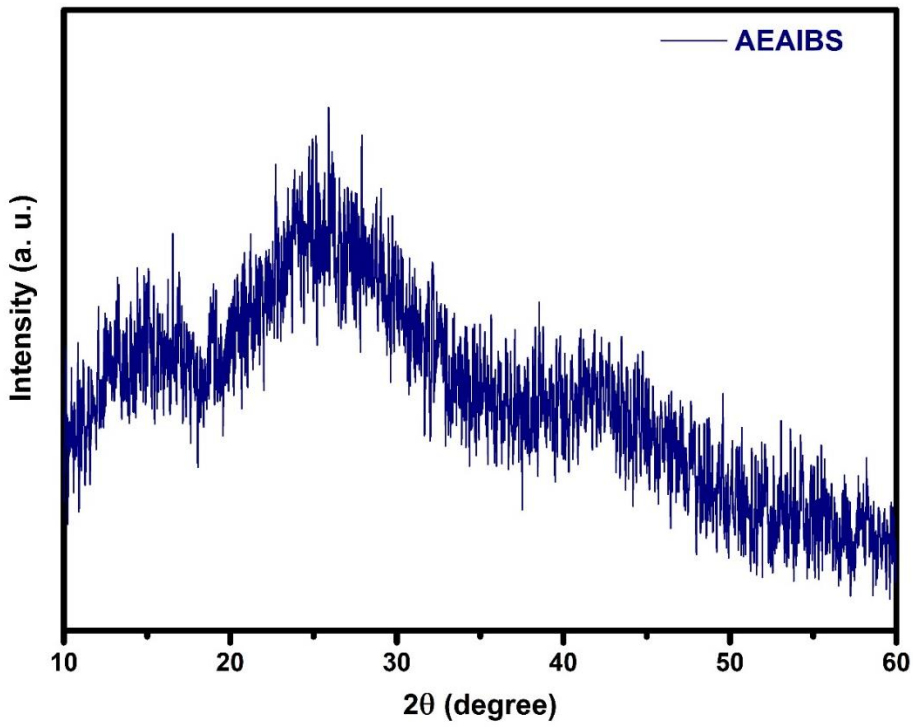

Fig. 3.1: *XRD pattern of an undoped AEAlBS glass.*

3.3.2. PL characteristics of single Sm^{3+} ions doped AEAlBS glasses

The PL excitation spectrum recorded for BSG:0.1Sm glass under λ_{em} = 599 nm wavelength is shown in Fig. 3.2. The PL excitation spectra comprise a number of peaks attributed to the $4f - 4f$ transition of Sm^{3+} ions in the range from 300 to 500 nm. The dominant excitation peak was due to $^6H_{5/2} \rightarrow {}^4F_{7/2}$ transition pertaining to Sm^{3+} ions observed at 402 nm wavelength. The other remaining excitations were observed at 316, 342, 360, 373, 416, 438, 448 and 477 nm pertaining to the transitions from $^6H_{5/2}$ to numerous levels as depicted in Fig. 3.2 [98,99]. The result signifying that the as prepared Sm^{3+} doped AEAlBS glasses were effectively excited via n-UV LED chips effectively. In Fig. 2, orange-red solid line represents the PL emission profile observed for BSG:0.1Sm at λ_{ex} = 402 nm. The PL emission profile contains four peaks observed at 561, 599, 645 and 712 nm pertaining to the transition from $^4G_{5/2}$ level to various lower levels as depicted in Fig. 2. A transition observed at 561 nm ($^4G_{5/2} \rightarrow {}^6H_{5/2}$)

was due to magnetic dipole and another one observed at 645 nm ($^4G_{5/2} \rightarrow {}^6H_{9/2}$) was owing to forced electric dipole in nature. Whereas the transition $^4G_{5/2} \rightarrow {}^6H_{7/2}$ observed at 599 nm is owing to both forced electric as well as magnetic in nature as per the selection rules [89,100]. In Sm^{3+} ions doped AEAlBS glass, the forced electric transition is less intense as compared with magnetic dipole transition, which endorses that the Sm^{3+} can placed in more symmetric sites.

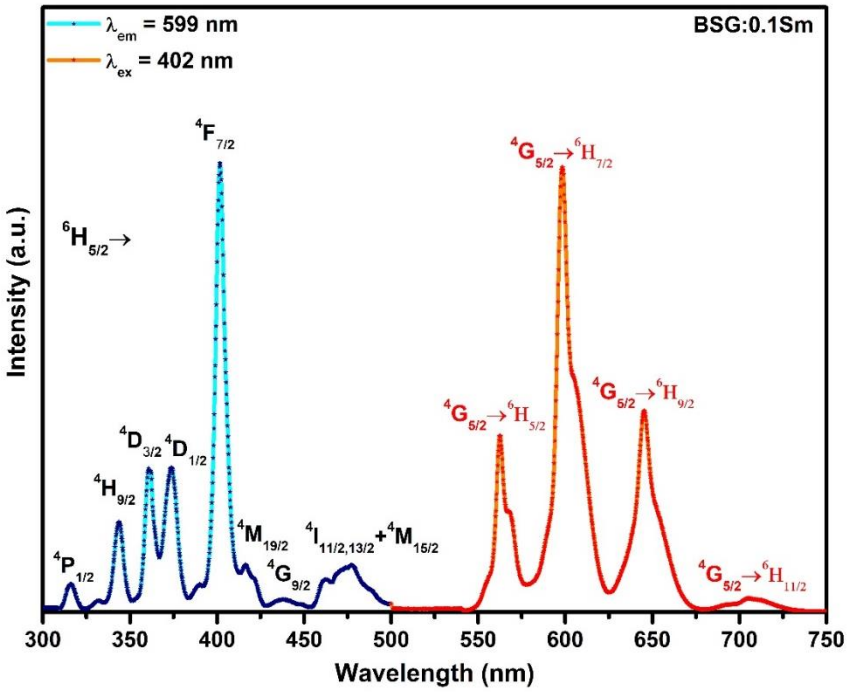

Fig. 3.2: PL excitation & PL emission spectrum of BSG:0.1Sm glass at λ_{em} = 599 and λ_{ex} = 402 nm, respectively.

On the way to optimize Sm^{3+} ion concentration in AEAlBS glasses, the Sm^{3+} ion concentration has been varied from 0.1 to 2.0 mol%. Fig. 3.3 signify the emission spectra for Sm^{3+} ions doped (0.10 to 2.0 mol%) AEAlBS glasses under λ_{ex} = 402 nm. As shown in Fig. 3.3, the intensity of the emission peaks surges up to 0.5 mol% of Sm^{3+} ion concentration and beyond diminishing due to concentration quenching resulted from non-radiative relaxations. The same thing has been depicted in the inset of Fig. 3. When the Sm^{3+} ions concentration was < 0.5 mol %, it can work as an isolated activator ion owing to faraway with nearest doping ions. As the

concentration of the Sm^{3+} ions increase, the distance of separation between the Sm^{3+} ions decrease and this will enhance the possibility of energy transfer among Sm^{3+} ions. This kind of non-radiative energy transfer from an excited Sm^{3+} ions (donors) to a nearby un-excited Sm^{3+} ions (acceptors) start occurring at 0.5 mol% of Sm^{3+} ion concentration in AEAlBS glasses and continues more aggressively beyond 0.5 mol% [101]. Finally, the PL emission investigations conducted on single Sm^{3+} ions doped AEAlBS glasses reveals the optimum concentration of Sm^{3+} ions in AEAlBS glass as 0.5 mol%.

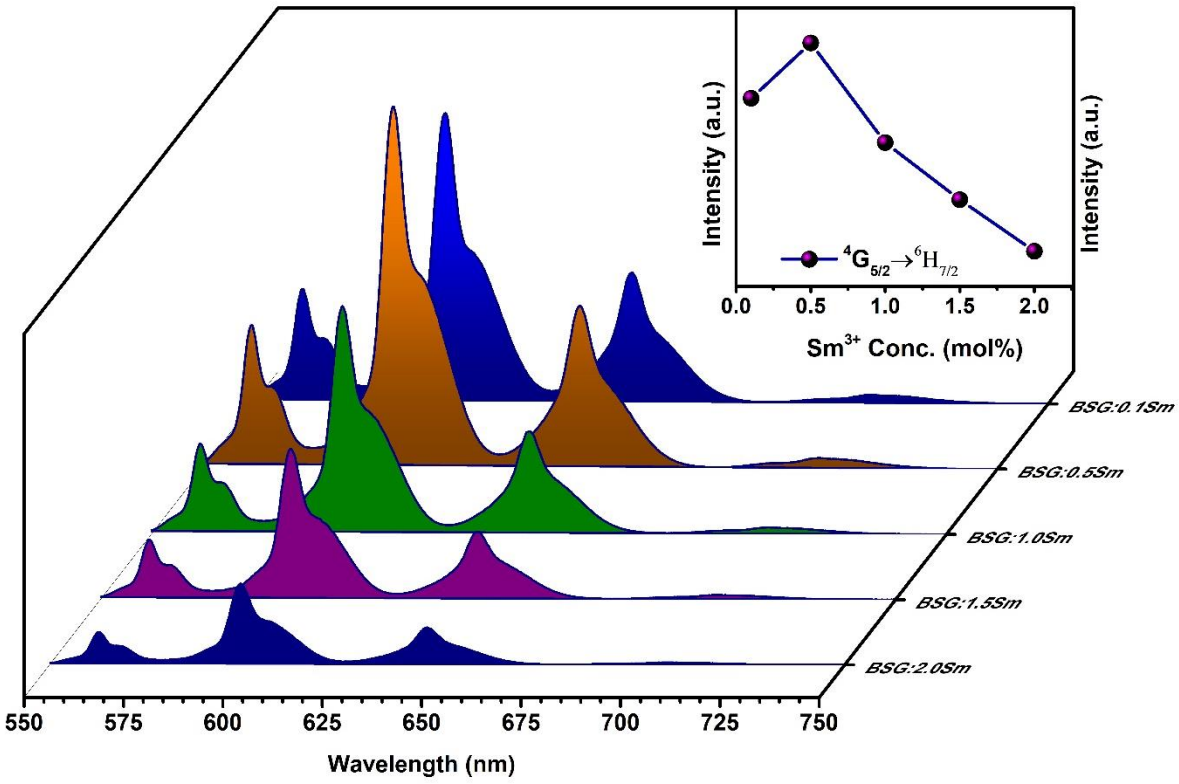

Fig. 3.3: PL emission spectra of Sm^{3+} ions doped AEAlBS glasses at λ_{ex} = 402 nm. Inset plot represents the change in PL emission intensity corresponding to $^4G_{5/2} \rightarrow {}^6H_{7/2}$ transition with Sm^{3+} ions concentration in AEAlBS glasses.

3.3.3. PL characteristics of single Eu^{3+} ions doped AEAlBS glasses

The PL excitation spectrum of BSG:0.5Eu^{3+} glass was recorded by monitoring λ_{em} = 613 nm as existing in Fig. 3.4. The PL excitation spectrum consists several sharp peaks in 300 to 500 nm range. The observed peaks at placed at 316, 361, 381, 392, 416 and 464 nm wavelength pertaining to the transitions $^7F_0 \rightarrow {}^5H_6$, $^7F_0 \rightarrow {}^5D_4$, $^7F_0 \rightarrow {}^5L_7$, $^7F_0 \rightarrow {}^5L_6$, $^7F_0 \rightarrow {}^5D_3$ and $^7F_0 \rightarrow {}^5D_2$, respectively [102,103]. The most intense PL excitation was placed at 392 nm attributed to the $^7F_0 \rightarrow {}^5L_6$ transition of Eu^{3+} ions. In Fig. 3.4, red line represents the PL emission profile observed for BSG:0.5Eu at λ_{ex} = 392 nm. The PL emission spectrum exhibit several sharp peaks at 581, 593, 613, 652, and 699 nm ascribed to $^5D_0 \rightarrow {}^7F_0$, $^5D_0 \rightarrow {}^7F_1$, $^5D_0 \rightarrow {}^7F_2$, $^5D_0 \rightarrow {}^7F_3$, and $^5D_0 \rightarrow {}^7F_4$ transitions respectively [104,105]. The emission peak transition $^5D_0 \rightarrow {}^7F_1$ and $^5D_0 \rightarrow {}^7F_2$ characterize as magnetic dipole and forced electric dipole transition, respectively [105]. The most intense PL emission peak was placed at 613 nm attributed to $^5D_0 \rightarrow {}^7F_2$ transition of Eu^{3+} ions.

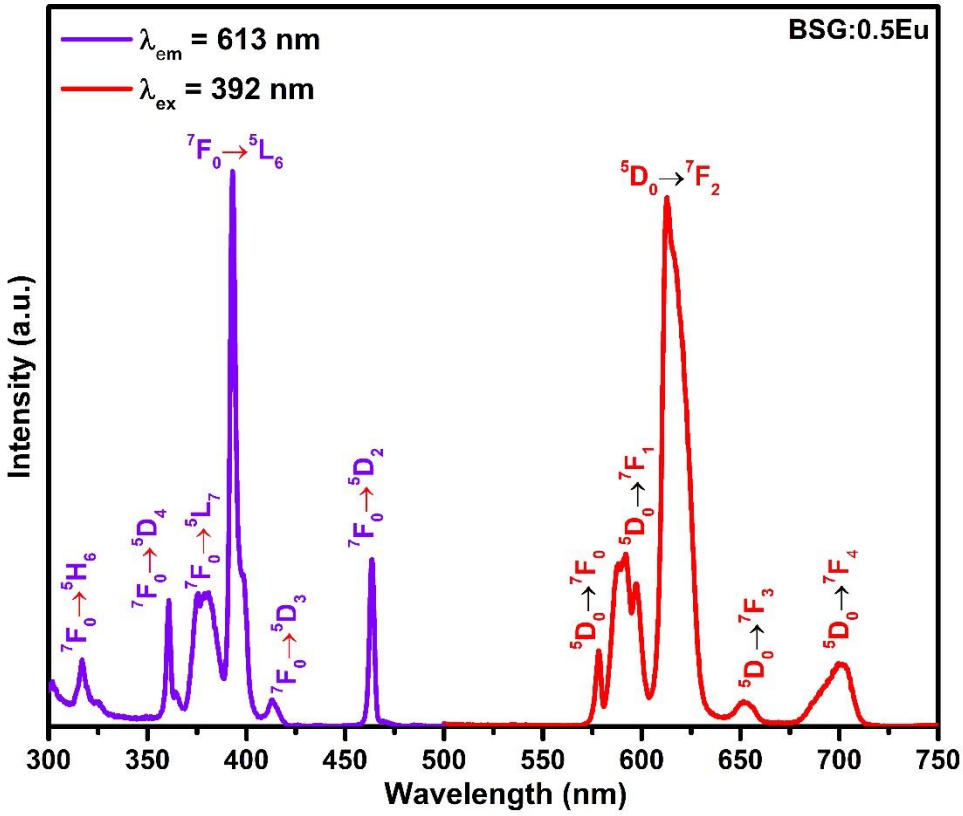

Fig. 3.4: PL excitation & emission spectrum of BSG:0.5Eu glass at λ_{em} = 613 and λ_{ex} = 392 nm, respectively.

3.3.4. PL emission characteristics of Sm^{3+}/Eu^{3+} co-doped AEAlBS glasses

PL excitation spectra for BSG:0.5Sm0.5Eu were recorded with monitoring excitation wavelength at 599 (pertaining to Sm) and 613 nm (pertaining to Eu). Fig. 3.5 represent the PL excitation spectra for BSG:0.5Sm0.5Eu at λ_{em} = 599 nm, which was similar to that observed for single Sm^{3+} doped AEAlBS glass. The observed peaks were centered at 316, 342, 360, 373, 402, 416, 438, 448 and 477 nm as deliberated earlier. When excitation spectrum was recorded for BSG:0.5Sm0.5Eu glass monitoring λ_{em} = 613 nm, a number of peaks were observed in 300

to 500 nm range related to Eu^{3+} along with Sm^{3+} ions present in the co-doped AEAlBS glass. The excitation peaks observed at 342, 402, 437 and 477 nm were related with Sm^{3+} as deliberated earlier, and the other peaks present at 320, 358, 383 392 and 464 nm were accredited to ($^7F_0 \rightarrow {}^5H_6$), ($^7F_0 \rightarrow {}^5D_4$), ($^7F_0 \rightarrow {}^5L_7$), ($^7F_0 \rightarrow {}^5L_6$) and ($^7F_0 \rightarrow {}^5D_2$) transitions of Eu^{3+} ions, respectively [13]. From the excitation spectra shown in Fig. 3.5, it is conspicuous that, Sm^{3+} ions (through its λ_{em}= 599 nm) are also competent enough along with Eu^{3+} ions (through its λ_{em} = 613 nm) to contribute for the emission related to Eu^{3+} ions in AEAlBS glasses.

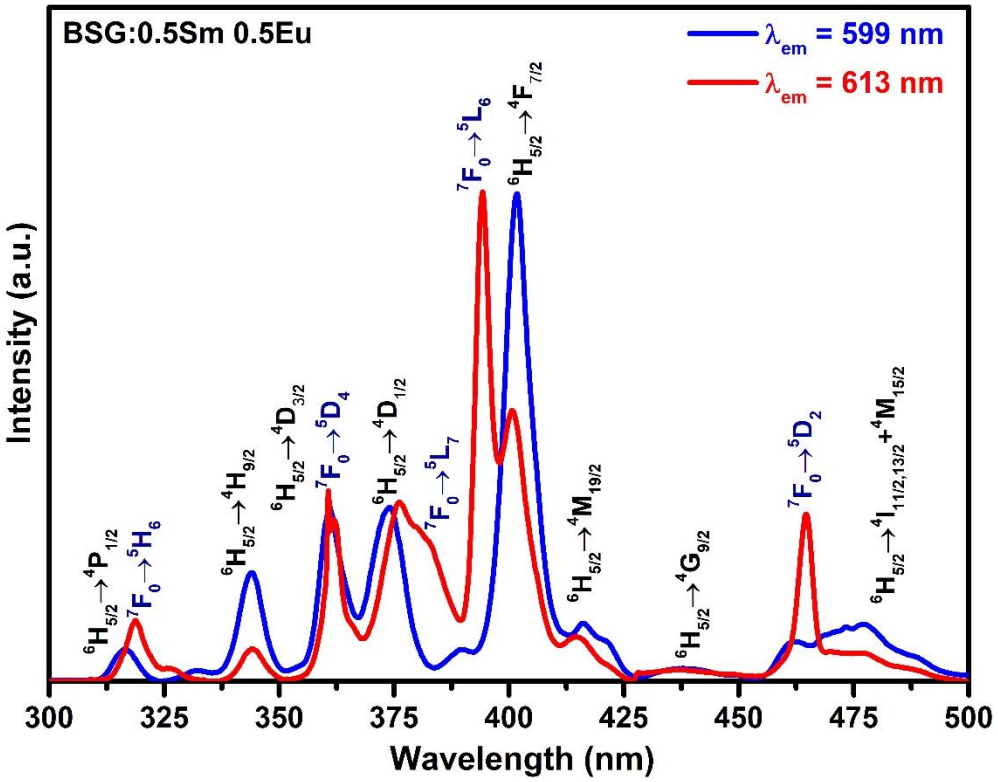

Fig. 3.5: PL excitation spectra of BSG:0.5Sm0.5Eu glass at λ_{em} = 599 and 612 nm**.**

The PL emission spectra pertaining to a series of Sm^{3+} & Eu^{3+} co-doped AEAlBS gasses with fixed Sm^{3+} concentration (x = 0.5 mol%) and varied Eu^{3+} concentration (y = 0.0, 0.1, 0.5, 1.0, 1.5 & 2.0 mol%) has been depicted in Fig. 3.6 under λ_{ex} = 402 nm (pertaining to Sm^{3+} ions).

The PL spectra include numerous peaks in 550-725 nm range under λ_{ex} = 402 nm for BSG:0.5Sm, which are attributed to $f-f$ transitions of Sm^{3+} ions. When Eu^{3+} ion concentration increases from y = 0.0 mol% to above, a number of new emission peaks arise owing to Eu^{3+} ions. These new peaks were centered at 578, 592, 613 and 700 nm attributed to ($^5D_0 \rightarrow {}^7F_0$), ($^5D_0 \rightarrow {}^7F_1$), ($^5D_0 \rightarrow {}^7F_2$) and ($^5D_0 \rightarrow {}^7F_4$) transitions related with Eu^{3+} ions respectively [85,106]. With gradual increase in Eu^{3+} ion concentration, the intensity of emission peaks pertaining to Eu^{3+} ions increase whereas the intensity of peaks pertaining to Sm^{3+} ions decrease simultaneously in the co-doped AEAlBS glasses. As the 402 nm wavelength is specific excitation peaks owing to ($^6H_{5/2} \rightarrow {}^4F_{7/2}$) transition related with Sm^{3+}, and observed PL result suggest that the part of excitation energy of sensitizer Sm^{3+} can transfer to the activator Eu^{3+} ions. Also, the plot in Fig. 3.7 represents the decrease in intensity of ($^4G_{5/2} \rightarrow {}^6H_{7/2}$) transition and increase in the intensity of ($^5D_0 \rightarrow {}^7F_2$) transition with surge of Eu^{3+} concentration in AEAlBS gasses at λ_{ex} = 402 nm. This outcome discloses that Sm^{3+} ions sensitize Eu^{3+} ions and by this means gives visible emission. The emission spectra evidently indorse that the part of ET form Sm^{3+} to Eu^{3+} ions and gives radiative emission.

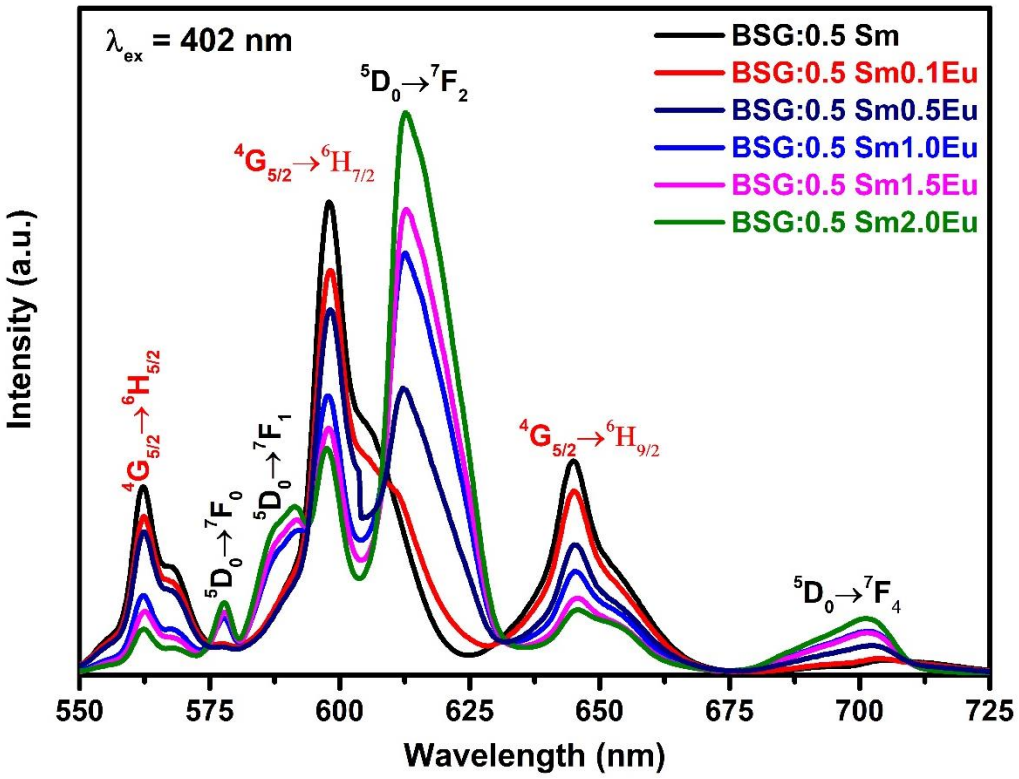

Fig. 3.6: PL emission spectra of BSG:0.5Sm, BSG:0.5Sm0.1Eu, BSG:0.5Sm0.5Eu, BSG:0.5Sm1.0Eu, BSG:0.5Sm1.5Eu and BSG:0.5Sm2.0Eu glasses at λ_{ex} = 402 nm.

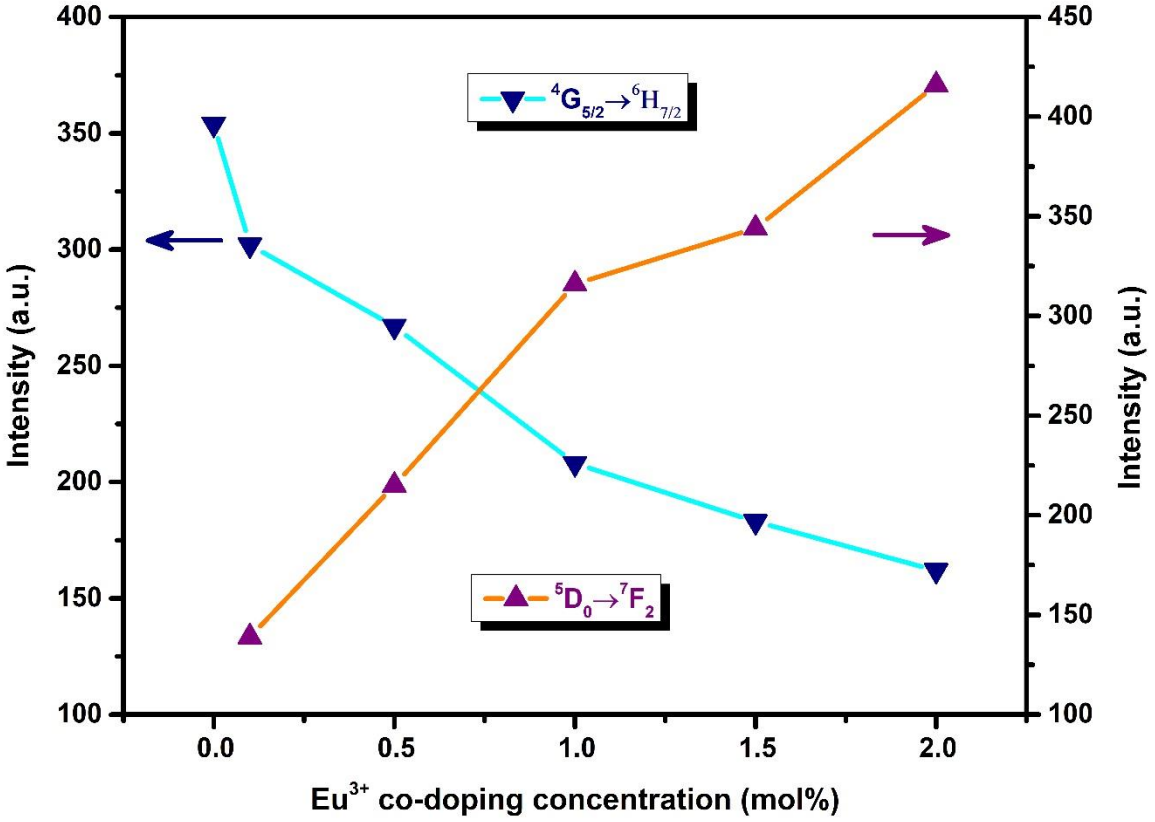

Fig. 3.7: The change in emission intensity corresponding to $^4G_{5/2} \rightarrow {}^6H_{7/2}$ and $^5D_0 \rightarrow {}^7F_2$ transition with co-doping concentration of Eu^{3+} ions in AEAlBS glasses.

The PL spectra for the Sm^{3+} & Eu^{3+} co-doped AEAlBS gasses have been recorded at λ_{ex} = 392 nm, as showing in Fig. 3.8. The PL spectra comprise a number of emission peaks at 578, 592, 613, 652 and 700 nm due to ($^5D_0 \rightarrow {}^7F_0$), ($^5D_0 \rightarrow {}^7F_1$), ($^5D_0 \rightarrow {}^7F_2$), ($^5D_0 \rightarrow {}^7F_3$) and ($^5D_0 \rightarrow {}^7F_4$) transitions of Eu^{3+} ions respectively, while the emission peaks associated to Sm^{3+} ions was absent [85]. These emission peaks were enhanced with surge in Eu^{3+} concentration in Sm^{3+}/Eu^{3+} co-doped AEAlBS gases. The absence of Sm^{3+} ions emission peaks can be due to 392 nm excitation, which is distinctive excitation wavelength of Eu^{3+} ion. The PL spectra for the co-doped gasses at λ_{ex} = 402 nm as well as λ_{ex} = 392 nm reveals that the Sm^{3+} act as an effective sensitizer for Eu^{3+} activator ions and part of ET to the Eu^{3+}, but not vice versa.

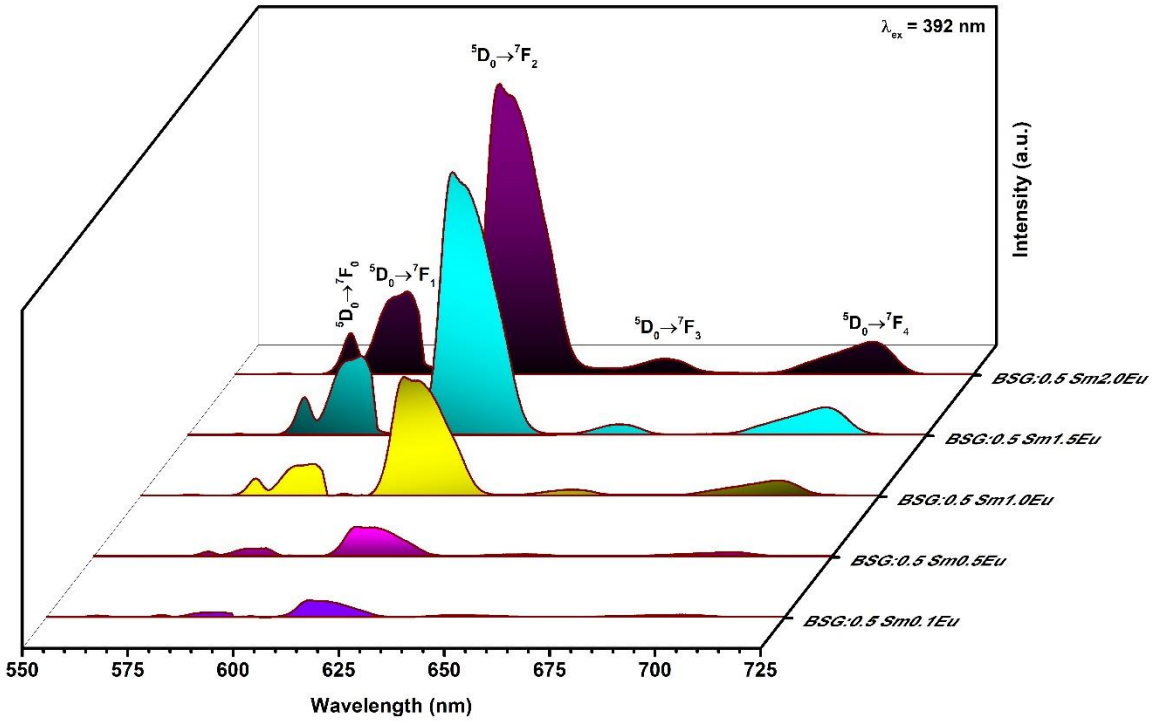

Fig. 3.8: PL emission spectra of BSG:0.5Sm0.1Eu, BSG:0.5Sm0.5Eu, BSG:0.5Sm1.0Eu, BSG:0.5Sm1.5Eu and BSG:0.5Sm2.0Eu glasses at λ_{ex} = 392 nm.

The combine energy level diagram of Sm^{3+}/Eu^{3+} ions can be clarifying the ET process as presented in Fig.3.9. The prepared co-doped glasses were pumped via near-UV excitation (402 & 392 nm). The excited electron transfers ground to respective excited sate and after certain period returns back via releasing radiative emission with some non-radiative relaxation as mentioned in Fig. 3.9. The lowest excited level for Sm^{3+} ion is $^4G_{5/2}$ having energy ~17,924 cm^{-1} and lowest excited energy level of Eu^{3+} ion is $^5D_0$ with energy ~17,277 cm^{-1}. The energy variance in between the above mentioned two energy states is very less ~647 cm^{-1} [107,108]. Hence, part of energy from $^4G_{5/2}$ level of Sm^{3+} ion was drifted to $^5D_0$ levels of Eu^{3+} ions. The outcome clearly agrees that Sm^{3+} ion functioned as a sensitizer and transfer the energy to the

Eu^{3+} activator ion in AEAlBS gasses. The ET mechanism mostly through exchange or multipolar interaction between the nearest lanthanide's ions. The type of multipolar interaction between lanthanide ions was recognized with help of Dexter's ET formula along with Reisfeld's approximation relation as follows [109,110]:

$$\frac{\eta_0}{\eta} \propto C^{n/3}$$

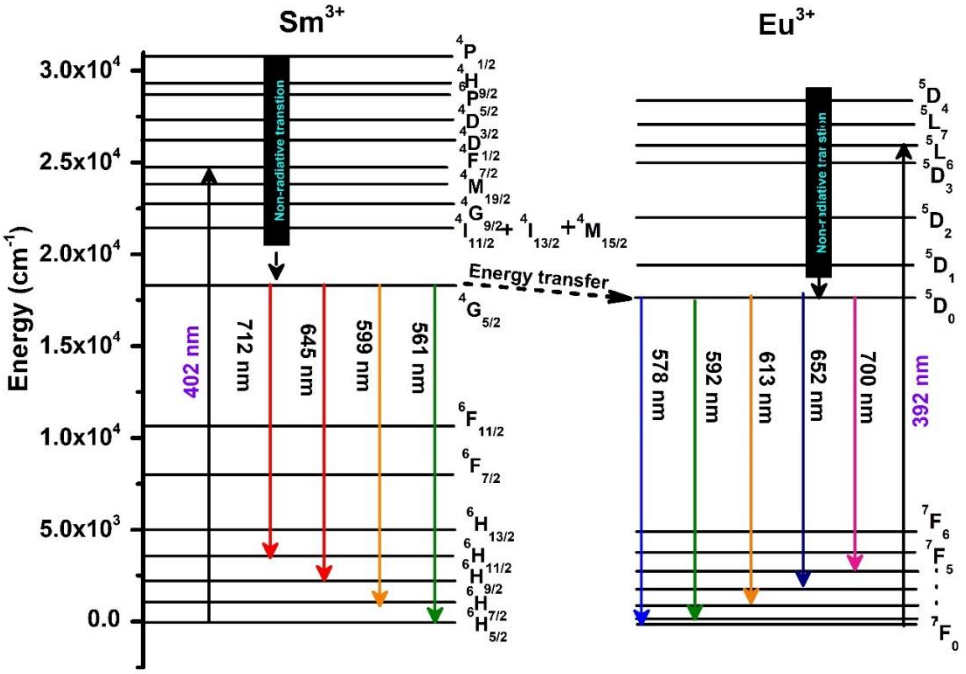

Fig. 3.9: Partial energy level diagram of Sm^{3+} and Eu^{3+} ions in AEAlBS glass with excitation, emission, and energy transfer.

in above relation η_0 and η signify the luminescence efficiency of Sm^{3+} in non-appearance and appearances of activator in AEAlBS gasses. C denotes the sum of the doping concertation of Sm^{3+} and Eu^{3+} ions. The estimated value of *n*, which defines the type multipolar interaction in AEAlBS gasses having n values equal to 6, 8 and 10 for dipole-dipole, dipole-quadrupole, and

quadrupole-quadrupole interaction, respectively. The η_0/η ratio related the ratio of emission intensities as bellow [108]:

$$\frac{I_{SO}}{I_S} \propto C^{n/3}$$

where I_{SO} signifies the ($^4G_{5/2} \rightarrow {}^6H_{7/2}$) emission intensity of single Sm^{3+} doped AEAlBS gasses and I_S denotes the ($^4G_{5/2} \rightarrow {}^6H_{7/2}$) intensity of Sm^{3+}/Eu^{3+} co-doped AEAlBS gasses. Fig.3.10. represents the I_{SO}/I_S versus $C^{n/3}$ plot at λ_{ex} = 402 nm. The best linear fitting was observed for n = 6, which reveals that the dipole-dipole nature of ET between the sensitizer (Sm^{3+}) to activator (Eu^{3+}) ions.

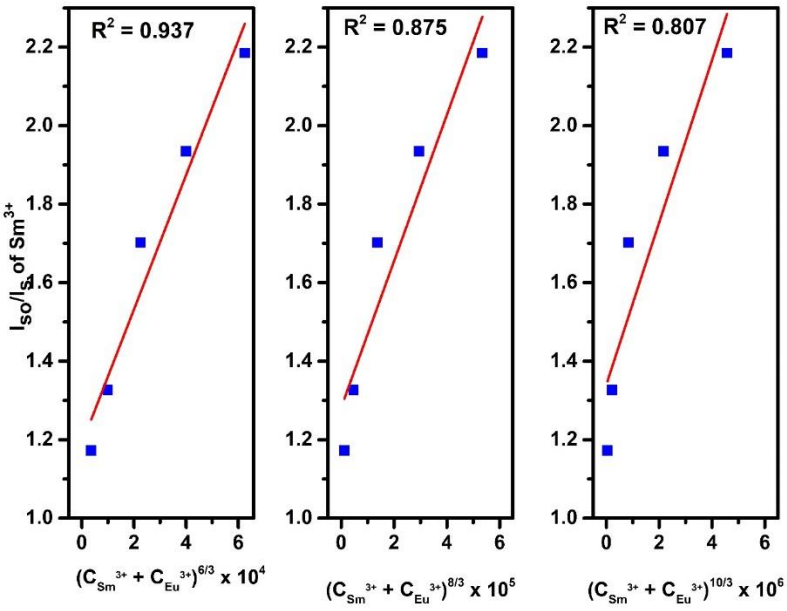

Fig. 3.10: Plot between I_{SO}/I_S for Sm^{3+} versus (a) $(C_{Dy+Eu})^{6/3}$, (b) $(C_{Dy+Eu})^{8/3}$ and (c) $(C_{Dy+Eu})^{10/3}$.

3.3.5. Commission Internationale dEclairage (CIE) chromaticity color coordinates

The CIE coordinates have been estimated based on the recorded the PL spectra at λ_{ex} = 402 nm. The CIE chromaticity color coordinates were enclosed in Table 3.1, also present in Fig. 3.11. The estimated CIE color coordinates for BSG:0.5Sm situated in orange region, which were nearest with the Nichia corporation developed amber LED [111,112].

Table 3.1: CIE color coordinates (*x, y*), CCT (K), PL decay time (ms), Sm^{3+} to Eu^{3+} energy transfer efficiency of Sm^{3+}/Eu^{3+} co-doped AEAlBS glasses at λ_{ex} = 402 and λ_{em} = 599 nm.

Sample name	CIE coordinates (*x, y*)	CCT Value (K)	PL decay time (ms)	Energy transfer efficiency η_T (%)
BSG:0.5Sm	(0.589, 0.408)	1720.58	1.583	0.00
BSG:0.5Sm0.1Eu	(0.587, 0.409)	1739.28	1.461	7.73
BSG:0.5Sm0.5Eu	(0.599, 0.397)	1743.42	1.394	11.94
BSG:0.5Sm1.0Eu	(0.624, 0.374)	1898.51	1.317	16.85
BSG:0.5Sm1.5Eu	(0.629, 0.369)	1988.10	1.281	18.96
BSG:0.5Sm2.0Eu	(0.632, 0.365)	2058.88	1.231	22.21

The CIE chromaticity color coordinates were tuned toward the red region as the Eu^{3+} concentration surge from 0.0 to 2.0 mol% in the co-doped AEAlBS glasses. Fig. 3.11 clearly signifies the change in CIE coordinates with co-doping. The correlated color temperature (CCT) was estimated empirically on basis of equation:

$$CCT = -437\left[\frac{x-x_e}{y-y_e}\right]^3 + 3601\left[\frac{x-x_e}{y-y_e}\right]^2 - 6861\left[\frac{x-x_e}{y-y_e}\right] + 5514.31$$

expressed by McCamy [62]. In above equation, (x, y) denotes the CIE coordinates for AEAlBS glasses and (x_e, y_e) represent the chromaticity epicenter having values of (0.338, 0.186). The estimated CCT values for Sm^{3+} & Eu^{3+} co-doped AEAlBS glasses were listed in Table 3.2. The outcomes reveal that the Sm^{3+} & Eu^{3+} co-doped AEAlBS glasses possess auspicious characteristics for n-UV pumped, tunable orange red constituent in warm white LEDs.

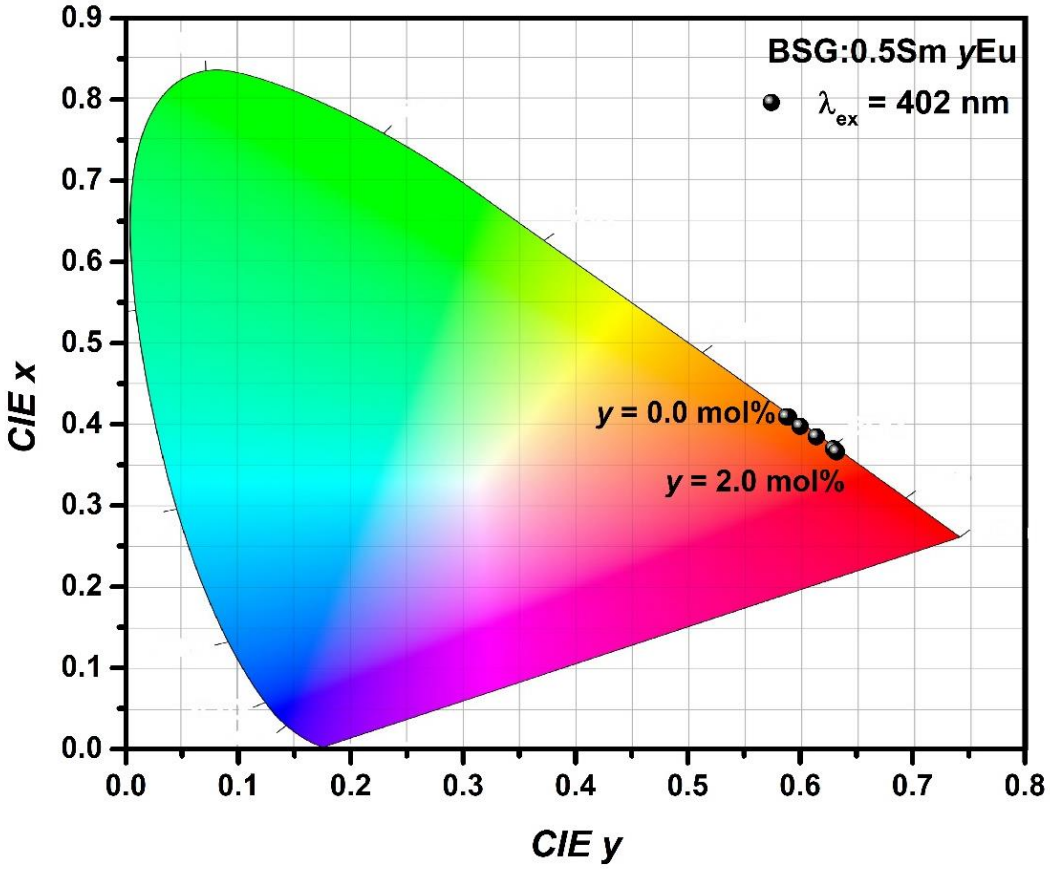

Fig. 3.11: CIE chromaticity coordinates of BSG:0.5Sm*y*Eu glasses (y = 0.1, 0.5, 1.0, 1.5 & 2.0 mol%) at λ_{ex} = 402 nm.

3.3.6. PL decay curve study

PL decay curve for BSG:0.5Sm and Sm^{3+}/Eu^{3+} co-doped AEAlBS gasses have been recorded at λ_{ex} = 402 nm. The decay curves (Fig. 3.12) for BSG:0.5Sm and Sm^{3+}/Eu^{3+} co-doped AEAlBS gasses were recorded and good fitted with bi-exponential expressed as [113,114]:

$$I(t) = I_o + A_1 exp\left(-\frac{t}{\tau_1}\right) + A_2\, exp\left(-\frac{t}{\tau_2}\right)$$

here I_o and *I(t)* express the PL intensity at time 0 second and t second, respectively. τ_1 and τ_2 signifies the slow and fast lifetimes in decay curve, respectively. A_1 and A_2 denotes two fitting constants. The recorded lifetime values for the co-doped glasses are varying with the Eu^{3+} ion co-doping concentration. The experimental lifetimes called as average decay time (τ_{avg}) for prepared glasses were assessed using formula as [115]:

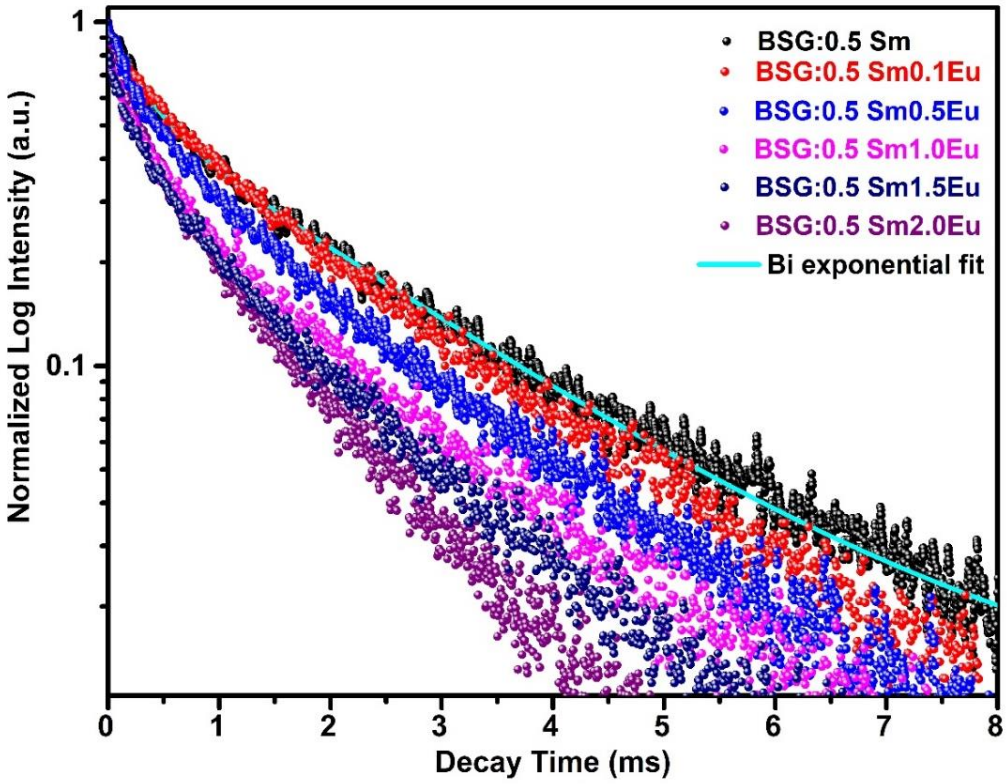

Fig. 3.12: PL decay curves of BSG:0.5Sm, BSG:0.5Sm0.1Eu, BSG:0.5Sm0.5Eu, BSG:0.5Sm1.0Eu, BSG:0.5Sm1.5Eu and BSG:0.5Sm2.0Eu glasses at λ_{ex} = 402 nm.

$$\tau_{avg} = \frac{A_1\tau_1^2 + A_2\tau_2^2}{A_1\tau_1 + A_2\tau_2}$$

τ_{avg} for the glasses have been tabulated in Table 3.2. The τ_{avg} value lessening from 1.583 ms to 1.231 ms when the Eu^{3+} ions concentration increase from y = 0.00 mol% to 2.0 mol%. With surge in Eu^{3+} ion concentration in Sm^{3+}/Eu^{3+} co-doped AEAlBS gasses, the decay accelerates and results in decrease in experimental lifetimes. Faster decay and decrease in lifetime values with surge in Eu^{3+} concentration in co-doped AEAlBS glasses reveals the possible energy transfer from sensitizer to activator. The decrement in τ_{avg} value may be due to the effectively ET from sensitizer Sm^{3+} to activator Eu^{3+} ions in AEAlBS glasses as shown in Fig. 3.13. The

ET efficiency (η_T) form Sm^{3+} to Eu^{3+} ions in co-doped AEAlBS glasses were estimated by using the following equation [116]:

$$\eta_T = 1 - \frac{\tau}{\tau_0}$$

where τ_0 and τ denotes the τ_{avg} value of the single Sm^{3+} doped and Sm^{3+}/Eu^{3+} co-doped AEAlBS glasses, respectively. The η_T are arranged in the Table 3.2. The observed result from Fig. 3.12 clearly specifies that the Sm^{3+} worked as an effective sensitizer for activator Eu^{3+} and ET efficiency increases with co-oping of Eu^{3+} ion concentration. The η_T for BSG:0.5Sm0.1Eu glass was found to be 7.73 % which was tripled as the Eu^{3+} ions concentration surge from *y* = 0.1 to 2.0 mol% in co-doping AEAlBS glasses.

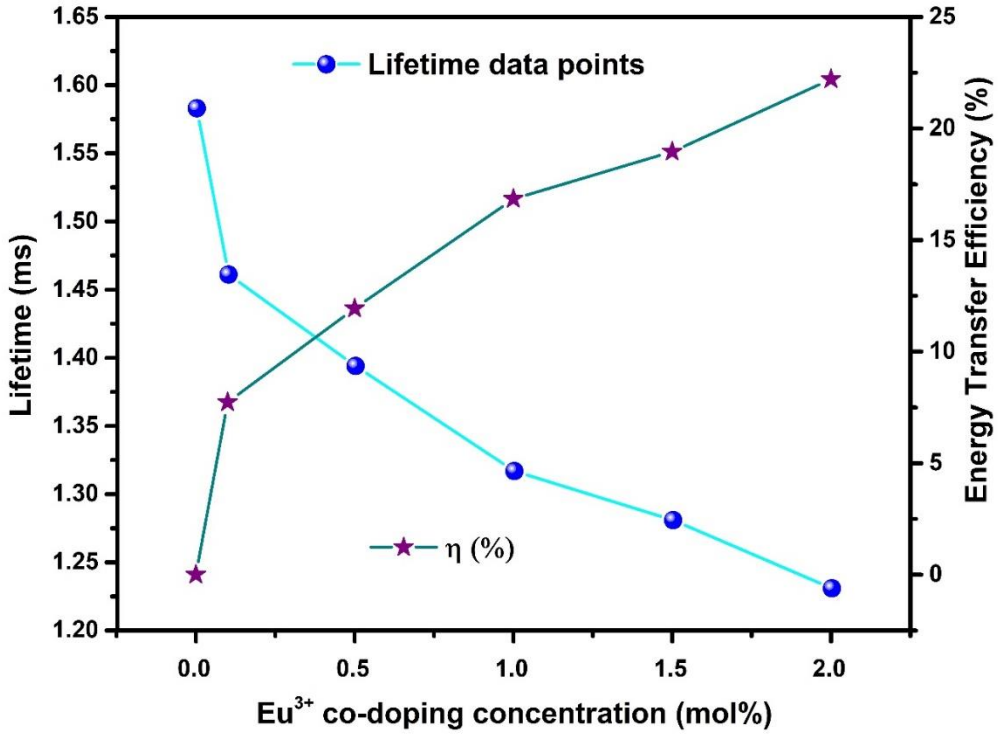

Fig. 3.13: The change in lifetime value and energy transfer efficiency with co-doping concentration of Eu^{3+} ions in AEAlBS glasses.

Additionally, I-H model was applied on the recorded decay curve for BSgG:0.5Sm2.0Eu glasses under the excitation wavelength at λ_{ex} = 402 nm and emission at λ_{em} = 599 nm wavelengths. The type of interaction was examined by employing the I-H model. As per this model, decay curve is given by the equation as follows [80]:

$$I_t = I_0 \exp\{\frac{-t}{\tau_o} - Q\left(\frac{t}{\tau_o}\right)^{\frac{3}{s}}\}$$

in above expression I_t is the PL intensity of the at time t (after excitation time), τ_o the lifetime value for the sensitizer Sm^{3+} ions in the non-appearance of the Eu^{3+}, respectively. Q denotes the energy transfer parameter. In the expression S signify a parameter, which defines the type of multipole interaction having values of S = 6, 8 and 10 designed for dipole-dipole, dipole-quadrupole interaction, quadrupole-quadrupole interactions, respectively [60]. The fitted curve can be seen in Fig. 14 having the parameter value S = 5.36 for BSG:0.5Sm2.0Eu glass. The value of the interaction parameter nearer to 6 reveals the multipolar interaction as dipole-dipole in nature among Sm^{3+} and Eu^{3+} ions. This result observed from I-H model is in consonance with the result composed by Dexter theory applied to the PL emission spectra.

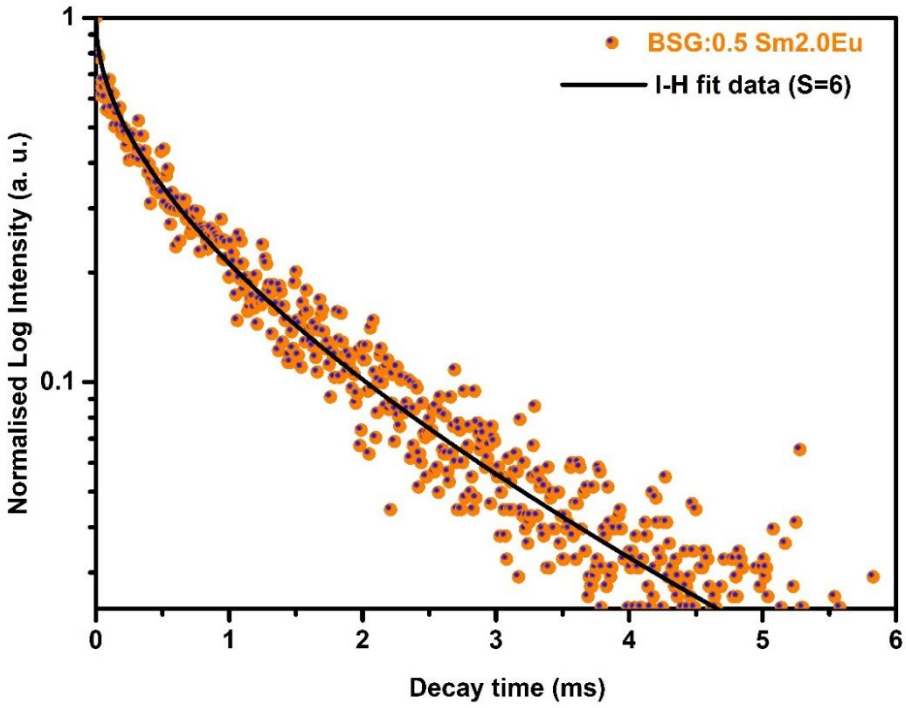

Fig. 3.14: PL decay curves of BSG:0.5Sm2.0Eu glasses with I-H fitting (S = 6) at λ_{ex} = 402 nm.

3.3.7. Temperature effect on PL properties

The temperature-dependent PL spectra for BSG:0.5Sm2.0Eu was recorded under the excitation of λ_{ex} = 402 nm. Fig. 3.15 confirmed that the emission intensity of Sm^{3+}/Eu^{3+} ions was lessened as the temperature enlarged from 27 to 200 °C. The PL intensity of all the peaks reduces with surge in temperature from room temperature to 200 °C. PL intensity drops to 94.34% at 150 °C and 91.30% at 200 °C, which specifies that the as-prepared glasses have excellent thermal stability.

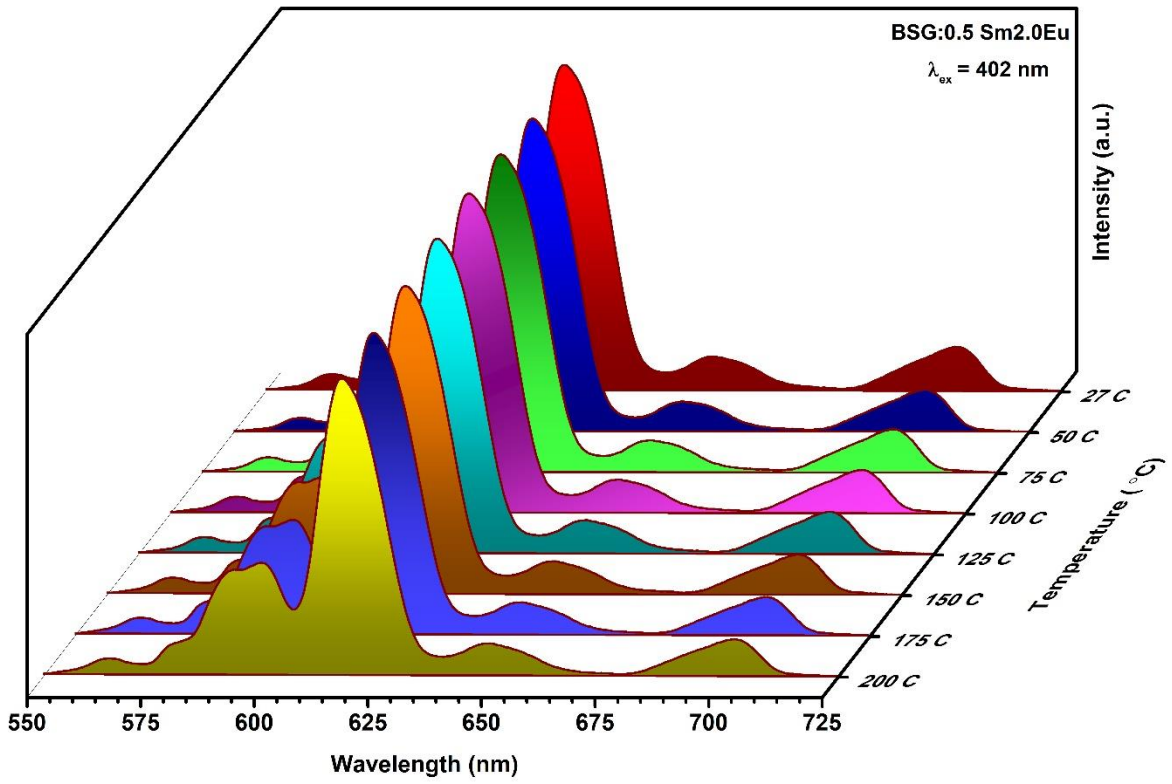

Fig.3.15: Temperature dependent emission spectra of BSG:0.5Sm2.0Eu glass at λ_{ex} = 402 nm.

The activation energy (ΔE_a) was assessed using the expression among the temperature and the luminescence intensity, given by the Arrhenian equation [117]:

$$I_T = \frac{I_0}{1 + C\ exp\left(-\frac{\Delta E}{K_B T}\right)}$$

in the expression I_0 and I_T signify the PL intensity at 27 °C or 300 K and T (K) temperature, respectively. C denotes an arbitrary constant and K_B denotes the Boltzmann constant. The activation energy for the as prepared glass can be estimated from the slope of the linearly fitted $ln((I_0/I_T)-1)$ versus $1/K_BT$ plot as described in Fig. 3.16. The activation energy was estimated to

be 0.139 eV for BSi:0.5Sm2.0Eu glass. Thus, temperature dependent luminescence properties of BSG:0.5Sm2.0Eu glass specify that the as prepared glass exhibits excellent thermal stability.

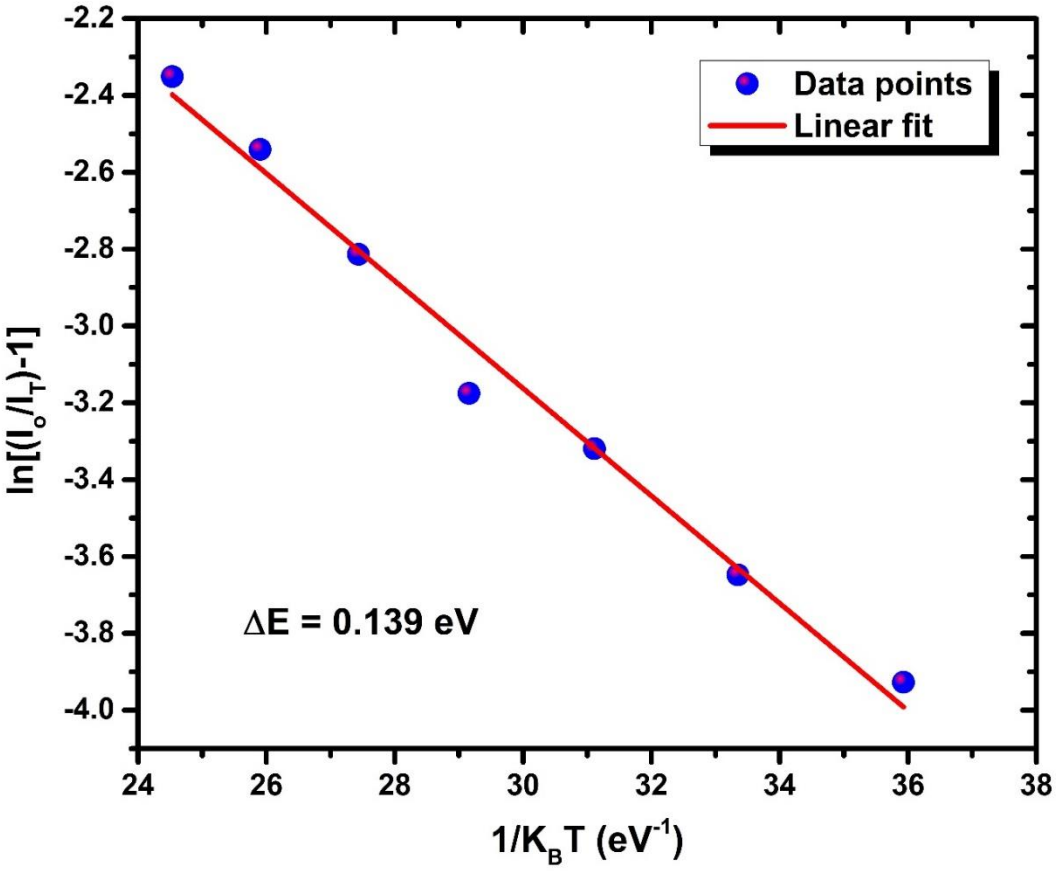

Fig.3.16: $\ln[(I_o/I_T)-1]$ versus $1/K_BT$ plot for BSG:0.5Sm2.0Eu.

3.4. Conclusions

Transparent, amorphous single Sm^{3+} ions doped and concoction of Sm^{3+}/Eu^{3+} ions co-doped AEAlBS glasses have been synthesized via employing melt quenching process and studied their structural, luminescent characteristics to have an insight into their utility in photonic devices applications under near UV excitation. A broad hump observed in XRD reveals the amorphous/ non-crystalline nature of the as prepared undoped AEAlBS glass. The PL spectra under 402 nm excitation exhibit several peaks ascribed to ($^4G_{5/2}\rightarrow{}^6H_{5/2}$),

($^4G_{5/2}\rightarrow{}^6H_{7/2}$), ($^4G_{5/2}\rightarrow{}^6H_{9/2}$) and ($^4G_{5/2}\rightarrow{}^6H_{11/2}$) transitions related with Sm^{3+} ions in AEAlBS glasses. The optimum emission intensity was attained for 0.5 mol% Sm^{3+} ions doped AEAlBS glasses. Sm^{3+} ion works as effective sensitizer for Eu^{3+} activator ion in AEAlBS glasses and part of ET from Sm^{3+} to Eu^{3+} ions. The tunable emission spectra were recorded under 402 excitation wavelengths. The energy transfer between Sm^{3+} to Eu^{3+} in co-doped AEAlBS glasses was proved to be dipole-dipole in nature via employing Dexter's ET formula, Reisfeld's approximation and I-H model on decay curves. The η_T for BSG:0.5Sm glass was found to be 7.73 % which was tripled as the Eu^{3+} ions concentration surged from y = 0.1 to 2.0 mol%. The CIE coordinates for single Sm^{3+} doped glasses fell in orange region, which was change towards red region with surge in co-doping of Eu^{3+} ion in AEAlBS glasses. The lifetime value (λ_{ex} = 402 nm) was reducing with surge in Eu^{3+} ion co-doping concentration, which correspondingly specify the ET from Sm^{3+} to Eu^{3+}. The temperature-dependent emission analysis reveals that the as prepared glasses have excellent thermal stability with ΔE = 0.139 eV. All the results obtained finally contemplate the effective applicability of the as prepared multifunctional orange/red emitting Sm^{3+}/Eu^{3+} co-doped AEAlBS glasses under n-UV excitation.

CHAPTER 4

Intense Green Emitting, Thermally Stable Optical Characteristics of Tb^{3+} Ions Incorporated Bao-SrO-Al_2O_3-B_2O_3-SiO_2 Glasses for Photonic Devices

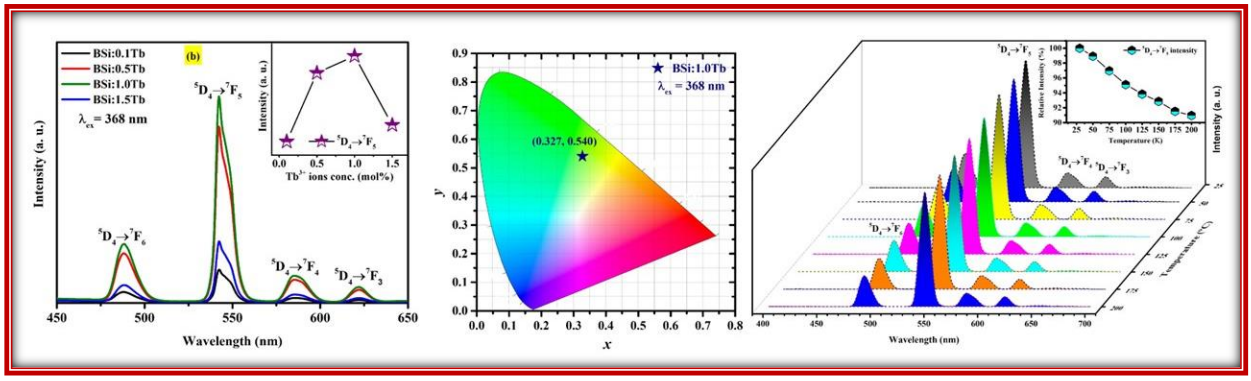

<u>Part of this work has been communicated to an international journal</u>

<u>Optical Materials (2024) (Impact Factor: 3.80)</u>

A series of Tb^{3+} activated transparent barium strontium alumino borosilicate (BaSrAlBSi) glasses were prepared via melt quenching routes and detailed studied their optical characteristics for advanced laser and lighting appliances applications. The diffraction pattern defined the amorphous nature of the prepared transparent BaSrAlBSi glass. The UV visible spectrum shows the various absorption in n-UV visible and NIR range owing to Tb^{3+} ions. BSi:Tb glasses were proficiently near-UV excited, which emits blue, green, yellow and red light corresponding peaks situated at 487, 543, 587 and 623 nm, respectively. The maximum

photoluminescence (PL) emission intensity was observed for 1.0 mol% Tb^{3+} doped BaSrAlBSi glass. Beyond the 1.0 mol% the concentration quenching mechanism was recognized via applying the Dexter theory. The PL lifetimes were showing the decrease in decay time with upsurge in Tb^{3+} content. I-H model was used to identify the type of non-radiative energy mechanism, which is found to be dipole-dipole in nature. TD-PL characteristics demonstrate the very less effect of temperature dependency on PL intensity and shows the good thermal stability of BSi:1.0Tb glass. The observed results anticipate that the direct utility of the as prepared transparent Tb^{3+} doped BaSrAlBSi glasses as n-UV pumped with green emitting constituent for photonic device applications.

4.1. Introduction

In current eras, non-crystalline glass materials activated with trivalent RE ions been considered as most active components in many areas such as industries, advance laser, light, solar cell, optical communications and other photonic devices [118–120]. The utility and applicability and fame of these RE activated glasses was mainly owing to its advantageous properties such as transparency, ease of manufacture process with desired size & shape, higher thermal stability, lower production cost, long life spam etc. [121–124]. Also, the RE activated glass has been a potential wavelength converter for ultra-violet (UV)/ blue pumped white emission in white light emitting diodes (w-LEDs), which can overcome the demerits such as low color rendering index, thermal stability, high correlated color temperature etc. Correspondingly, these RE activated glasses functioned as encapsulant along with wavelength converter. Furthermore, w-LEDs attached with the RE activated glassed doesn't required organic epoxy resin binder and protect from adversely effects on luminous efficiency at high temperatures [124,125].

The desired characteristics of glasses have been mainly depending on glass compositions, such glass formers, modifiers and respective dopants ions. There are variety of inorganic glass host available like borate, germinate, tungstate, phosphate, silicate, borosilicate etc. [9,96]. Among these, the inorganic borosilicate glass can be a potential glass host having own high transparency, less melting temperature, less thermal expansion coefficient, high thermal stability, high corrosive resistant etc. [67,97]. These characteristics were very important for the applicability in numerous areas of current lighting, lasers, solar cells, displays, automation many more. In borosilicate glass host, alkaline earth oxides were considered as an appropriate network modifier, which can enhance the chemical stability, lessen glass structure, significant compaction of the glass network [68]. Furthermore, by adding the metal oxides such as Al_2O_3 functioned as network modifier, which can improve the critical distance, reduces the phonon emission, enhance the mechanical chemical, thermal stability thermal resistance of the host along with radiative emission [17,49]. Based on the characteristics required for glass host, BaO-SrO-Al_2O_3-B_2O_3-SiO_2 (BaSrAlBSi) glass composition selected to synthesize, transparent, thermally mechanically stable glass with exceptional photonic properties, which can directly applicable in optical devices.

Tri/divalent RE ions have a number of energy states and absorbing the spectrum ranges from UV to infrared and emitting in visible as well as IR region via down conversion/up-conversion mechanism, which can applicable in lasers and advanced photonic device [16,126]. In trivalent state RE ions, the incompletely occupied $4f$ elctrons shells protected by 5s2/5p6 orbitals and gives the sharp excitation radiative emission [49,92]. Among these lanthanides, Tb^{3+} ions can effectively absorb near UV/blue light and emits visible green light [61,127,128]. As $^5D_4 \rightarrow {}^7F_5$ transition of Tb^{3+} ion provides the information about the threshold value in a four-level laser system, which can be used for a biological probe owing to sharp emission with long

spontaneous lifetime and good quantum efficiency. Recently, Tb^{3+} activated numerous glass host have been prepared reported for photonic devices applications.

In this research work, a number of Tb^{3+} activated BaSrAlBSi glasse have been prpeared via melt quenching routes with varying the activater concnetration and studied their structural, vibrational, optical charcteriscts in detailed. Absorption, photoluminescence (PL), Commission Internationale dEclairage (CIE) and PL lifetime characteristics have been investigated in detail to appropriateness of the Tb^{3+} activated BaSrAlBSi glass as primary color emitting effetcitve component in laser, w-LEDs and other optical devices.

4.2. Experimental

4.2.1. Preparation of Tb^{3+} activated BaSrAlBSi Glasses

A sequence of Tb^{3+} activated BaSrAlBSi glasses were synthesized via melt quenching method having chemical composition as follows:

$$10\ BaO - 10\ SrO - (10\text{-}m)\ Al_2O_3\text{-}50B_2O_3\text{-}20SiO_2 -: m\ Tb_4O_7$$

in above chemical compositions, Tb^{3+} ions concentration varies as m = 0.1, 0.5, 1.0 and1.5 mol% and synthesized glasses are BSi:0.1Tb, BSi:0.5Tb, BSi:1.0Tb, BSi:1.5Tb & BSi:2.0Tb, respectively.

The precursor $BaCO_3$, $SrCO_3$, Al_2O_3**,** H_3BO_3**,** SiO_2 and Tb_4O_7 chemicals have been used to synthesize Tb^{3+} activated BaSrAlBSi glass. All the precursor chemicals were weighed in desired quantity via using electric balance and ground using the mortar and pestle in acetone medium. After a certain time, the homogeneously grounded mixer was kept in crucible and put in furnace for melting. The furnace temperature swiftly rises from room temperature to 1250°C at 5 °C per minute. After a certain time at 1250°C, powder turns into melting sate and homogeneously melted chemicals were quickly quenched in two heated (300°C) brass plates.

To eliminate the air bubbles stress and prevent thermal shock, the prepared transparent BaSrAlBSi glass was annealed at 350°C for 3.5 hrs. Finally, the Tb^{3+} activated BaSrAlBSi glasses have been prepared for structural, optical and other investigations.

4.2.2. Characterizations of Tb^{3+} activated BaSrAlBSi Glasses

The structural property of the BaSrAlBS glass was been examined by diffraction pattern attained from XRD (Bruker, D8 advance) in $10° \leq 2\theta \geq 60°$ range. FT-IR spectroscopy has been used to identify the various vibrational groups present in the prepared glass. Photoluminescence (PL) characteristics have been obtained via spectrofluorophotometer (Jasco, FP-8300) at room temperature. Spectrofluorophotometer (Edinburgh, FLS920) was used to record PL decay curves. Temperature dependent PL spectra were characterized with setup connected with sample heating assembly, Xenon light source and detector (FLAME-S-XR1-ES, Ocean optics).

4.3. Results and discussion

4.3.1. Diffraction pattern analysis

The diffraction pattern for 1.0 mol% Tb^{3+} activated BaSrAlBSi glass has been recorded as display in Fig. 4.1. The recorded patterns exhibit broad hump with short of any crystalline peaks, which signifies the glassy amorphous nature of Tb^{3+} activated BaSrAlBSi glass.

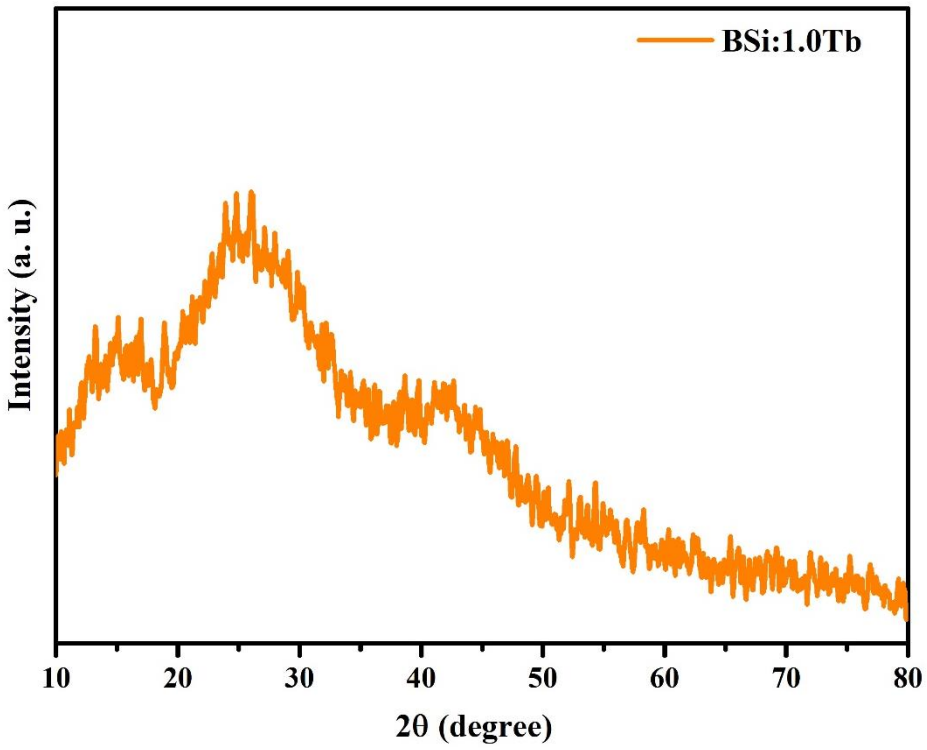

Fig. 4.1: *XRD pattern of 1.0 mol% Tb^{3+} doped BaSrAlBSi glass (BSi:1.0Tb).*

4.3.2. FT-IR analysis

FT-IR spectrum of BSi:1.0Tb glass was recorded in 400-4000 cm^{-1} range at room temperature 27˚C as seen in Fig. 4.2. The observed spectrum contains a number of vibrational peaks situated at 685, 1027, 1241,1371, 2076, 2342, 2932 and 3648 cm^{-1}. The band at 685 may be observed due to bending B-O-B of borate network. A vibration peaks located at 1027 cm^{-1} may be for the reason that of the stretching vibration formed by BO_4 di-borate groups. Asymmetric stretching of B—O bonds related peaks from orthoborate group was situated at 1241 cm^{-1} and vibration at 1371 cm^{-1} is attributed to presence of pyriborate, orthoborate groups containing BO_3 [119,129]. The band observed at 2932 cm^{-1} and 3674 cm^{-1} are observed owing to asymmetric and symmetric vibrations of water molecule presented in KBr and sample pallet.

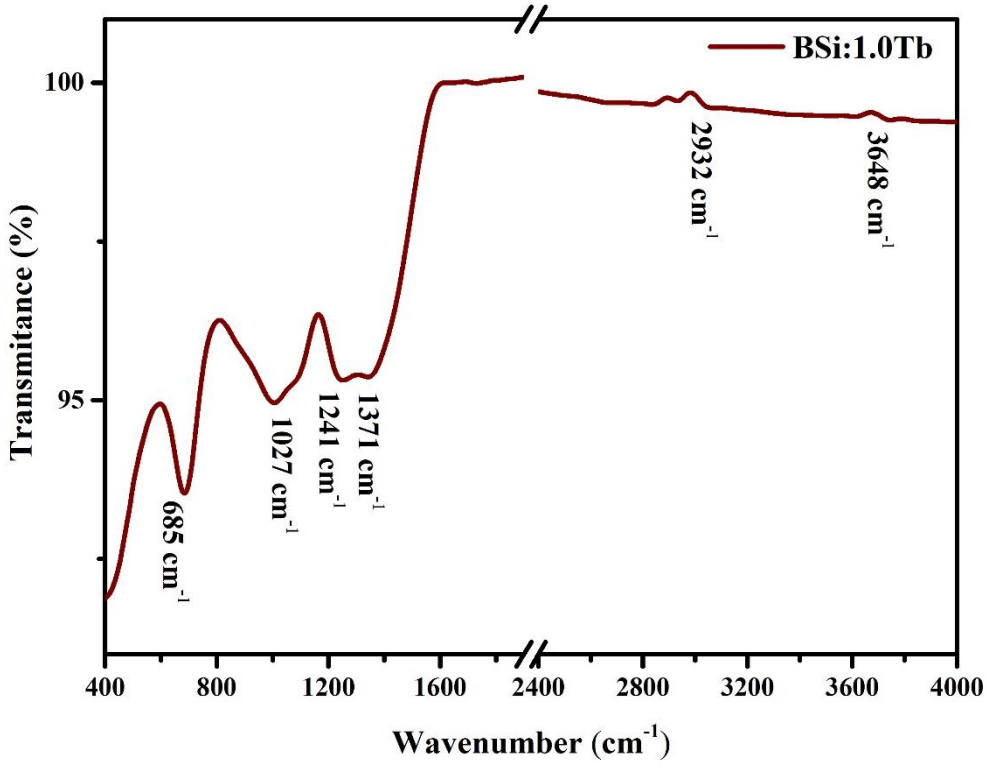

Fig. 4.2: *FT-IR spectrum of BSI:1.0Tb glass.*

4.3.3. UV- vis absorption spectrum analysis

The UV- vis absorption spectrum of the Tb^{3+} activated BaSrAlBSi glass has been recorded as shown in Fig. 4.3. The recorded spectrum comprises several peaks in 300-2500 nm range. The absorption spectra comprise a number of peaks at 370, 486, 1920 and 2210 nm associated to f-f- transitions of Tb^{3+} ions as described in Fig.4.3 [130]. These transitions were related to electric dipole were follow | J|≤ 6 selection rule, on the other hand magnetic dipole transition followed | J |=0, +1 rule. Optical band gap is one of the parameters, which can evaluate using absorption spectrum with the help of the Davis and Mott relation as follows [125]:

$$\alpha(v) = \left(\frac{B}{hv}\right)\left(hv - E_{opt}\right)^{n}$$

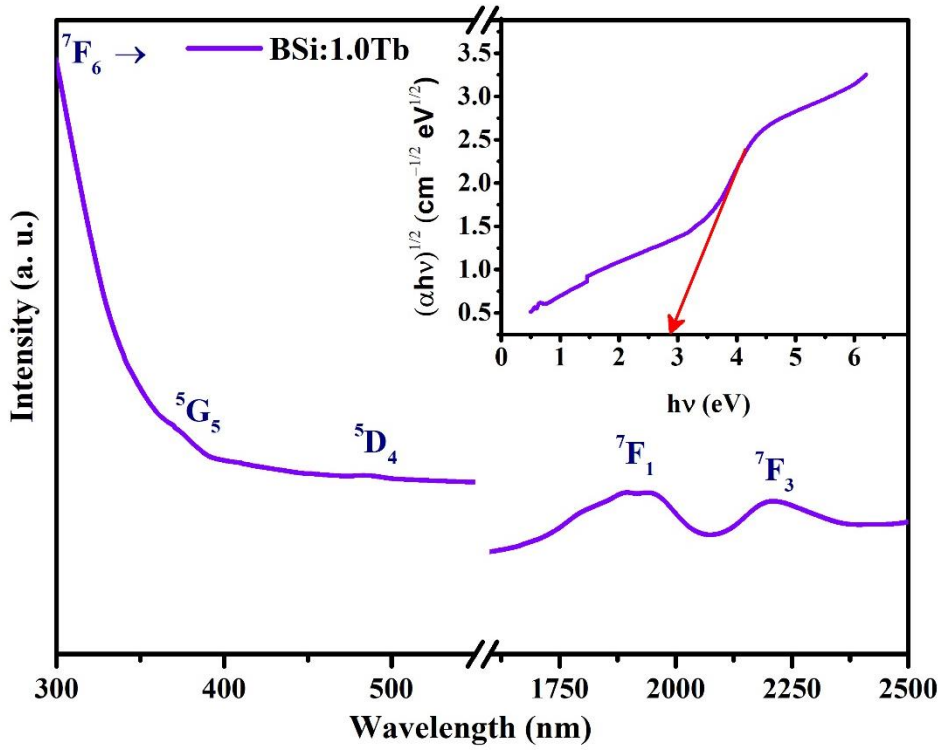

***Fig. 4.3**: UV absorption spectrum of 1.0 mol% Tb^{3+} doped BaSrAlBSi glass. Inset plot shows the indirect optical bandgap Tauc plot for BSi:1.0Tb glass.*

in above equation $h\nu$, E_{opt} and B were photon energy, optical bandgap of glass and band tailing parameter, respectively. n represent a parameter and affirm the type of transition. For indirect allowed transitions value of $n = 2$. The $\alpha(\nu)$ was evaluated using the following equation [131]:

$$\alpha(\nu) = \left(\frac{1}{d}\right) ln\left(\frac{I_0}{I_T}\right)$$

$ln\,(I_0/I_T)$ and d are absorbance and glass thickness, respectively. The E_{opt} value was evaluated via Tauc's plot by extrapolating the linear part as presented in inset of Fig. 4.3. The indirect E_{opt} of BSi:1.0Tb was estimated to be 2.94 eV.

4.3.4. PL Characteristics of Tb^{3+}activated BaSrAlBSi Glasses

The PL characteristics for all the Tb^{3+}activated BaSrAlBSi glasses have been recorded at ambient temperature. The PL excitation spectrum of BSi:1.0TB glass from 300 to 500 nm wavelength range by keeping fix the emission wavelength at 542 nm as visible in Fig. 4. The excitation profile contains a number of excitation peaks in the near ultraviolet (n-UV) and blue region. The experimental excitation peaks situated at 317, 340, 351, 368, 378, and 486 nm were attributed to the transitions from ground level ($^7F_6$) to $^5H_7$ + $^5D_0$, $^5L_7$+ $^5G_3$, $^5L_9$+$^5D_2$, $^5G_6$, $^5G_6$ +$^5D_3$ and $^5D_4$ levels states, respectively. Among all excitation, the peaks at 351, 368 and 378 nm were comparatively higher than the other peaks, which were used as an excitation wavelength (λ_{ex}=351, 368 & 378 nm) to record PL emission characteristics.

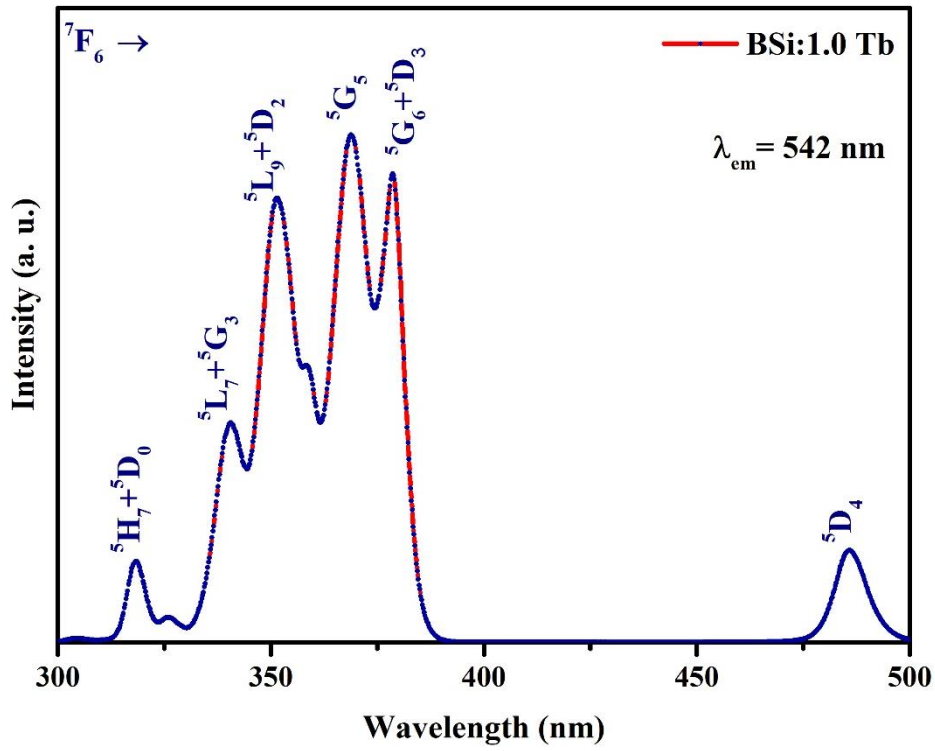

Fig. 4.4: *The excitation spectrum of the BSi:1.0Tb glass by keeping the emission wavelength at 542 nm.*

The emission profiles have been recorded of all the as prepared transparent numerous Tb^{3+} doped BaSrAlBSi glasses under different excitation wavelength as illustrated in Fig.4.5 (a, b & c). The emission profile exhibits four peaks situated at 487, 543, 587, 623 nm corresponding to transitions from $^5D_4$ to various $^7F_{(J = 6, 5, 4 \& 3)}$ energy levels of Tb^{3+} ions. Among the blue, green, yellow and red peaks, the most intense peak is green owing to $^5D_4 \rightarrow {}^7F_5$ transition and follow the Laporte-forbidden selection rule. The second most intense peak is blue peak at 488 due to the $^5D_4 \rightarrow {}^7F_6$ transition, which related the magnetic dipole transition ($\Delta J = \pm 1$). The emission intensity fluctuates with doping concentration as demonstrated from emission profile.

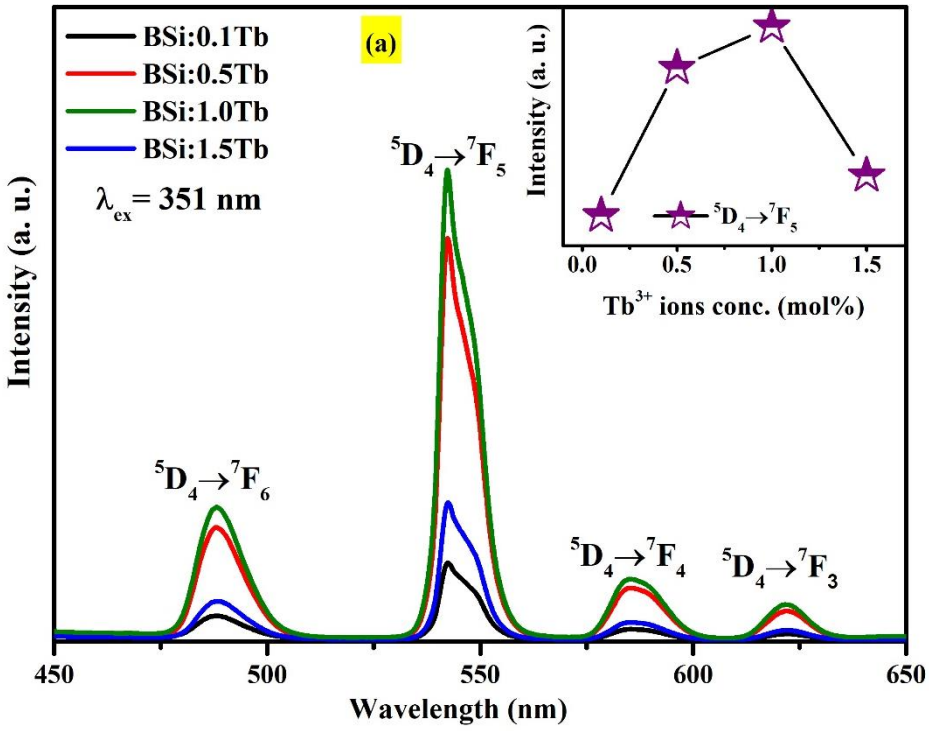

Fig. 4.5: *PL spectra of BaSrAlBSi glass with varying the Tb^{3+} doping concertation from 0.01 to 1.5 mol% at excitations wavelength of (a) 351 nm. The inset image of all plots shows the changes in ($^5D_4 \rightarrow {}^7F_5$) intensity with Tb^{3+} ions concentration.*

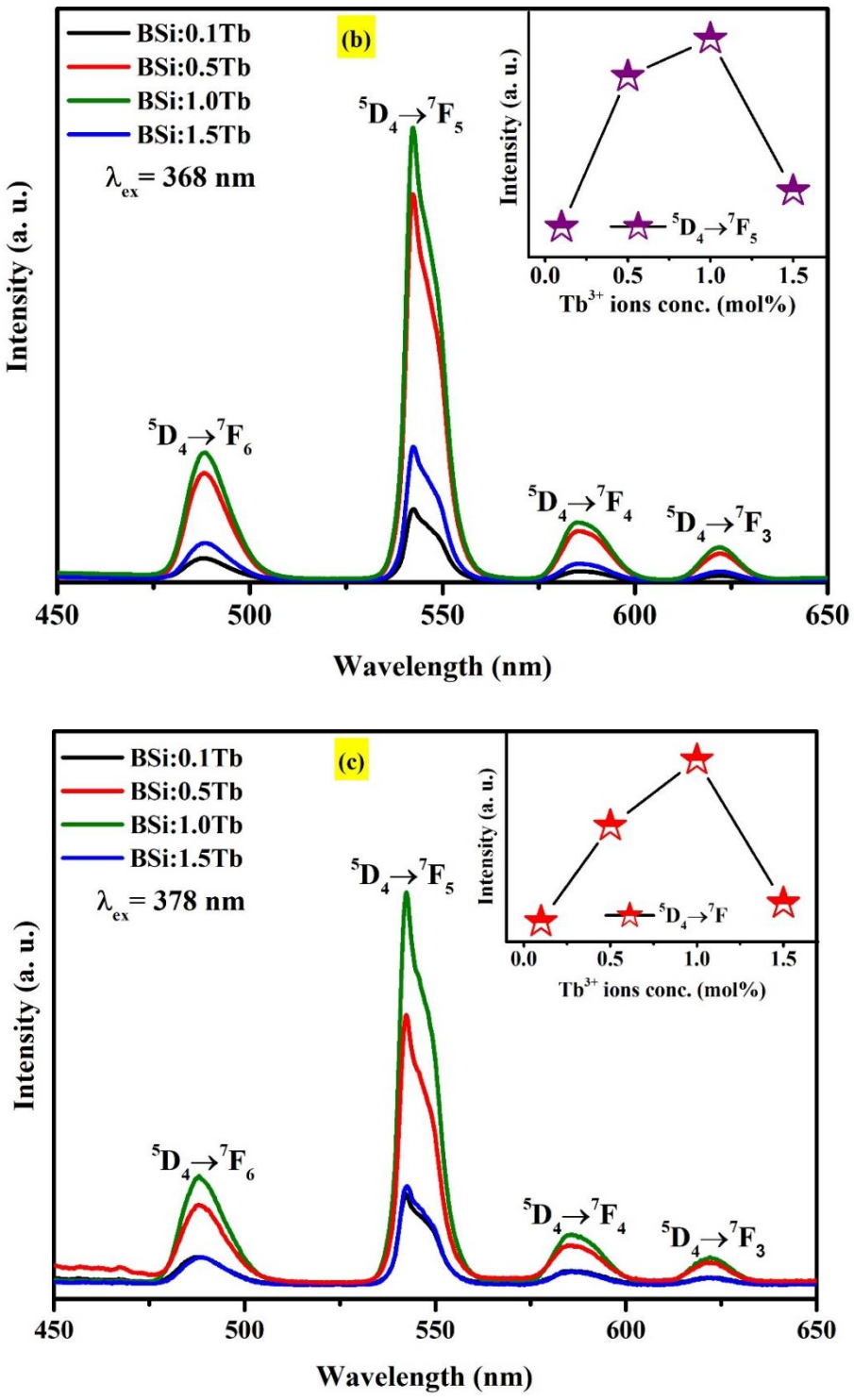

Fig. 4.5: *PL spectra of BaSrAlBSi glass with varying the Tb^{3+} doping concertation from 0.01 to 1.5 mol% at excitations wavelength of (b) 368 and (c) 378 nm. Inset image of all plots shows the changes in ($^5D_4 \rightarrow {}^7F_5$) intensity with Tb^{3+} ions concentration.*

To optimize the emission intensity with doping concentration, the various doped glasses have been prepared. As of Fig. 4.5 (a, b & c) and their inset plot evident that the emission intensity intensifies gradually up to 1.0 mol% of Tb^{3+} ions in BaSrAlBSi glasses and beyond this concentration diminish owing to the quenching effect. Reduction in emission intensity after 1.0 mol% of Tb^{3+} ions in BaSrAlBSi glasses may be ascribed to the non-radiative multipole-multipole interaction or cross-relaxation (CR) process among Tb^{3+}ions [132–134]. The quenching mechanism can be recognized via employing Dexter theory. As per the theory emission intensity (I) related with the activator concentration (x) given below:

$$\log\left(\frac{I}{x}\right) = c - \frac{s}{3}\log(x) \tag{3}$$

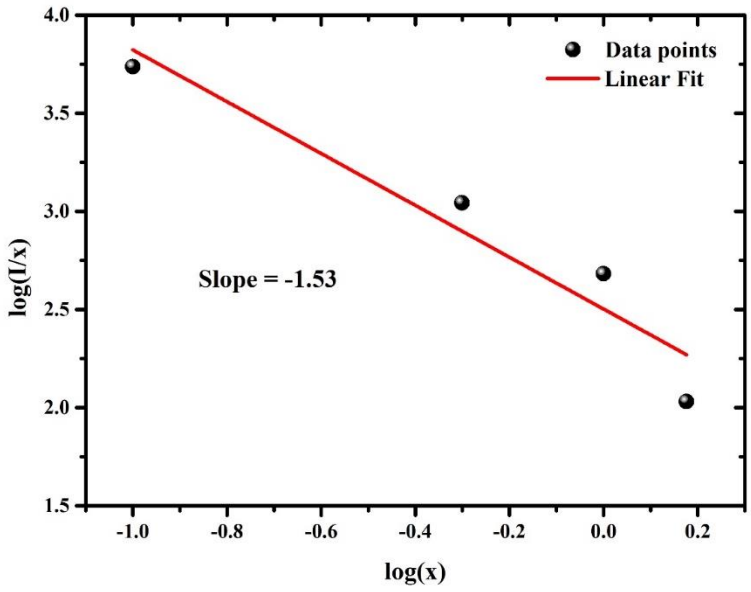

Fig. 4.6: *Dexter plot for Tb^{3+} doped BaSrAlBSi glass.*

in the above equation, c denotes the constant and s denotes fitting parameter. The fitting parameter having values were s = 10, 8, and 6 for quadrupole-quadrupole (q-q), quadrupole-dipole (q-d) and dipole-dipole (d-d) interactions, respectively [135]. According to the Dexter theory, graph plotted between $\log\left(\frac{I}{x}\right)$ and $\log(x)$ and linearly fitted as demonstrated in Fig.4.6.

The slope of linearly fitted plot was found to be -1.53, which gives the s parameter value of 4.59. On the basis of s parameter of Dexter theory, it was recognized that the non-radiative energy transfer between Tb^{3+} ions is dipole-dipole in nature. From the PL emission spectra, it was noticed that 1.0 mol% of Tb^{3+} ion is optimum concentration in BaSrAlBSi glass and gives intense green emission.

Furthermore, the PL mechanism, probable cross-relaxation (CR) channels and resonant energy transfer (RET) were illustrated by using the partial energy level diagram for doped BaSrAlBSi glasses as demonstrated in Fig. 4.7. Energy level diagram clarified the PL excitation, emission, process decorative in the green emitting glass pumped via n-UV (351, 368 & 378 nm) light attributed the respective transition in numerous energy levels [132,136,137].

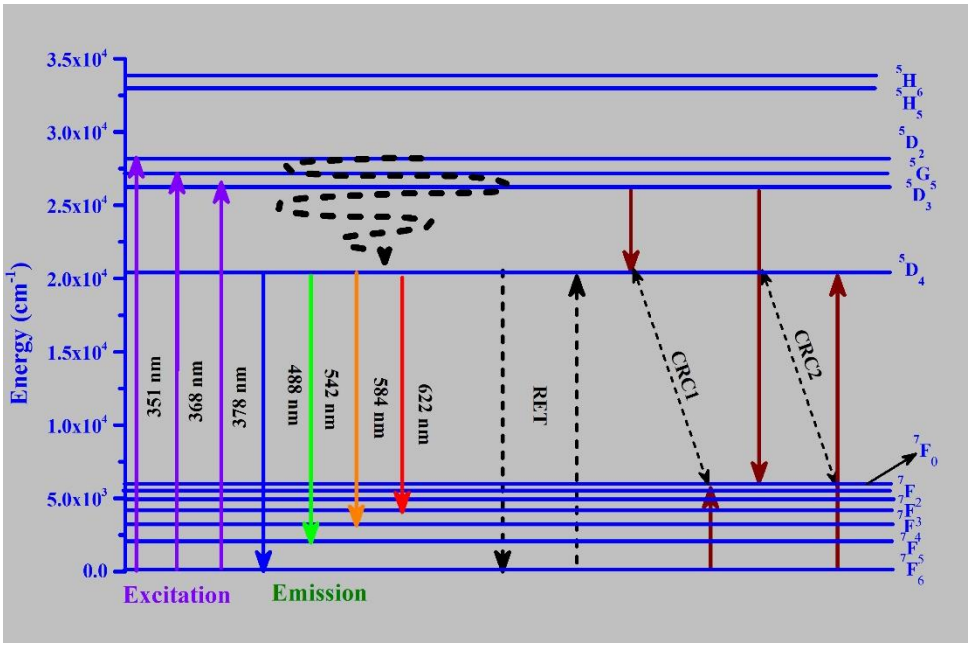

Fig. 4.7: *Partial energy level diagram of Tb^{3+} doped BaSrAlBSi glass.*

On the basis of difference between energy levels of Tb^{3+} ions, the probable CR channels and RET are as follows:

$$CR1: {}^5D_3/{}^7F_6 \rightarrow {}^7F_0/{}^5D_4$$

$$CR2: {}^5D_3/{}^7F_6 \rightarrow {}^5D_4/{}^7F_0$$

$$RET: {}^5D_4/{}^7F_6 \rightarrow {}^7F_6/{}^5D_4$$

4.3.5. CIE chromaticity

The CIE chromaticity coordinates were assessed using the emission profile for Tb^{3+} doped BaSrAlBSi glasses under λ_{ex} = 368 nm. All the assessed CIE chromaticity coordinates were listed in table 1. Fig, 4.8 visibly indicates the CIE color coordinates for BSi:1.0Tb was fall in green region, which is adjacent with the green emitting component by European Broadcasting Union illuminant (0.290, 0.600). The CCT was evaluated with help of McCamy formula [138]:

$$CCT = -449n^3 + 3525n^2 – 6823.2n + 5520.3 \quad (5)$$

Glass sample	CIE coordinates (*x, y*)	CCT (K)	Lifetime (ms)
BSi:0.1Tb	0.341, 0.414	5267	2.739
BSi:0.5Tb	0.327, 0.540	5621	2.684
BSi:1.0Tb	0.343, 0.469	5429	2.631
BSi:1.5Tb	0.326, 0.474	5661	2.617

where $n=\frac{x-x_e}{y-y_e}$, x_e=0.332, y_e=0.186. The CCT values for Tb^{3+} doped BaSrAlBSi glasses under λ_{ex} = 368 nm have been tabulated in Table 4.1 and confirmed cool (≥5000K) green light.

Table 4.1. *CIE coordinates (x, y), CCT (K) and average lifetime (ms) of Tb^{3+} doped BZLP glasses.*

The aforesaid results make known that the Tb^{3+} doped BaSrAlBSi glasses have propitious features for n-UV pumped, green component in photonic devices.

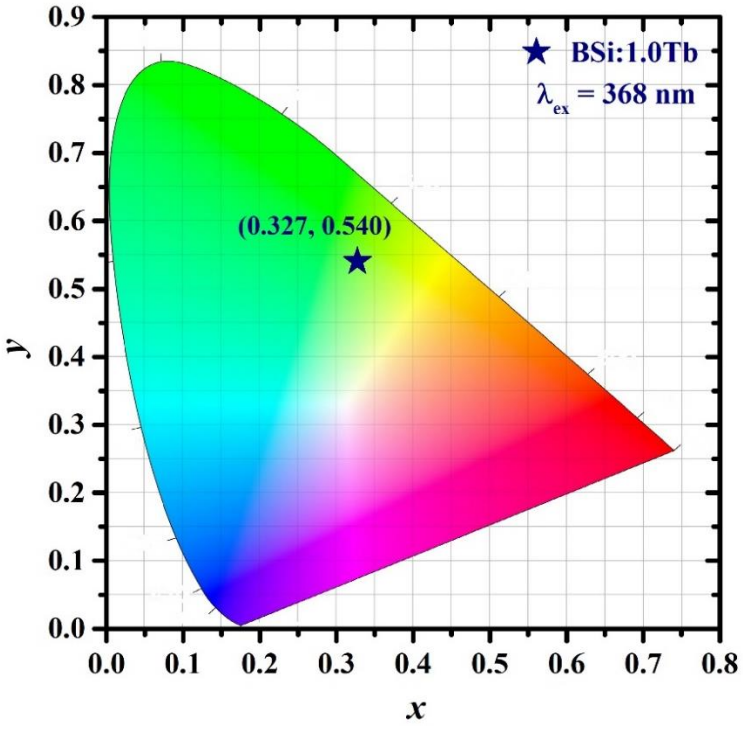

Fig. 4.8: *CIE color coordinates for optimized BSI:1.0Tb glass.*

4.3.6. PL decay study

PL lifetime curve of Tb^{3+} doped BaSrAlBSi gasses were obtained at λ_{ex} = 368 nm with monitoring the λ_{em} = 542 nm as displayed in Fig 4.9. The lifetime curves were exponential in nature and fitted with following equation: [113,114]:

$$I(t) = I_o + A_1 exp\left(-\frac{t}{\tau_1}\right) + A_2\, exp\left(-\frac{t}{\tau_2}\right)$$

I_o and $I(t)$ show 542 nm emission intensity at time 0 second and t second, respectively. A_1 and A_2 are constants. τ_1 and τ_2 are two lifetime values. PL lifetime decreases with upsurge in doping

concentrationof Tb^{3+} ions. The decrement in lifetime can be due to the non-radiative energy transfer among Tb^{3+} ion. The average lifetime (τ_{avg}) was evaluated via given formula [115]:

$$\tau_{avg} = \frac{A_1\tau_1^2 + A_2\tau_2^2}{A_1\tau_1 + A_2\tau_2}$$

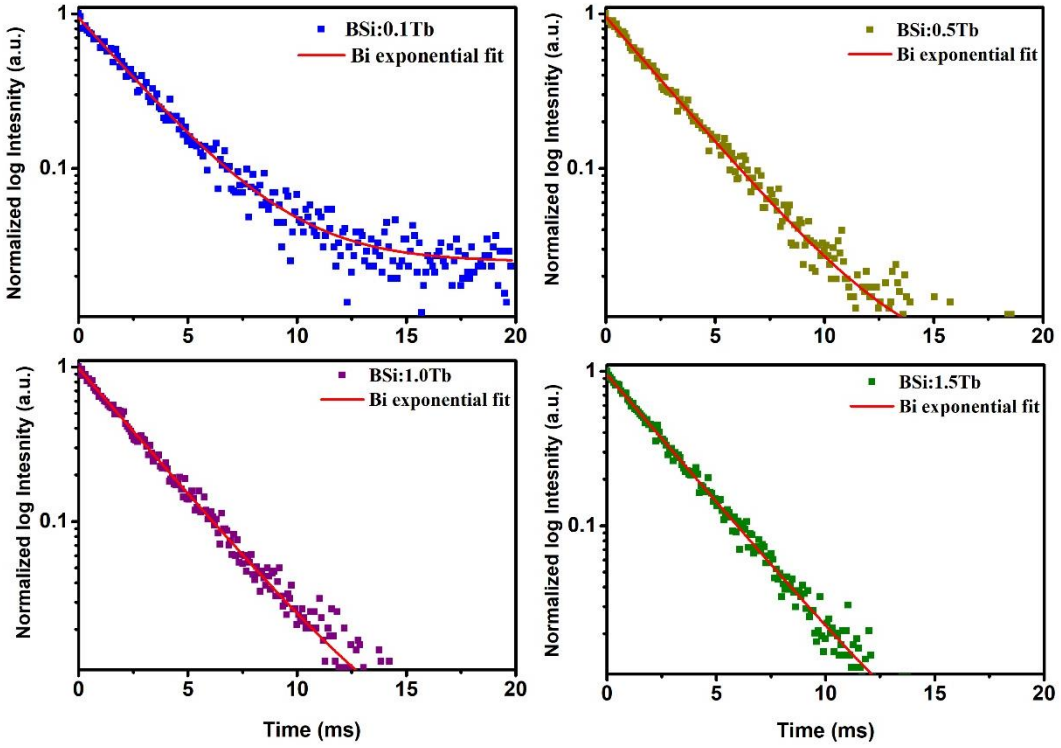

Fig.4.9: *PL lifetime curves for Tb^{3+} doped BaSrAlBSi glasses at 368 nm excitation and emission at 542 nm.*

The average lifetime was arranged in Table 4.1. The result indicated the decrease in τ_{avg} from 2.739 ms to 2.617 ms with upsurge the Tb^{3+} ions content from 0.1 mol% to 1.5 mol%.

The non-radiative energy transfer among Tb^{3+} ion can be identified via employing the I-H model on PL lifetime curve. According to the I-H model [80]:

$$I_t = I_0 \exp\{\frac{-t}{\tau_o} - Q\left(\frac{t}{\tau_o}\right)^{\frac{3}{s}}\}$$

here I_t is the emission intensity of the at time t, τ_o the lifetime value. Q represents the energy transfer parameter. The value of S = 6, 8 and 10 for d-d, q-d and q-q interactions, respectively [60]. The I-H fitted lifetime curve was shown in Fig. 4.10 and parameter value is found S = 5.61 for optimized glass, which confirms the dipole-dipole type of interaction among Tb^{3+} ions and well agreement with Dexter's theory results.

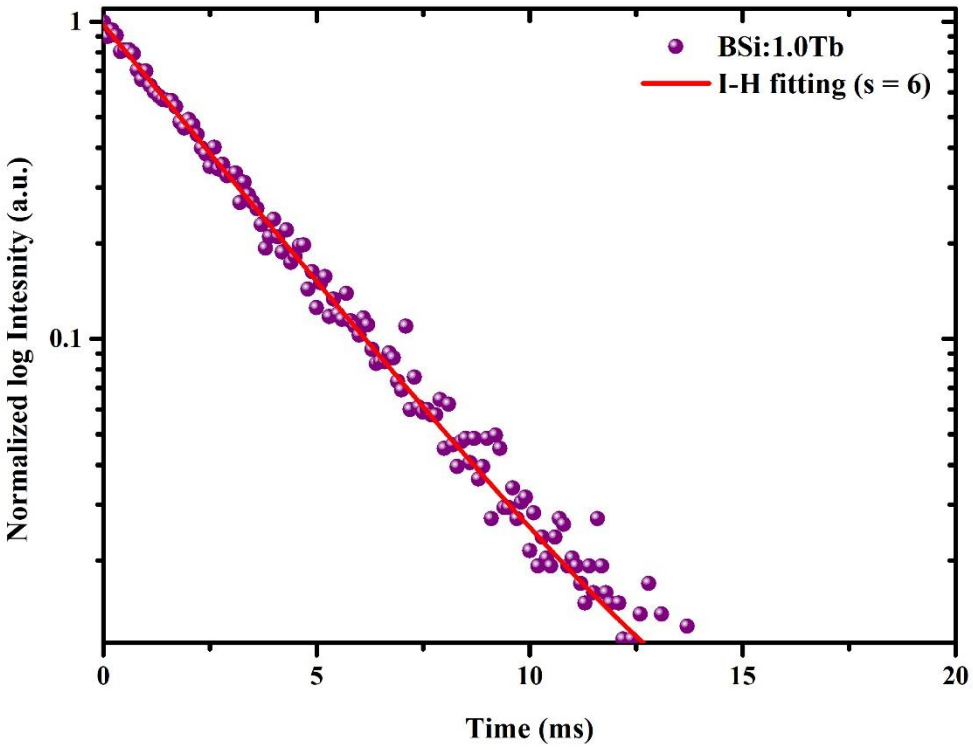

Fig. 4.10: *PL lifetime curve of BSi:1.0Tb glass with I-H fitting (S = 6).*

4.3.7. Temperature effect on PL properties

The effect temperature on PL properties of optimized glass was examined via TD-PL spectra. The TD-PL spectra for BSi:1.0Tb was recorded in 27 to 200°C range at λ_{ex} = 368 nm as display in Fig. 4.11. TD-PL spectra revealed that the very less diminishing in emission intensity with rise in temperature from atmospheric temperature to 200 °C. The emission intensity diminishes to 93.85 % at 150 °C and 90.54 % at 200 °C, which approves that the

BSi:1.0Tb glass has exceptional thermal stability. Furthermore, the activation energy (ΔEa) of BSi:1.0Tb glass was evaluated using the equation as follows [117]:

$$I_T = \frac{I_0}{1 + C\ exp\left(-\frac{\Delta Ea}{K_B T}\right)}$$

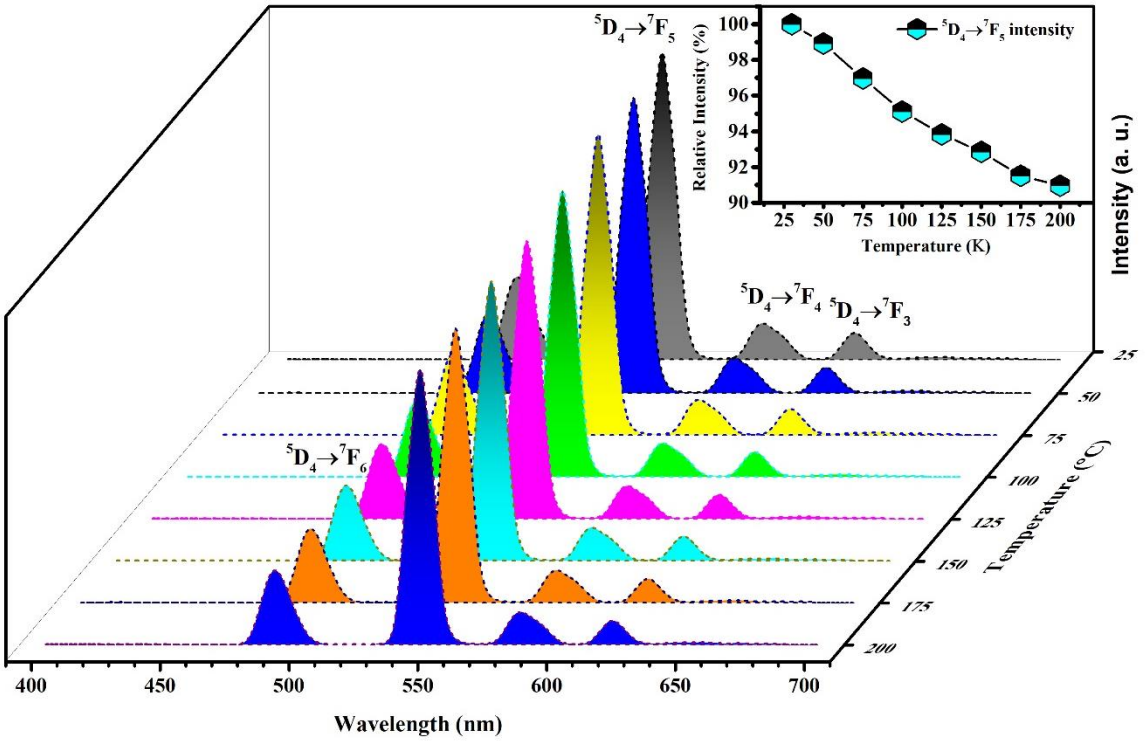

Fig.4.11: *Temperature dependent emission spectra of optimized glasses at temperature range from 27 to 200℃ at excitation wavelength of 368 nm. Inset plot shows the reduction in ($^5D_4 \rightarrow {}^7F_5$) emission intensity with temperature.*

here I_0 and I_T indicate emission intensity at different temperature. K_B symbolizes the Boltzmann constant. C designates an arbitrary constant. The value of ΔEa was assessed using the $ln((I_0/I_T)-1)$ versus $1/K_BT$ plot as designated in Fig. 4.12. The ΔEa was 0.126 eV for BSi:1.0Tb glass. Accordingly, TD-PL spectra of BSi:1.0Tb glass validate that the glass exhibits appropriate thermal stability and useful for lighting and photonic device applications.

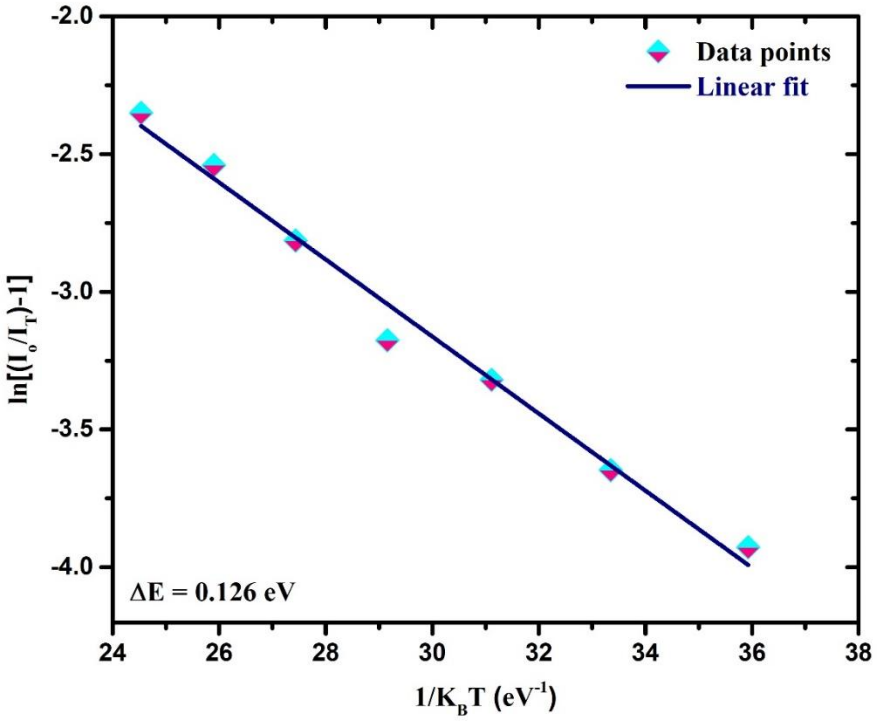

***Fig. 4.12**: ln[(I$_o$/I$_T$)-1] and (1/K$_B$T) plot for BSi:1.0Tb glass.*

4.4. Conclusions

A series of transparent Tb^{3+} doped BaSrAlBSi glasses have been produced via melt quenching method and examined structural, optical features for advanced laser and lighting appliances. XRD and FT-IR profile discloses the non-crystalline nature and presented functional groups of glass. The absorption spectrum shows the various peaks owing to Tb^{3+} ions situated in n-UV visible and NIR region. Based on the absorption profile, indirect E_{opt} was estimated to be 2.94 eV for BSi:1.0Tb. The transparent glass was excited by n-UV light and emits the blue, green, yellow and red light owing to transitions from $^5D_4$ to various $^7F_{(J = 6, 5, 4 \& 3)}$ energy levels of Tb^{3+} ions. The most intense emission peak was observed at 542 nm under n-UV source corresponding to $^5D_4 \rightarrow {}^7F_5$ transition and follow the Laporte-forbidden selection rule. The optimum emission intensity was conquered for 1.0 mol% Tb^{3+} ions doped

BaSrAlBSi glasses. The maximum photoluminescence (PL) emission intensity was observed for 1.0 mol% Tb^{3+} doped BaSrAlBSi glass. Beyond the 1.0 mol% the dipole-dipole type of non-radiative energy transfer was recognized with the help of the Dexter theory. The PL lifetimes were showing the decrease in decay time with upsurge in Tb^{3+} content. The I-H model confirmed the dipole-dipole type of non-radiative energy transfer mechanism among the nearest Tb^{3+} ions. The TDPL investigation unveils that the optimized BSi:1.0Tb glass has $\Delta E = 0.126$ eV, which shows good thermal stability The observed results anticipate that the direct utility of the as prepared transparent Tb^{3+} doped BaSrAlBSi glasses as n-UV pumped with green emitting constituent for photonic device applications.

CHAPTER 5

Energy Transfer and Thermally Stable White Light Illuminating Characteristics of Tb^{3+}/Sm^{3+} ions Activated BaO-SrO-Al_2O_3-B_2O_3-SiO_2 Glasses for W-LEDs

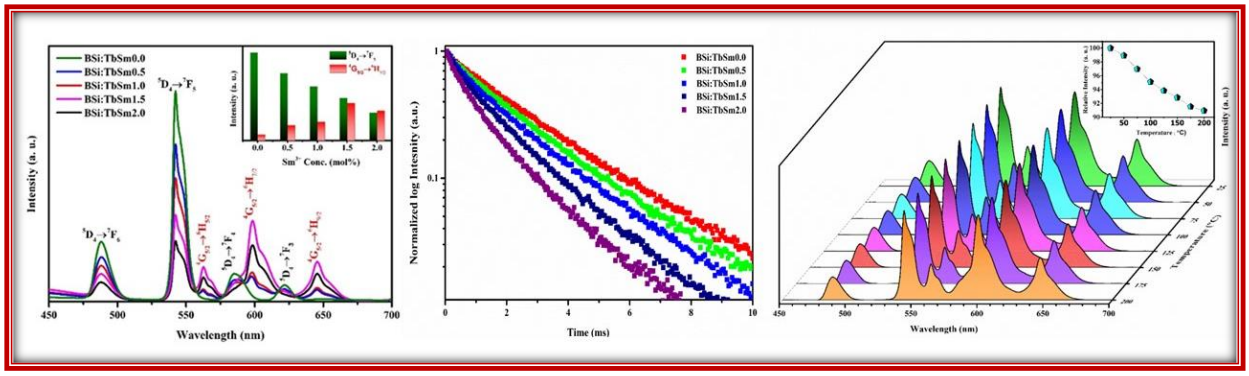

<u>Part of this work has been published in an International Journal</u>

<u>Optical Materials 145 (2023) 114446 (Impact Factor: 3.9)</u>

A number of Tb^{3+} and Tb^{3+}, Sm^{3+} incorporated barium strontium aluminium borosilicate (BaSrAlBSi) glasses were prepared, and their optical properties were carefully examined for use in high-tech lighting and laser applications. The transparent BaSrAlBSi glass's amorphous nature was established by the XRD pattern. The absorption profile demonstrates the various peaks from n-UV to NIR range caused by the Tb^{3+} as well Sm^{3+} ions in BaSrAlBSi glass. The as prepared glass with 1.0 mol% of Tb^{3+} (BSi:Tb1.0) glasses gives

emission in blue, green, yellow and red light owing to the transition from $^5D_4$ to various $^7F_{(J = 6, 5, 4 \& 3)}$ under λ_{ex}=379 nm. The as prepared glass with 1.0 mol% of Sm^{3+}(BSi:Sm1.0) glasses exhibit the emission spectra green to red region, caused by the transitions from $^4G_{5/2}$ to $^6H_{5/2}$, $^6H_{7/2}$, $^6H_{9/2}$, and $^6H_{11/2}$ of the Sm^{3+} ions. The Tb^{3+}/Sm^{3+} co-doped BaSrAlBS glasses exhibit a mixture of blue, green, and orange-red light when excited at 379 nm, whereas they red-orange light when excited at 402 nm. The PL lifetimes demonstrated a reduction in decay time as Sm^{3+} concentration increased in Tb^{3+} doped BaSrAlBSi glass. The sort of non-radiative energy process was determined using the Inokuti Hirayama (I-H) model, and it turns out to be a dipole-dipole in the environment. CIE coordinates show the green emission was tuned towards warm white region via co-doping of Sm^{3+} in Tb^{3+} doped BaSrAlBSi glasses. The strong thermal stability of BSi:TbSm1.0 glass is confirmed via temperature dependent emission profile, which reveals that temperature dependence on PL intensity has a very small impact. The observed results indicate that the transparent BSi:TbSm1.0 glasses as made will be directly useful for photonic device applications as n-UV pumped with the green warm white and orange emitting component.

5.1. Introduction

Energy conservation is a current topic that receives a lot of consideration because the globally energy usage is continually rising. In the continuation of energy conservation, White light-emitting diodes (w-LEDs) have been regarded as a next-generation light source for indoor and outdoor illumination. As w-LEDs have superior characteristics such as energy savings, high efficiency, environmental friendliness, compact size, and other factors over fluorescent lamp. In the present day, trivalent rare-earth (RE) ion-activated non-crystalline glass materials have been regarded as the most active components in several fields, including advanced

laser, solar cell, light, optical communications, and other photonic devices [118–120]. The practicality, application, and fame of these RE activated glasses were largely due to their beneficial qualities, including transparency, simplicity of fabrication with desired size and shape, greater thermal stability, cheaper production costs, extended life span, etc. [123,124,129]. Additionally, the RE-activated glass has the potential to convert wavelengths for UV/blue driven white emission in white light emitting diodes (w-LEDs), which might help them overcome drawbacks like a poor color rendering index, thermal instability, and high associated color temperature, among others. In accordance, these RE-activated glasses served as a wavelength converter and encapsulant. Additionally, the RE-activated glass used to attach the w-LEDs prevents negative impacts on illuminating efficacy at elevated temperatures by not requiring an organic epoxy resin binder. [124,139].

Glass compositions, such as glass formers, modifiers, and appropriate dopants ions, have significantly influenced the envisioned characteristics of glasses. Numerous inorganic glass hosts are available, including borosilicate, tungstate, phosphate, borate, germinate, and silicate. [9,96]. A suitable glass host among them is inorganic borosilicate glass, which has properties such as high transparency, low melting point, a low thermal expansion coefficient, excellent thermal stability, strong corrosion resistance, etc. [67,97]. These qualities were crucial for their use in many fields, including modern lighting, displays, solar cells, lasers, automation, and many others. Alkaline earth oxides were thought to be a suitable network modifier for borosilicate glass hosts because they may improve chemical stability, reduce glass structure, and significantly condense the glass network [68]. As a network modifier, the addition of metal oxides like Al_2O_3 may also increase the critical distance, decrease phonon emission, improve the mechanical chemistry, thermal stability, thermal resistance of the host, as well as radiative emission. [17,49]. In current studies, BaO-SrO-Al_2O_3-B_2O_3-SiO_2 (BaSrAlBSi) glass

composition was chosen to synthesize transparent, thermally mechanically robust glass with remarkable photonic properties, which may directly use in optical devices, based on the requirements necessary for glass hosts.

Tri/divalent RE ions can be used in modern photonic devices such as lasers since they have a variety of energy states and can absorb wavelengths from ultraviolet to infrared while also emitting in the visible and IR regions [16,126]. As The incompletely occupied 4f electron shells in trivalent state RE ions are shielded by 5s2/5p6 orbitals and produce a strong excitation radiative emission [49,92]. One of these lanthanides, Tb^{3+}, emits visible green light after absorbing near UV/blue light [61,127,128]. As the Tb^{3+} ion's transition reveals the four-level laser system's threshold value, it may be employed as a biological probe because of its acute emission, extended spontaneous lifetime, and high quantum efficiency. Tb^{3+} activated many glass hosts have recently been created and described for use with photonic devices [80,140]. To achieve the necessary luminous characteristics, the relevant RE ions can be combined with ions in the host lattice. Sm^{3+} is an effective activator for generating orange/red-orange emissions under UV or n-UV sources. White light emission as well as multicolored light emission are both possible at certain concentrations of Tb^{3+} and Sm^{3+} RE ions in a single host material.

In this study, Tb^{3+} and Tb^{3+}/Sm^{3+} incorporated BaSrAlBSi glasses were prepared using melt quenching methods and then carefully examined their structural, vibrational, and optical characteristics. The applicability of the Tb^{3+}/Sm^{3+} incorporated glass as the major colour emitting effective component in lasers, w-LEDs, and other optical devices has been thoroughly explored. This includes absorption, photoluminescence (PL), and PL lifespan properties and other optical charactersitics.

5.2. Experimental

5.2.1. Tb^{3+}/Sm^{3+}activated BaSrAlBSi glasses preparation

Single ions (Tb^{3+} & Sm^{3+}) activated BaSrAlBSi glasses have been prepared via melt quenching rout with chemical composition as:

$$10\ BaO - 10\ SrO - (10\text{-}m)\ Al_2O_3\text{-}50B_2O_3\text{-}20SiO_2 -: m\ Tb_4O_7$$

$$10\ BaO - 10\ SrO - (10\text{-}n)\ Al_2O_3\text{-}50B_2O_3\text{-}20SiO_2 -: n\ Sm_2O_3$$

in above chemical compositions, Tb^{3+} ions concentration is as m = 1.0 mol% glasses named as BSi:Tb1.0 and Sm^{3+} ions concentration is as n = 1.0 mol% glasses named as BSi:Sm1.0.

$$10BaO - 10SrO- (10\text{-}m)Al_2O_3\text{-}50B_2O_3\text{-}20SiO_2 -: mTb_4O_7, nSm_2O_3$$

The precursor $BaCO_3$, $SrCO_3$, Al_2O_3**,** H_3BO_3**,** SiO_2 and Tb_4O_7 chemicals have been used to synthesize Tb^{3+} activated BaSrAlBSi glass. The concentrations used for n are 0.0, 0.5, 1.0, 1.5, and 2.0 mol%, while the value of m was set at 1.0 mol% and glasses named as BSi:TbSm0.0, BSi:TbSm0.5, BSi:TbSm1.0, BSi:TbSm1.5, and BSi:TbSm2.0, respectively. All of the precursor chemicals were measured according to the appropriate amount using an electric balance, and they were all pulverized in an acetone medium using a mortar and pestle. The uniformly ground mixer was held in a crucible and placed in a furnace for melting after a certain amount of time. The furnace's temperature increased quickly, by 5 °C every minute, from ambient to 1250 °C. After a predetermined period at 1250 °C, powder transforms into melting state, and uniformly melted chemicals are immediately cooled in two heated brass plates at 300 °C. The created clear BaSrAlBSi glass was annealed at 350 °C for 3.5 hours to remove air bubble stress and avoid thermal sock. For structural, optical, and other research, the Tb^{3+}/Sm^{3+} integrated glasses have finally been created.

5.2.2. Characterizations techniques

Structural property of the BaSrAlBS glass has been examined by diffraction pattern attained from X-ray diffraction (XRD) (Bruker, D8 advance) in $10° \leq 2\theta \geq 60°$ range. UV-vis absorption spectroscopy has been obtained from the spectrophotometer (Jasco, V770). Photoluminescence (PL) characteristics have been obtained via spectrofluorophotometer (Jasco, FP-8300) at room temperature. Spectrofluorophotometer (Edinburgh, FLS920) was used to record PL decay curves. Temperature dependent PL spectra were characterized with setup connected with sample heating assembly, Xenon light source and detector (FLAME-S-XR1-ES, Ocean optics).

5.3. Results and discussion

5.3.1. Diffraction pattern analysis

Fig. 5.1 represents the XRD pattern for BSi:TbSm1.0 glass that has been activated with 1.0 mol% Tb^{3+} as well as 1.0 mol% Sm^{3+}. The wide hump and lack of any crystalline peaks in the measured patterns indicate the glassy amorphous nature of BSi:TbSm1.0 glass.

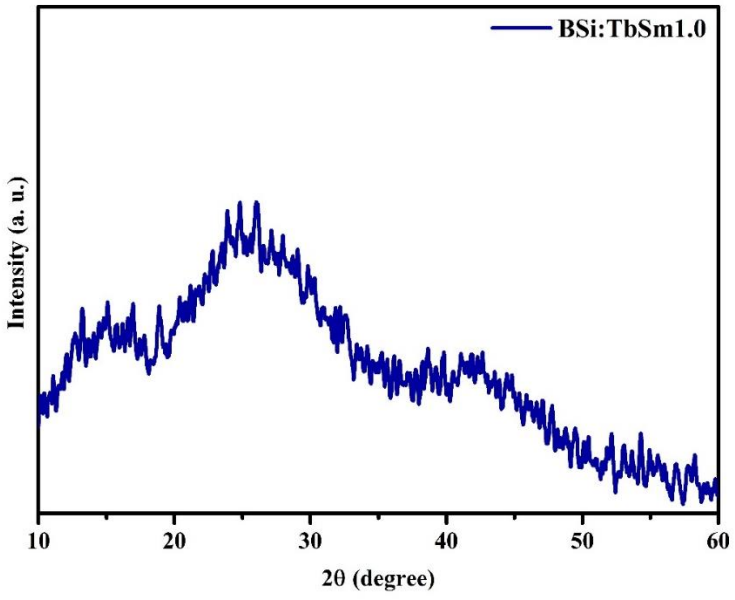

Fig. 5.1: *XRD pattern of BSi:TbSm1.0 glass.*

5.3.2. UV- vis absorption spectrum analysis

UV absorption profile for the prepared Tb^{3+}, Sm^{3+} and Tb^{3+}/ Sm^{3+} activated BaSrAlBSi glasses were obtained at room temperature as displayed in Fig. 5.2. The UV profile exhibits the number of absorption peaks in 300-2500 nm range. There are many peaks in the absorption spectrum at wavelengths of 370, 486, 1920, and 2210 nm that are related to f-f- transitions of Tb^{3+} ions [130]. These transitions, which were connected to electric dipoles, adhered to the |J|=0, +1 rule whereas magnetic dipole transitions followed the | J|≤ 6 selection criteria. Sm^{3+} activated glass shows the absorption spectrum has various peaks in UV to infrared rang owing transitions from $^6H_{5/2}$ to $^4F_{7/2}$, $^6F_{11/2}$, $^6F_{9/2}$, $^6F_{7/2}$, $^6F_{5/2}$, and $^6F_{3/2}$. The band allocations follow the information provided in the paper by Carnal et al. Other absorption bands were prevented from appearing in the UV-Vis region by the host glass's significant absorption. The absorption profile of Tb^{3+}/Sm^{3+} co-doped glasses were also demonstrated in Fig.2. The absorption profile includes various band owing to transition related to both Tb^{3+}/Sm^{3+} ions. Using the absorption spectrum and the Davis and Mott relation, it is possible to calculate the optical band gap, one of the parameters [125]:

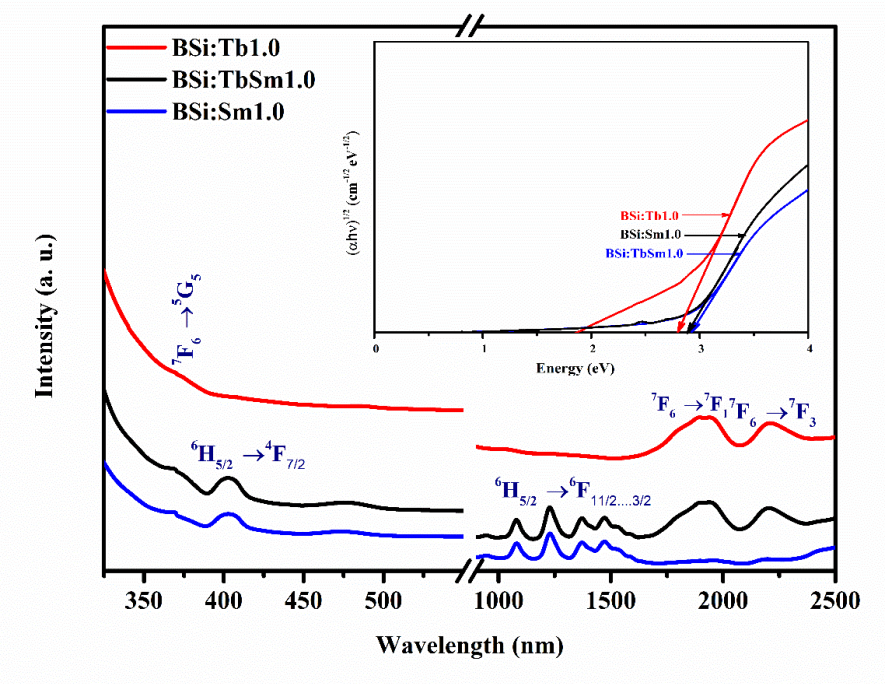

Fig. 5.2: *UV spectra of BSi:Sm1.0, BSi:Tb1.0, BSi:TbSm1.0, glasses. Inset plot shows the Tauc's plot for the BSi:Sm1.0, BSi:Tb1.0 and BSi:TbSm1.0 glasses.*

$$\alpha(\nu) = \left(\frac{B}{h\nu}\right)\left(h\nu - E_{opt}\right)^n$$

in above equation $h\nu$, E_{opt} and B were photon energy, optical bandgap of glass and band tailing parameter, respectively. n represent a parameter and affirm the type of transition. For indirect allowed transitions value of n = 2. The $\alpha(\nu)$ was evaluated using the following equation [131]:

$$\alpha(\nu) = \left(\frac{1}{d}\right) ln\left(\frac{I_0}{I_T}\right)$$

$ln\,(I_0/I_T)$ and d are absorbance and glass thickness, respectively. The E_{opt} value was evaluated via Tauc's plot by extrapolating the linear part as presented in inset of Fig. 5.2. The indirect E_{opt} of BSi:Tb1.0, BSi:Sm1.0 and BSi:TbSm1.0 were estimated to be 2.94, 2.98 and 3.09 eV, respectively.

5.3.3. PL analysis of Tb^{3+} activated BaSrAlBSi Glasses

The PL characteristics for all the Tb^{3+}activated BaSrAlBSi glasses have been recorded at ambient temperature. The PL excitation spectrum of BSi:Tb1.0 glass from 300 to 500 nm wavelength range by keeping fix the emission wavelength at 542 nm as visible in Fig. 5.3. The excitation profile contains several excitation peaks in the near ultraviolet (n-UV) and blue region. The experimental excitation peaks situated at 317, 340, 351, 368, 378, and 486 nm were attributed to the transitions from ground level ($^7F_6$) to $^5H_7$ + $^5D_0$, $^5L_7$+ $^5G_3$, $^5L_9$+$^5D_2$, $^5G_6$, $^5G_6$ +$^5D_3$ and $^5D_4$ levels states, respectively [141]. Among all excitation, the peaks at 351, 368 and 379 nm were comparatively higher than the other peaks, which were used as an excitation wavelength (λ_{ex}=379 nm) to record PL emission characteristics.

The emission profiles have been recorded of all the prepared transparent numerous Tb^{3+} doped BaSrAlBSi glasses under different excitation wavelength as illustrated in Fig.3 (PL). The emission profile exhibits the four peaks situated at 487, 543, 587, 623 nm corresponding to transitions from $^5D_4$ to various $^7F_{(J = 6, 5, 4 \& 3)}$ energy levels of Tb^{3+} ions. Among the blue, green, yellow and red peaks, the most intense peak is green owing to $^5D_4 \rightarrow {}^7F_5$ transition and follow the Laporte-forbidden selection rule. The second most intense peak is blue peaks at 488 due to the $^5D_4 \rightarrow {}^7F_6$ transition, which related the magnetic dipole transition ($\Delta J = \pm 1$). The emission intensity fluctuates.

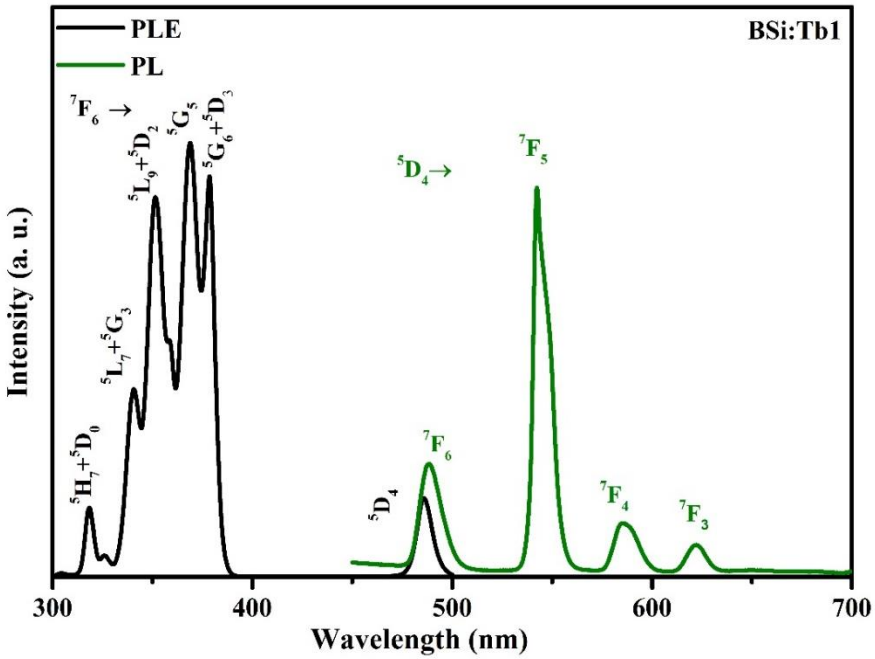

Fig. 5.3: *The excitation and emission spectrum of the BSi:Tb1.0 glass by keeping fix the emission wavelength at 542 and excitation wavelength at 368 nm.*

with doping concentration as demonstrated from emission profile. To optimize the emission intensity with doping concentration, various doped glasses have been prepared. As of Fig. 5.3 and their inset plot it is evident that the emission intensity intensifies gradually up to 1.0 mol% of Tb^{3+} ions in BaSrAlBSi glasses and beyond this concentration diminish owing to the quenching effect. Reduction in emission intensity after 1.0 mol% of Tb^{3+} ions in BaSrAlBSi glasses may be ascribed to the non-radiative multipole-multipole interaction or cross-relaxation (CR) process among Tb^{3+}ions [132–134]. From the PL emission spectra, it was noticed that 1.0 mol% of Tb^{3+} ion is optimum concentration in BaSrAlBSi glass and gives intense green emission.

5.3.4. PL analysis of Sm^{3+} activated BaSrAlBSi glasses

The excitation wavelength must be determined in order to use rare earth doped glass in various optoelectronic devices. In order to do this, the emission at 602 nm wavelength was

monitored while the excitation spectrum in the region of 300 to 500 nm was recorded. The excitation spectrum of glass is seen in the blue spectrum in Fig. 5.4, which supports the existence of numerous excitation peaks in both the blue and n-UV regions. These excitation peaks situated at 343, 360, 375, 402, 415, 436, and 475 nm, arises due to transitions from ground state $^6H_{5/2}$ to numerous levels of Sm^{3+} ion such as $^4H_{9/2}$, $^4D_{3/2}$, $^4D_{1/2}$, $^4F_{7/2}$, $^6P_{5/2}$, $^4G_{9/2}$ and $^4I_{13/2}$ + $^4I_{11/2}$ + $^4M_{15/2}$, respectively [142]. From the excitation spectra, it has been disclosed that the highest peak intensity at 402 nm. The recorded spectra also indicate that the as prepared glass can be efficiently excited by n-UV bare chip.

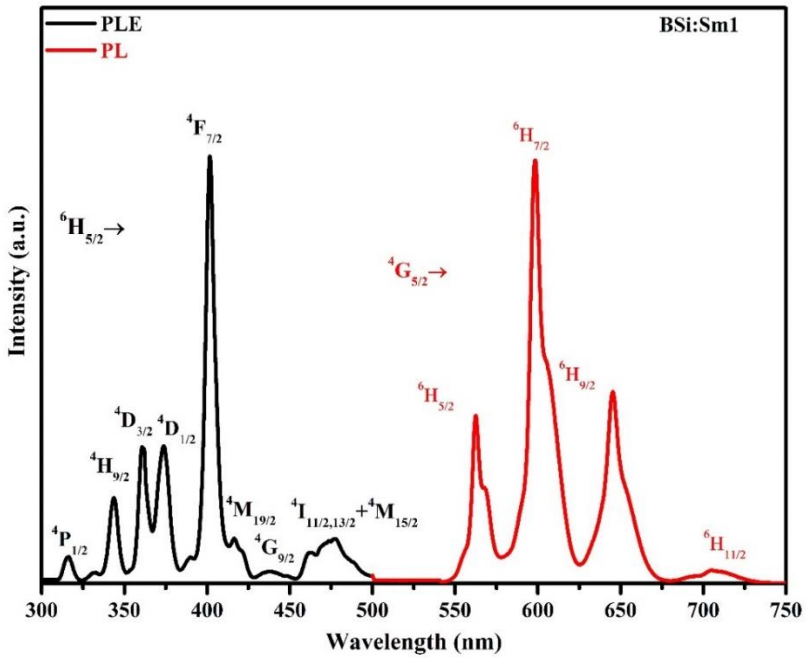

Fig. 5.4: *Excitation and emission spectrum of BSi:Sm1.0 glass at λ_{em} = 602 and λ_{ex} = 402 nm, respectively.*

Fig. 5.4 (PL) illustrates the emission spectra of the as-made the BSi:Sm1.0 under the n-UV excitation (λ_{ex} = 402 nm) and the emission pattern under 402 nm excitation was observed in the 500 to 750 nm region. Four peaks in the emission spectra, centered at 561, 602, 648, and 704 nm, respectively, are caused by the transitions of the Sm^{3+} ions from $^4G_{5/2}$ to $^6H_{5/2}$, $^6H_{7/2}$, $^6H_{9/2}$, and $^6H_{11/2}$ respectively. According to the spectroscopic selection rules, the transitions

$^4G_{5/2} \rightarrow {}^6H_{5/2}$ and $^4G_{5/2} \rightarrow {}^6H_{7/2}$ are magnetic dipoles, but the transitions $^4G_{5/2} \rightarrow {}^6H_{9/2}$ and $^4G_{5/2} \rightarrow {}^6H_{11/2}$ is forced electric dipoles. As a result, the $^4G_{5/2} - {}^6H_{7/2}$ transition has a mixture of both the transitions characteristics [120,143]. The main peak among these PL peaks is centered at 602 nm and is found in the reddish orange area. Hypersensitive in nature, the ligand atoms' crystal fields had an impact on the strength of the forced electric dipoles transition. The surroundings of the crystal field had no effect on the magnetic dipole transition. The magnetic dipole transitions were dominant over the electric dipoles transition in the present Sm^{3+} activated glass system. The result indicates that there was greater symmetry and that there was no departure from the nature of inversion symmetry [6].

5.3.5. PL analysis of Tb^{3+}/ Sm^{3+} activated BaSrAlBSi Glasses

Based on the Dieke's energy level diagram, energy can be transferred between two rare earth ions. The rare earth ion in the high fluorescent state transfers energy to another rare earth ion in the lower state. When it comes to Tb^{3+} and Sm^{3+} ions, Tb^{3+} has a greater fluorescent excited state than the Sm^{3+} ion. Therefore, the energy transfer from Tb^{3+} to Sm^{3+} may occur. Fig. 5.5 shows the excitation spectra of BSi:TbSm1.0 glass as measured from emission at 602 and 542 nm. Sm^{3+} excitation lines were seen in the excitation spectra of BSi:TbSm1.0 through tracking emission at 602 nm, whereas Tb^{3+} peak emission was visible at 542 nm. 379 and 402 nm were determined to be the proper excitation lines for the series of co-doped Tb^{3+}/ Sm^{3+} activated BaSrAlBSi glasses based on the BSi:TbSm1.0 excitation spectra.

Emission spectra for the Tb^{3+}/ Sm^{3+} activated BaSrAlBSi glasses were recorded under 379 and 402 nm excitation wavelength. The emission profile exhibits the four peaks situated at 487, 543, 587, 623 nm corresponding to transitions from $^5D_4$ to various $^7F_{(J = 6, 5, 4 \& 3)}$ energy levels of Tb^{3+} ions for BSi:TbSm0.0 glasses at λ_{ex} =379 nm as presented in Fig.5.6. When the content

of Sm^{3+} ions included in Tb^{3+} doped BaSrAlBSi glasses, the new emission peaks were arising at 561, 602 and 648 nm caused by the transitions from $^4G_{5/2} \rightarrow {}^6H_{5/2}$, $^4G_{5/2} \rightarrow {}^6H_{7/2}$, $^4G_{5/2} \rightarrow {}^6H_{9/2}$ of Sm^{3+} ions. The intensity of these arises emission peaks were enhancing with increment of content of Sm^{3+} ions. Simultaneously some emission peaks related to Tb^{3+}ions can get reduces with increment of

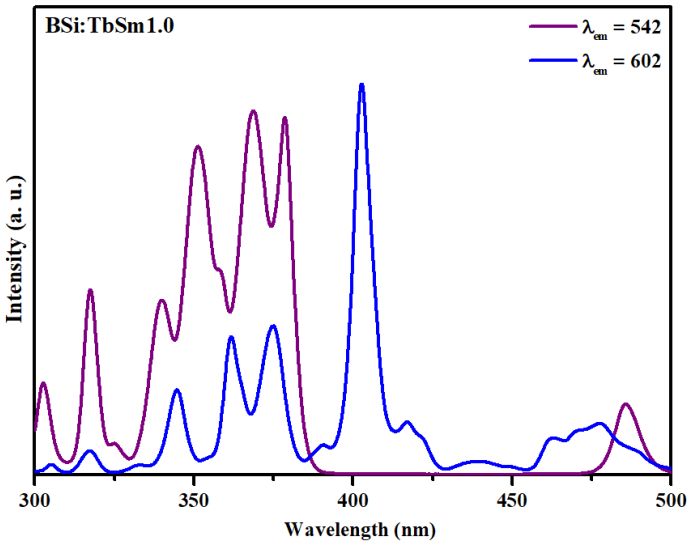

Fig. 5.5: *Excitation spectra of BSi:TbSm1.0 glass at λ_{em} = 542 and 602 nm.*

content of Sm^{3+} ions up to 1.5 mol%. Beyond this concentration, all emission peaks intensity gets reduced owing to concentration effect-based emission effect [144]. The reduction in Tb^{3+} ions emission and enhancement in Sm^{3+} ions emission confirmed the energy transfer from Tb^{3+} sensitizer ions to Sm^{3+} activator ions. The inset plot also indicates the change the emission peaks related $^4G_{5/2} \rightarrow {}^6H_{7/2}$ and $^5D_4 \rightarrow {}^7F_5$ transition with change in Sm^{3+} activator ions concentrations. Emission spectra for the Tb^{3+}/ Sm^{3+} activated BaSrAlBSi glasses were also recorded at λ_{ex} =402 nm as represented in Fig.7. the spectra exhibit the emission peaks at 561, 602 and 648 nm instigated.

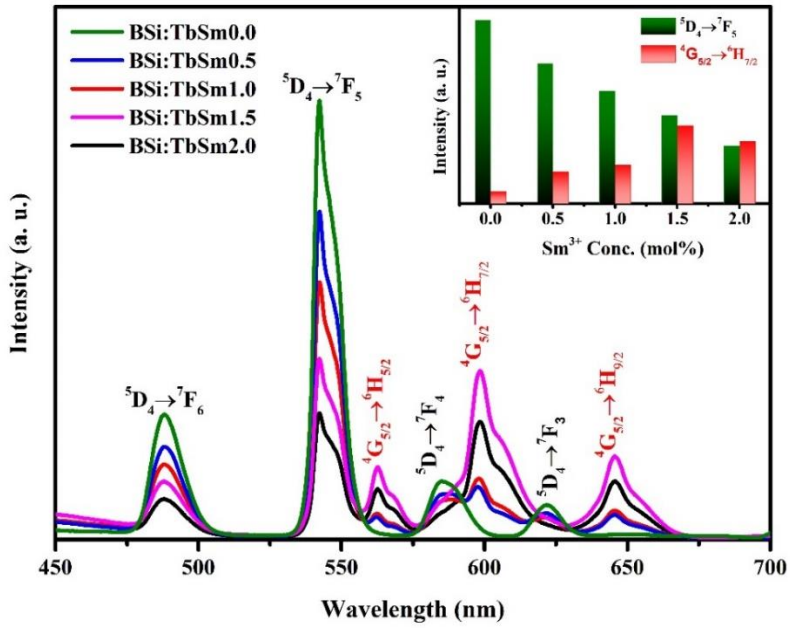

Fig. 5.6: *Emission spectra of BSi:TbSm0.0, BSi:TbSm0.5, BSi:TbSm1.0, BSi:TbSm1.5 and BSi:TbSm2.0 glasses at λ_{ex} = 368 nm. Inset plot shows the change emission intensity for the $^5D_4 \rightarrow {}^7F_5$ and $^4G_{5/2} \rightarrow {}^6H_{7/2}$ transitions with upsurge in Sm^{3+} ions concertation.*

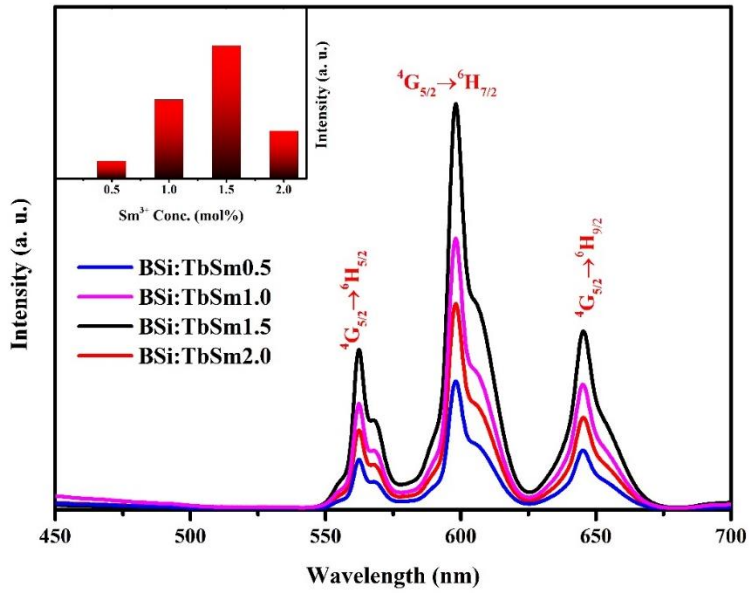

Fig. 5.7: *Emission spectra of BSi:TbSm0.0, BSi:TbSm0.5, BSi:TbSm1.0, BSi:TbSm1.5 and BSi:TbSm2.0 glasses at λ_{ex} = 402 nm. Inset plot shows the change emission intensity for $^4G_{5/2} \rightarrow {}^6H_{7/2}$ transitions with upsurge in Sm^{3+} ions concertation.*

by the transitions from $^4G_{5/2} \rightarrow {}^6H_{5/2}$, $^4G_{5/2} \rightarrow {}^6H_{7/2}$, $^4G_{5/2} \rightarrow {}^6H_{9/2}$ of Sm^{3+} ions, which are analogous with normal Sm^{3+} doped BaSrAlBSi glasses. The result indicates the charge transfer takes place from Tb^{3+} sensitizer ions to Sm^{3+} activator ions, not vice versa. The inset plot also indicates the change the emission peaks related $^4G_{5/2} \rightarrow {}^6H_{7/2}$ with change in Sm^{3+} activator ions concentrations.

The partial energy levels of the Tb^{3+} and Sm^{3+} ions seen in Fig. 5.8 can be used to provide insight on the energy transfer process. The co-doped glasses with Tb^{3+}/Sm^{3+} ions have been successfully stimulated by n-UV radiations, as shown in Fig. 5.8, based on PL data. The intermediate levels of Tb^{3+} and Sm^{3+} ions then experience a specific non-radiative transition. Afterward the Tb^{3+} ions exhibits the four peaks situated at 487, 543, 587, 623 nm corresponding to transitions from $^5D_4$ to various $^7F_{(J = 6, 5, 4 \& 3)}$ energy levels. While Sm^{3+} ions give four emissions

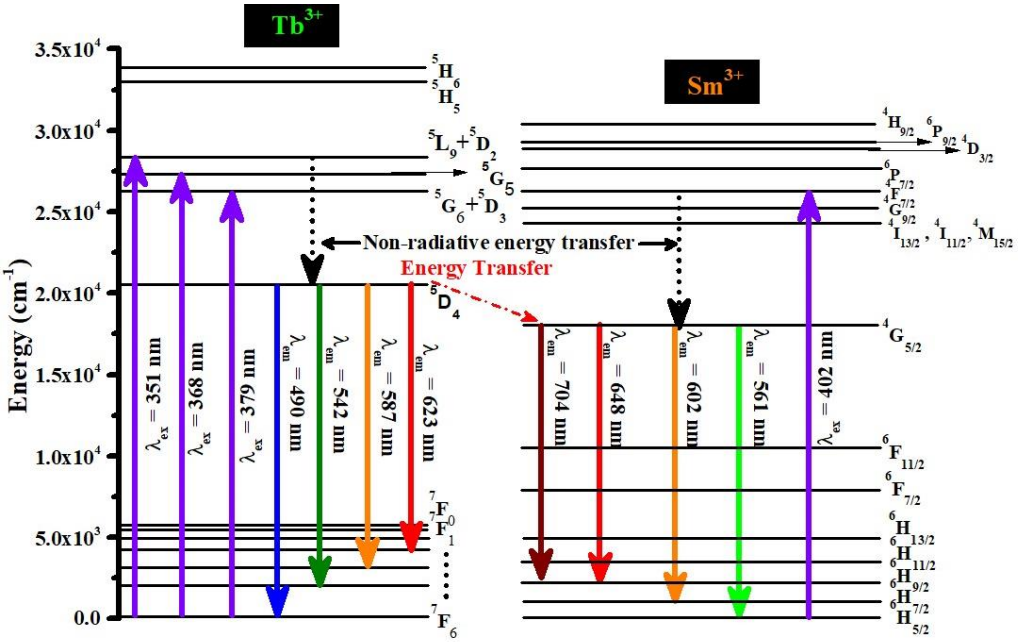

Fig. 5.8: *Partial energy level diagram of Sm^{3+} and Eu^{3+} ions in BaSrAlBSi glass with excitation, emission and energy transfer.*

peaks centered at 561, 602, 648, and 704 nm caused by the transitions of the ions from $^4G_{5/2}$ to $^6H_{5/2}$, $^6H_{7/2}$, $^6H_{9/2}$, and $^6H_{11/2}$ respectively. In addition to the individual emission, Tb^{3+} to Sm^{3+} ion energy transfer also occurs. The energy transfer takes happen because the prepared glasses' $^5D_4$ Tb^{3+} ion energy levels are higher than the $^4G_{5/2}$ Sm^{3+} energy levels. The Tb^{3+} ions in BaSrAlBSi glasses transferred some of the energy they had taken from the Tb^{3+} ions to the Sm^{3+} ions due to the lower energy difference between both energy levels, as shown partial energy level diagram.

Rare earth doped glasses predominantly employ multipolar exchange interaction, which may be divided into three types of interaction: quadrupole and quadrupole, dipole and dipole, and dipole and quadrupole. By combining Reisfeld's approximation with Dexter's multipolar exchange interaction expression, the forms of energy transfer among the closest doped ions were examined as follows [61,129]:

$$\frac{\eta_0}{\eta} \propto C^{n/3}$$

The symbols η_0 and η indicate, respectively, the radiant quantum efficiency of the sensitizer Tb^{3+} ions and the quantum efficiency of the sensitizer Tb^{3+} ions with Sm^{3+} (activator). The letter C stands for the combined concentration of activator and sensitizer ions. In the equation above, n represents the type of multipolar exchange interaction. The value of n can be 6, 8, or 10 depending on how dipoles, dipoles-quadrupoles, and quadrupoles interact with one another. The relationship between the radiation intensities below and the ratio between η_0 and η is depicted [145]:

$$\frac{I_{SO}}{I_s} \propto C^{n/3}$$

In the equation above, I_{SO} and I_S stand for the emission intensities of Tb^{3+} and Sm^{3+}, respectively. The graph of I_{SO}/I_S versus $C^{n/3}$ where n=6, 8, and 10, may also be seen in Fig.5.9.

In Tb^{3+}/ Sm^{3+} activated BaSrAlBSi glasses, the energy transfer from Tb^{3+} to Sm^{3+} is caused by the non-radiative dipole-dipole interaction, as shown by the best linear fit for n=6.

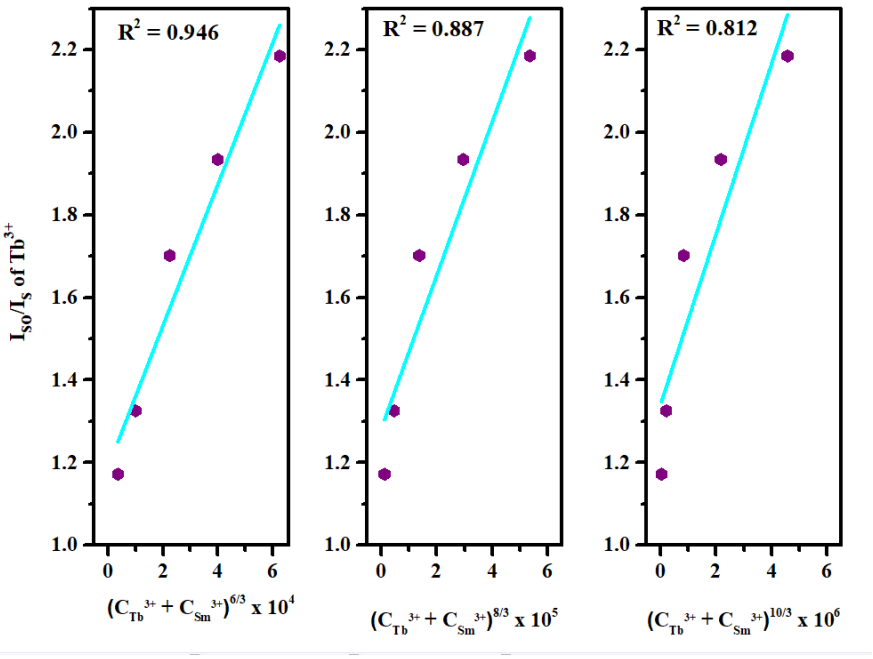

Fig. 5.9: *Plot between* I_{SO}/I_S *for* Sm^{3+} *versus (a)* $(C_{Tb+Sm})^{6/3}$, *(b)* $(C_{Tb+Sm})^{8/3}$ *and (c)* $(C_{Tb+Sm})^{10/3}$.

5.3.6. CIE chromaticity

Using the emission profile for Tb^{3+}/ Sm^{3+} activated BaSrAlBSi glasses at λ_{ex} = 379 nm, the CIE chromaticity coordinates were evaluated. Table 1 contains a list of every CIE chromaticity coordinate that was evaluated. The CIE color coordinates for BSi:TbSm1.0 are clearly seen in Fig.10: fell in the green region, which is close to the green emission component of the illuminant used by the European Broadcasting Union (0.290, 0.600). The green emission was tuned towards white region via co-doping of Sm^{3+} in Tb^{3+} doped BaSrAlBSi glasses. The McCamy formula was used to assess the CCT [138]:

$$CCT = -449n^3 + 3525n^2 – 6823.2n + 5520.3 \quad (5)$$

here n= $\frac{x-x_e}{y-y_e}$, y_e=0.186, x_e=0.332. Table 1 lists the CCT values for Tb^{3+} doped BaSrAlBSi glasses at λ_{ex} = 379 nm and indicates cool (>5000K) green light. These CCT values were tuned towards warm white region having CCT<5000K with co-doping of Sm^{3+} ions. The aforesaid results make known that the Tb^{3+}/ Sm^{3+} activated BaSrAlBSi glasses has propitious features for n-UV pumped, warm white light component in lighting devices.

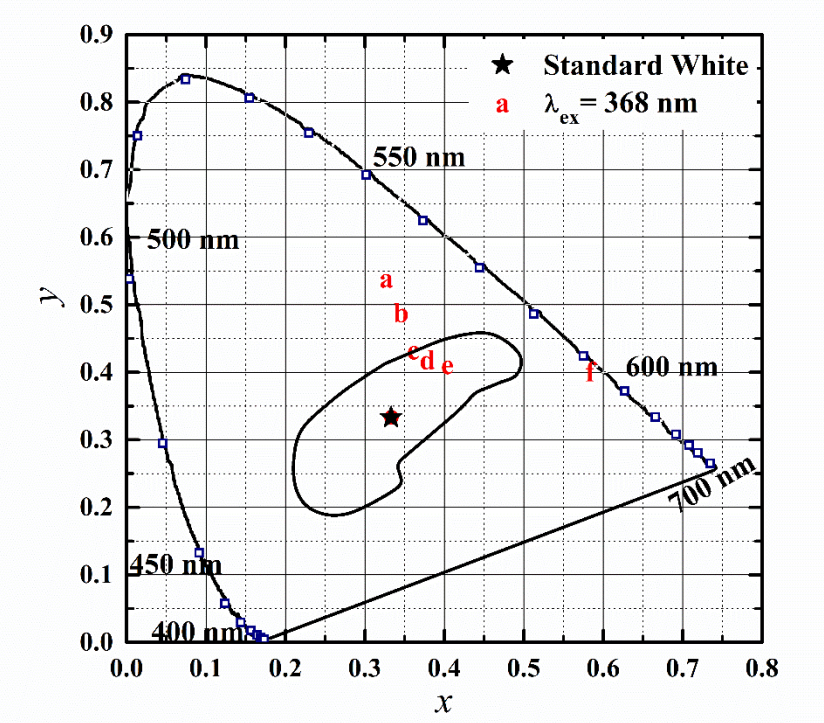

Fig. 5.10: *CIE chromaticity coordinates of (a) BSi:TbSm0.0, (b) BSi:TbSm0.5, (c) BSi:TbSm1.0, (d) BSi:TbSm1.5, (e) BSi:TbSm2.0 at λ_{ex} = 368 nm and (f) BSi:TbSm1.5 λ_{ex} = 402 nm.*

5.3.7. PL decay study

PL lifetime curve of Tb^{3+}/ Sm^{3+} activated BaSrAlBSi gasses were obtained at λ_{ex} = 379 nm with monitoring the λ_{em} = 542 nm as demonstrated in Fig 5.11. The lifetime curves were exponential in nature and fitted with following equation [113,114]:

$$I(t) = I_o + A_1 exp\left(-\frac{t}{\tau_1}\right) + A_2 exp\left(-\frac{t}{\tau_2}\right)$$

I_o and $I(t)$ show 542 nm emission intensity at time 0 second and t second, respectively. τ_1 and τ_2 are two lifetime values. A_1 and A_2 are constants. PL lifetime decreases with upsurge in doping concentrationof Tb^{3+} ions. The decrement in lifetime can be due to the non-radiative energy transfer among Tb^{3+} ion. The average lifetime (τ_{avg}) was evaluated via given formula [115]:

$$\tau_{avg} = \frac{A_1\tau_1^2 + A_2\tau_2^2}{A_1\tau_1 + A_2\tau_2}$$

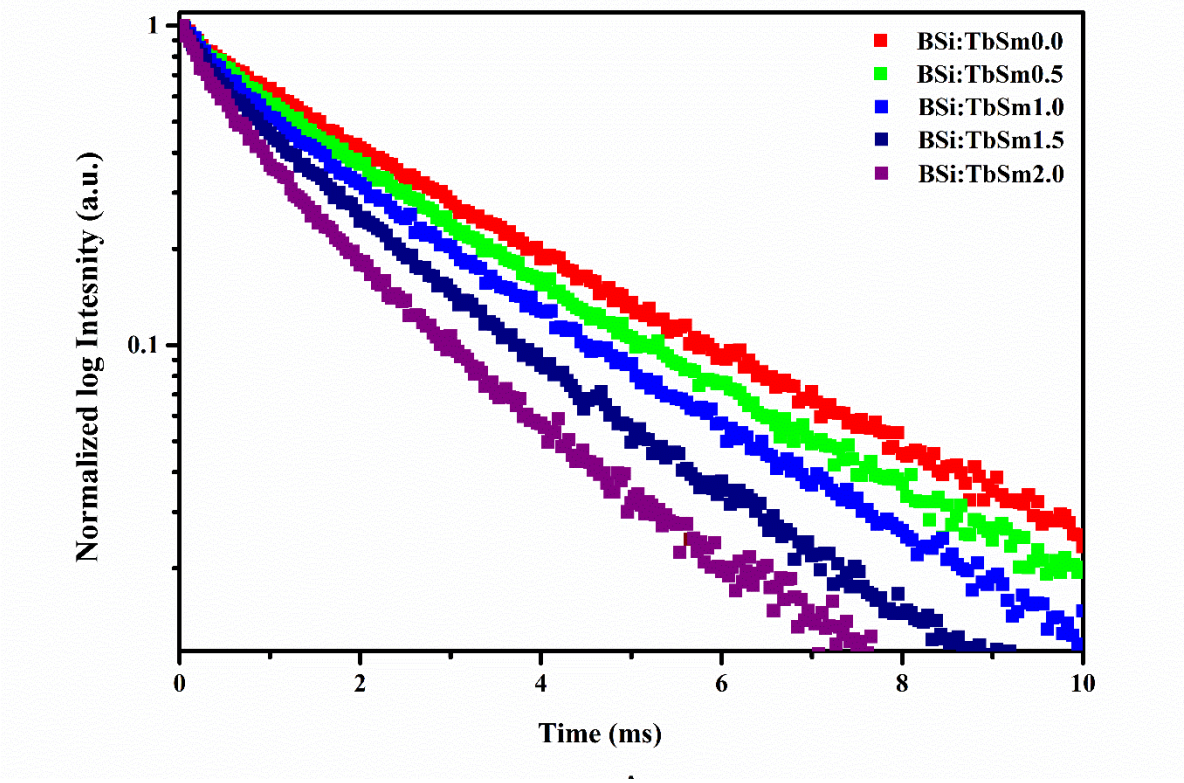

Fig. 5.11: *PL decay curves of BSi:TbSm0.0, BSi:TbSm0.5, BSi:TbSm1.0, BSi:TbSm1.5 and BSi:TbSm2.0 glasses at λ_{ex} = 368 nm.*

The average lifetime was arranged in Table 5.1. The result indicated the decrease in τ_{avg} from 2.739 ms to 2.617 ms with upsurge the Tb^{3+} ions content from 0.1 mol% to 1.5 mol%.

Additionally, the connection as follows was used to determine the energy transfer efficiency:

$$\eta_T = 1 - \frac{\tau_d}{\tau_{d0}}$$

The lifetimes of the glasses doped with Tb^{3+} ions and Sm^{3+}, respectively, are shown by the symbols $\tau_d$and τ_{d0}. The parameter for η_T is shown in Table 5.1. When the Sm^{3+} ion concentration is increased, Fig. 5.12 shows how lifespan and energy transfer efficiency in co-doped BZLP glasses modify. The result strongly suggests that when Sm^{3+} ions grow in amount, the η_T parameter increases. Six times as much energy transfer was likely to occur when the amount of Sm^{3+} ions in Tb^{3+}/ Sm^{3+} activated BaSrAlBSi glasses increased from 0.0 mol% to 2.0 mol%.

Table 5.1: *CIE color coordinates (x, y), CCT (K), decay time (ms), Tb^{3+} to Sm^{3+} energy transfer efficiency of Tb^{3+}/ Sm^{3+} co-doped BASrAlBSi glasses.*

Sample name	Excitation Wavelength (nm)	CIE coordinates (*x, y*)	CCT(K)	Lifetime (ms)	Energy transfer efficiency η_T (%)
BSi:Tb1.0	368	(0.327, 0.540)	5661	2.631	0.00
BSi:TbSm0.5	368	(0. 356, 0.489)	5123	2.523	4.15
BSi:TbSm1.0	368	(0. 361, 0.434)	4734	2.391	9.12
BSi:TbSm1.5	368	(0.379, 0.419)	4356	2.182	17.06
BSi:TbSm2.0	368	(0.441, 0.430)	4133	1.981	24.71
BSi:TbSm1.5	402	(0.589, 0.410)	-	-	-

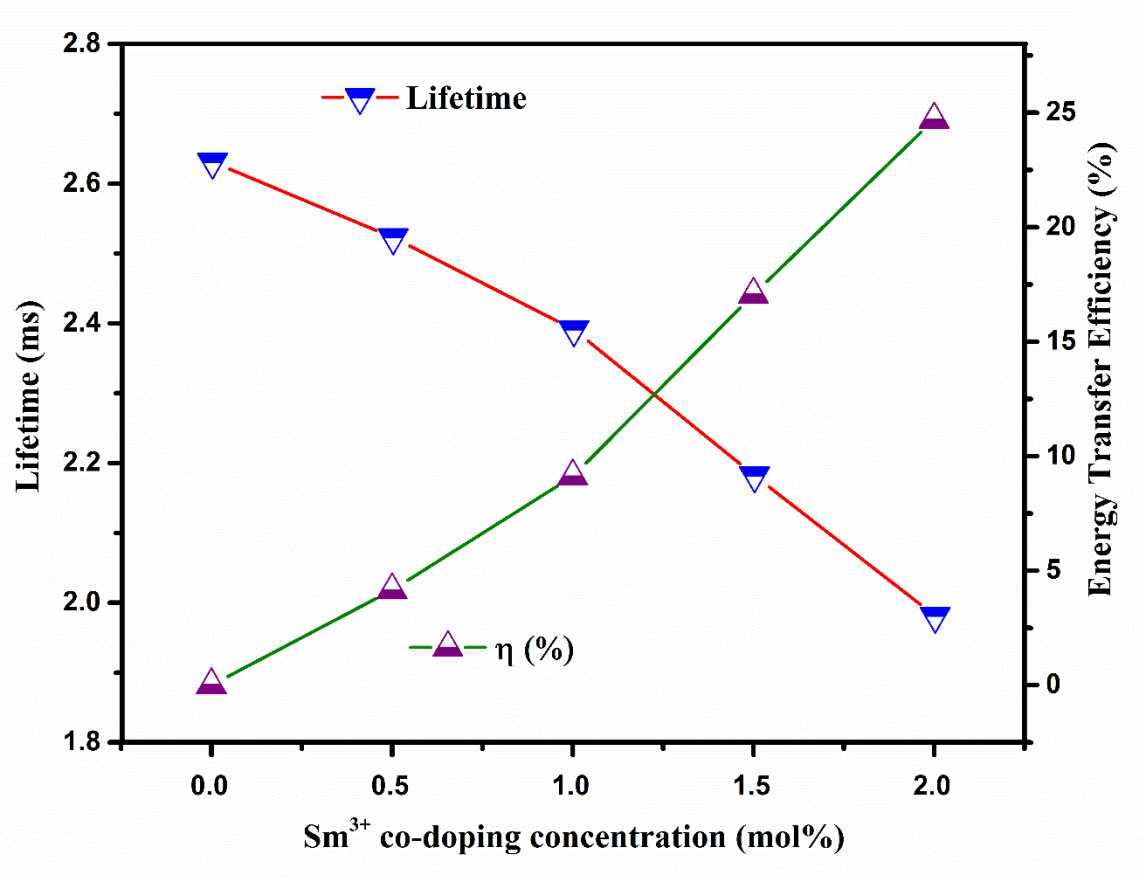

Fig. 5.12: *The change in lifetime value and energy transfer efficiency with co-doping concentration of Sm^{3+} ions in BSi:Tb1.0 glasses.*

The energy transfer mechanism between Tb^{3+} and Sm^{3+} ion can be recognized by using the Inokuti- Hirayama (I-H) model on lifetime curve as follows [80]:

$$I_t = I_0 \exp\{\frac{-t}{\tau_o} - Q\left(\frac{t}{\tau_o}\right)^{\frac{3}{s}}\}$$

I_t in this instance is the lifetime value, which is the emission intensity of the at time t. Energy transfer parameter Q is represented by dipole-dipole, quadrupole-dipole and quadrupole-quadrupole interactions, respectively, have S values of 6, 8, and 10 [36]. The I-H fitted lifetime curve is depicted in Fig. 5.13, and for optimized BSi:TbSm1.0 glass, parameter value S = 5.461

is discovered. This value confirms the dipole-dipole type of interaction between Tb^{3+} and Sm^{3+} ions and is in good agreement with the findings of Dexter's theory.

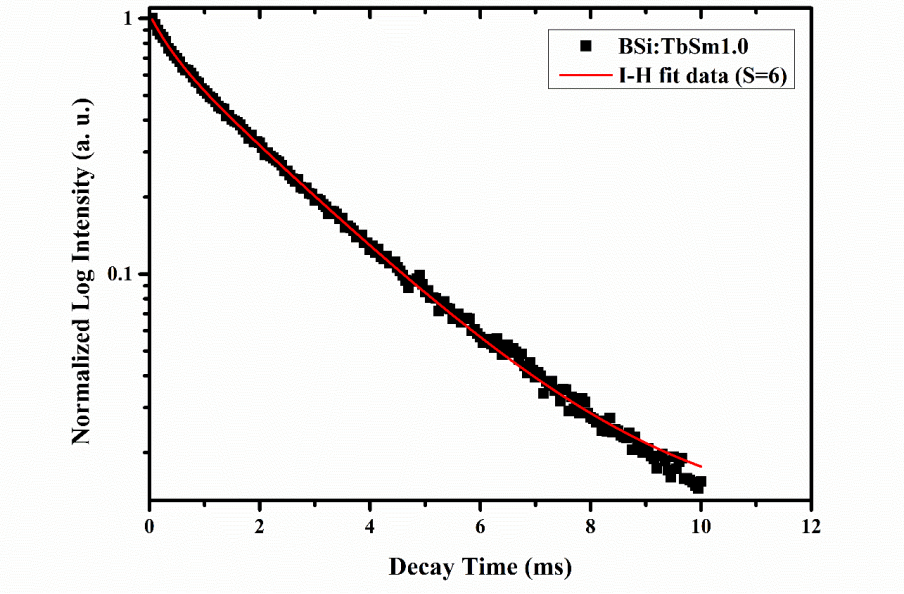

Fig. 5.13: *I-H fitted decay curves of BSi:TbSm1.0 glasses at λ_{ex} = 368 nm.*

5.3.8. Temperature effect on PL properties

Temperature-dependent emission spectra were used to analyze the PL profile at various temperatures. As shown in Fig. 5.14 (a, b), the emission profile for BSi:TbSm1.0 glass was seen in the temperature range of 25 to 200 C at λ_{ex} = 379 and 402 nm. According to temperature-dependent emission spectra, there is a very little decrease in emission strength when temperature increases from room temperature to 200 °C. The emission intensity decreases to 91.24% at 200 °C and 93.31% at 150 °C, demonstrating the outstanding thermal stability of the BSi:TbSm1.0 glass. Additionally, the activation energy (ΔEa) of prepared optimized BSi:TbSm1.0 glass was assessed via equation as follows [117]:

$$I_T = \frac{I_0}{1 + C\ exp\left(-\frac{\Delta Ea}{K_B T}\right)}$$

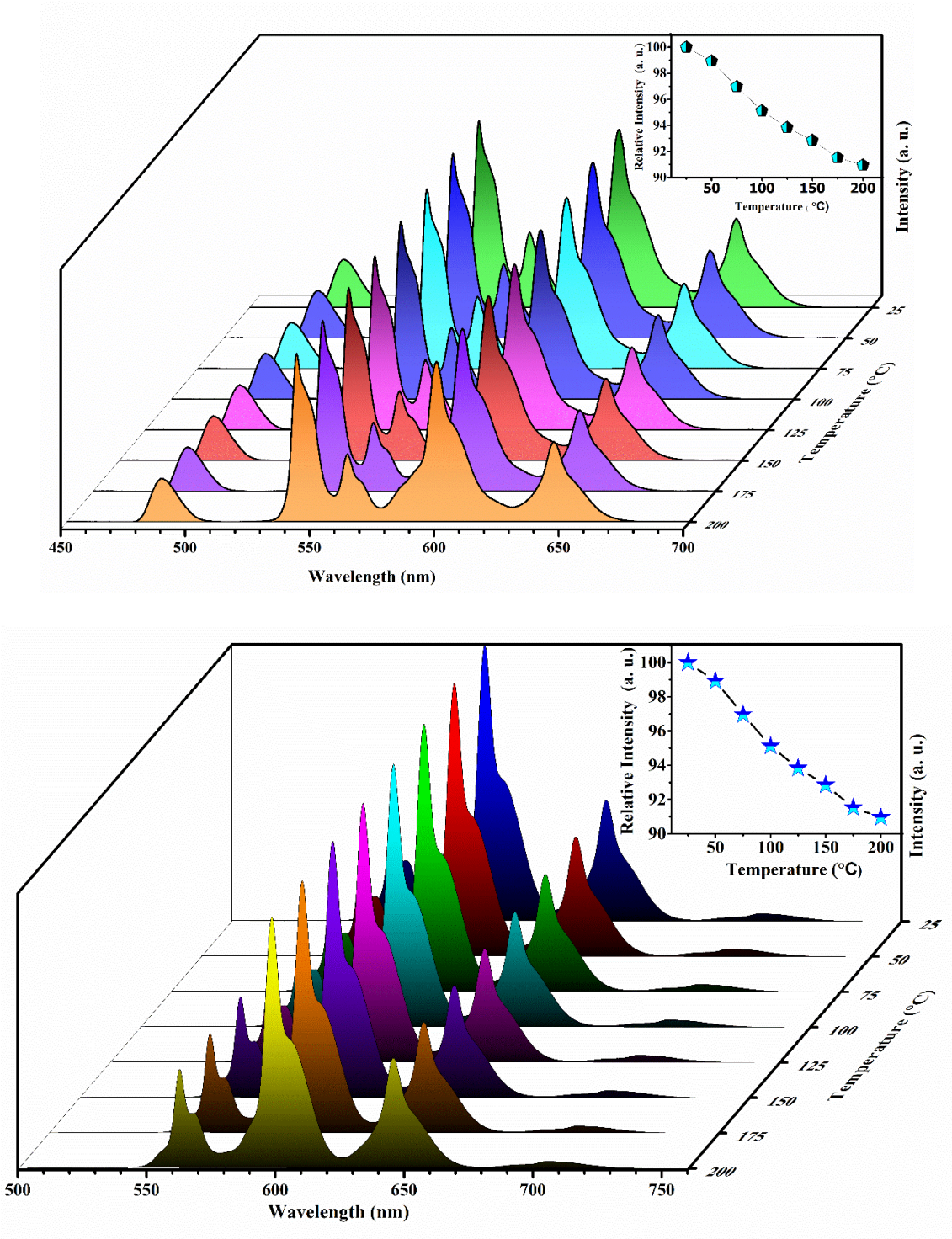

Fig.5.14: (a) *Temperature dependent emission spectra of BSi:TbSm1.5 glass at* λ_{ex} *= 368 nm.*

(b) *Temperature dependent emission spectra of BSi:TbSm1.5 glass at* λ_{ex} *= 402 nm.*

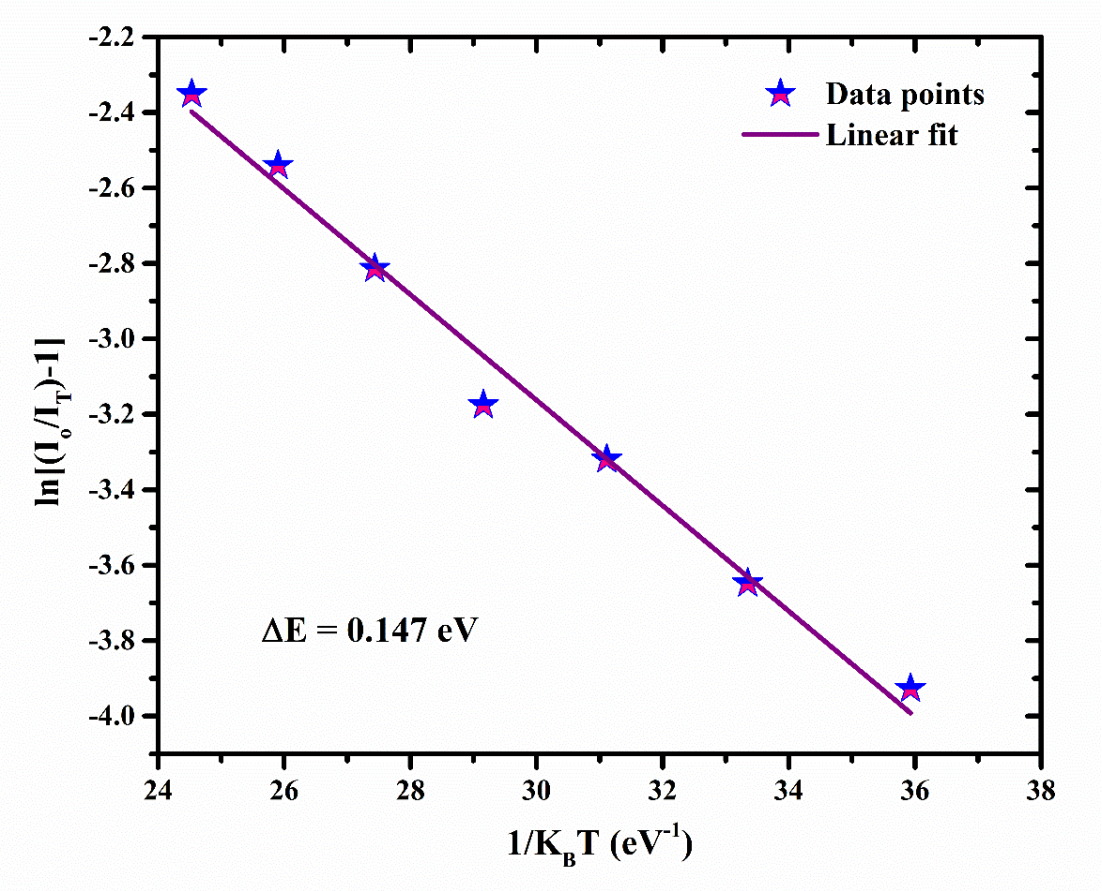

Fig.5.15: *ln[(I$_o$/I$_T$)-1] versus 1/K$_B$T plot for BSi:TbSm1.5 glass at λ$_{ex}$ = 368 nm.*

I_0 and I_T in the Arrhenian equation denote the PL intensity at 25 °C and a specific temperature T, respectively. C and K_B denote the Boltzmann constant and an arbitrary constant. The *ln((I$_0$/I$_T$)-1)* versus *1/K$_B$T* plots are prepared based on temperature-dependent emission characteristics, and fitted with linear equations for both emission characteristics as shown in Fig.5.15. According to emission spectra at λ_{ex} = 379 nm, respectively, the activation energy for Tb^{3+}/ Sm^{3+} activated BaSrAlBSi glass is 0.147 eV. A possible red and white emitting component in luminous devices, the Tb^{3+}/ Sm^{3+} activated BaSrAlBSi emits thermally stable white as well as orange emission, according to temperature dependent emission properties.

5.4. Conclusions

Transparent Tb^{3+}, Sm^{3+} and Tb^{3+}/Sm^{3+} activated BaSrAlBSi glass have been prepared successfully via melt quenching method. XRD profile reveals the non-crystalline nature of Tb^{3+}/Sm^{3+} activated BaSrAlBSi glass. The absorption spectra were used to calculate the glasses' optical band gap. Under 379 nm excitation, the glass that had been doped with Tb^{3+} showed a strong emission peak at 542 nm. Its utility as a green emitting component for photonic devices is suggested by the CIE chromaticity coordinates. The reddish orang emission peak at 602 nm under 402 nm excitation was seen in BSi:Sm1.0 glass and can a potential use for manufacturing in orange LEDs and display devices. By adjusting the Sm^{3+} concentration, the emission color of Tb^{3+}/Sm^{3+} co-doped BaSrAlBSi glasses adjusted from yellowish-green to warm-white via energy transfer process as confirmed from emission and CIE diagram. By using the I-H model on the decay curves and the Dexter and Reisfeld's theory based on the emission spectra, it was shown that the energy transfer from Tb^{3+} ($^5D_4$) to Sm^{3+} ($^4G_{5/2}$) happens via dipole-dipole interaction. The temperature dependent emission profile unveils that the BSi:TbSm1.0 glass has $\Delta E = 0.147$ eV, which shows good thermal stability. The identified results demonstrate that the transparent Tb^{3+}/Sm^{3+} activated BaSrAlBSi glasses can be directly useful for photonic device applications as n-UV pumped with warm white light as well orange light emitting in w-LEDs and photonic devices.

CHAPTER 6

Summary and Future Scope of Research Work

An overview of the overall study effort and the conclusions drawn from the data are presented in the sixth chapter of this dissertation. This chapter also looks at future directions for this study and how it could be used to inform future research directions.

6.1. Summary

Glass science and technology experts have prepared a range of glasses utilizing different glass formers and network formers, and they have examined the spectroscopic characteristics of different glasses. The goals of this thesis were outlined in chapter 1 and included creating high-quality optical glasses doped with specific RE ions and maximizing the environment for a variety of photonic uses. Glasses were effectively prepared with the use of single and co-doped RE ions, such as Sm^{3+}, Tb^{3+}, Sm^{3+}/Tb^{3+}, and Sm^{3+}/Eu^{3+} using the melt quenching process. The many characterization methods that we employed in our research, as well as the melt-quenching method, were covered in detail in chapter 2.

In 3rd chapter, transparent, amorphous single Sm^{3+} ions doped and concoction of Sm^{3+}/Eu^{3+} ions co-doped AEAlBS glasses have been synthesized via employing melt quenching process and studied their structural, luminescent characteristics to have an insight into their utility in photonic devices applications under near UV excitation. A broad hump

observed in XRD reveals the amorphous/ non-crystalline nature of the as prepared un-doped AEAlBS glass. The PL spectra under 402 nm excitation exhibit several peaks ascribed to ($^4G_{5/2}\rightarrow{}^6H_{5/2}$), ($^4G_{5/2}\rightarrow{}^6H_{7/2}$), ($^4G_{5/2}\rightarrow{}^6H_{9/2}$) and ($^4G_{5/2}\rightarrow{}^6H_{11/2}$) transitions related with Sm^{3+} ions in AEAlBS glasses. The optimum emission intensity was attained for 0.5 mol% Sm^{3+} ions doped AEAlBS glasses. Sm^{3+} ion work as effective sensitizer for Eu^{3+} activator ion in AEAlBS glasses and part of ET from Sm^{3+} to Eu^{3+} ions. The tunable emission spectra were recorded under 402 excitation wavelengths. The energy transfer between Sm^{3+} to Eu^{3+} in co-doped AEAlBS glasses was proved to be dipole-dipole in nature via employing Dexter's ET formula, Reisfeld's approximation and I-H model on decay curves. The η_T for BSG:0.5Sm glass was found to be 7.73 % which was tripled as the Eu^{3+} ions concentration surged from y = 0.1 to 2.0 mol%. The CIE coordinates for single Sm^{3+} doped glasses were fall in orange region, which was change towards red region with surge in co-doping of Eu^{3+} ion in AEAlBS glasses. The lifetime value (λ_{ex} = 402 nm) was reducing with surge in Eu^{3+} ion co-doping concentration, which correspondingly specify the ET from Sm^{3+} to Eu^{3+}. The temperature-dependent emission analysis reveals that the as prepared glasses have excellent thermal stability with ΔE = 0.139 eV. All the results obtained finally contemplates the effective applicability of the as prepared multifunctional orange/red emitting Sm^{3+}/Eu^{3+} co-doped AEAlBS glasses under n-UV excitation.

Chapter 4 describes a series of transparent Tb^{3+} doped BaSrAlBSi glasses and examined their structural, optical features for advanced laser and lighting appliances. XRD and FT-IR profile discloses the non-crystalline nature and presented functional groups of glass. The absorption spectrum shows the various peaks owing to Tb^{3+} ions situated in n-UV visible and NIR region. Based on the absorption profile, indirect E_{opt} was estimated to be 2.94 eV for BSi:1.0Tb. The transparent glass was excited by n-UV light and emits the blue, green, yellow

and red light owing to transitions from $^5D_4$ to various $^7F_{(J = 6, 5, 4 \& 3)}$ energy levels of Tb^{3+} ions. The most intense emission peak was observed at 542 nm under n-UV source corresponding to $^5D_4 \rightarrow {}^7F_5$ transition and follow the Laporte-forbidden selection rule. The optimum emission intensity was conquered for 1.0 mol% Tb^{3+} ions doped BaSrAlBSi glasses. The maximum photoluminescence (PL) emission intensity was observed for 1.0 mol% Tb^{3+} doped BaSrAlBSi glass. Beyond the 1.0 mol% the dipole-dipole type of non-radiative energy transfer was recognized with the help of the Dexter theory. The PL lifetimes were show the decrease in decay time with upsurge in Tb^{3+} content. The I-H model was confirmed the dipole-dipole type of non-radiative energy transfer mechanism among the nearest Tb^{3+} ions. The TDPL investigation unveils that the optimized BSi:1.0Tb glass has $\Delta E = 0.126$ eV, which shows good thermal stability The observed results anticipates that the direct utility of the as prepared transparent Tb^{3+} doped BaSrAlBSi glasses as n-UV pumped with green emitting constituent for photonic device applications.

Chapter 5 explain about the transparent Tb^{3+}, Sm^{3+} and Tb^{3+}/Sm^{3+} activated BaSrAlBSi glass and their numerous optical and energy transfer characteristics. XRD profile reveals the non-crystalline nature of Tb^{3+}/Sm^{3+} activated BaSrAlBSi glass. The absorption spectra were used to calculate the glasses' optical band gap. Under 379 nm excitation, the glass that had been doped with Tb^{3+} showed a strong emission peak at 542 nm. Its utility as a green emitting component for photonic devices is suggested by the CIE chromaticity coordinates. The reddish orang emission peak at 602 nm under 402 nm excitation was seen in BSi:Sm1.0 glass and can a potential use for manufacturing in orange LEDs and display devices. By adjusting the Sm^{3+} concentration, the emission color of Tb^{3+}/Sm^{3+} co-doped BaSrAlBSi glasses adjusted from yellowish-green to warm-white via energy transfer process as confirmed from emission and CIE diagram. By using the I-H model on the decay curves and the Dexter and Reisfeld's theory

based on the emission spectra, it was shown that the energy transfer from Tb^{3+} ($^5D_4$) to Sm^{3+} ($^4G_{5/2}$) happens via dipole-dipole interaction. The temperature dependent emission profile unveils that the BSi:TbSm1.0 glass has $\Delta E = 0.147$ eV, which shows good thermal stability. The identified results demonstrate that the transparent Tb^{3+}/Sm^{3+} activated BaSrAlBSi glasses can be directly useful for photonic device applications as n-UV pumped with warm white light as well orange light emitting in w-LEDs and photonic devices.

The above-mentioned noteworthy results all attest to the potential utility of the RE doped/co-doped BaSrAlBSi glasses produced in the thesis for photonic applications, including solid-state lasers, LED lighting, photovoltaic cells, and optical amplifiers.

6.2. Scope for future work

A lot of research has been done on luminescent glass, and further research can be done by using the thesis work as a foundation. Some of the research projects that will be undertaken in the future include: -

- To improve the luminous characteristics of our glass substrate by adjusting the combination of distinct co-doped RE ions.
- Evaluating the prepared materials' efficacy in comparison to materials that are used commercially.
- To use prepared glasses and fabricate efficient w-LEDs.
- To increase the glass's usefulness for additional potential uses, like temperature sensors, lasers, and optical fiber applications.

References

[1] M. Rodríguez Chialanza, R. Faccio, H. Bentos Pereira, R. Marotti, Opt Mater (Amst) 123 (2022) 111890.

[2] B.P. Choudhary, N.B. Singh, (2023) 79–112.

[3] M. Giordano, D. Leporini, M.P. Tosi, (1996) 1–392.

[4] J.D. Musgraves, J. Hu, L. Calvez, (2019) 1851.

[5] J.L. Mass, R.E. Stone, M.T. Wypyski, Prehistory and History of Glassmaking Technology (1998) 121–145.

[6] D. Crossley, The Prehistory and History of Glassmaking Technology (1998) 167–179.

[7] H. Wen, G. Jia, C.-K. Duan, P.A. Tanner, Physical Chemistry Chemical Physics 12 (2010) 9933–9937.

[8] H. Wu, X. Zhang, C. Guo, J. Xu, M. Wu, Q. Su, IEEE Photonics Technology Letters 17 (2005) 1160–1162.

[9] H. Wen, B.M. Cheng, P.A. Tanner, RSC Adv 7 (2017) 26411–26419.

[10] P. Vani, G. Vinitha, M.I. Sayyed, M.M. AlShammari, N. Manikandan, Nuclear Engineering and Technology 53 (2021) 4106–4113.

[11] K. Maheshwari, Ravita, A. Prasad, Y. Tayal, A.S. Rao, Opt Mater (Amst) 140 (2023).

[12] S. Kumar Ray, Y.K. Kshetri, S. Wohn Lee -, P. Linna Guo, Y. Wang, J. Zhang, al -, nanotubes Zepeng Li, J. Wang, L. Wang, E. Erol, N. Vahedigharehchopogh, O. Kıbrıslı,

elikbilek Ersundu, A. Erç in Ersundu, Journal of Physics: Condensed Matter 33 (2021) 483001.

[13] Y. Wang, W. Zheng, Y. Lu, P. Li, S. Xu, J. Zhang, J Lumin 237 (2021) 118152.

[14] L.P. Naranjo, N.T.C. Oliveira, L.R.P. Kassab, C.B. de Araújo, J Lumin 238 (2021) 118225.

[15] X. Li, J. Cao, Y. Wei, Z. Yang, H. Guo, Journal of the American Ceramic Society 98 (2015) 3824–3830.

[16] C.B. Annapurna Devi, S. Mahamuda, M. Venkateswarlu, K. Swapna, A. Srinivasa Rao, G. Vijaya Prakash, Opt Mater (Amst) 62 (2016) 569–577.

[17] B.N.K. Reddy, B.D. Raju, K. Thyagarajan, R. Ramanaiah, Y.D. Jho, B.S. Reddy, Ceram Int 43 (2017) 8886–8892.

[18] K. Jha, M. Jayasimhadri, Journal of American Ceramic Society (2017) 1402–1411.

[19] A.G. Clare, P.F. Wachtel, J.D. Musgraves, Springer Handbooks (2019) 595–616.

[20] A. Zakery, S.R. Elliott, Springer Series in Optical Sciences 135 (2007) 1–193.

[21] Optical Nonlinearities in Chalcogenide Glasses and Their Applications (2007) 1–28.

[22] F. N, A. G, YMER Digital 21 (2022) 111–126.

[23] L.D. Pye, R. Locker, M.J. Plodinec, Materials Science Research 15 (1983) 627–637.

[24] M. Kuwik, J. Pisarska, W.A. Pisarski, Materials 13 (2020) 1–20.

[25] (n.d.).

[26] Introduction to Glass Science and Technology Second Edition, n.d.

[27] L.U. Khan, Z.U. Khan, Handbook of Materials Characterization (2018) 345–404.

[28] J. Zhou, Q. Liu, W. Feng, Y. Sun, F. Li, Chem Rev 115 (2014) 395–465.

[29] G. Blasse, B.C. Grabmaier, (1994).

[30] (n.d.).

[31] A. Escudero, M.E. Calvo, S. Rivera-ferna, (2013).

[32] P. Yasaka, J. Kaewkhao, in: Proceedings - 2015 4th International Conference on Instrumentation, Communications, Information Technology and Biomedical Engineering, ICICI-BME 2015, Institute of Electrical and Electronics Engineers Inc., 2016, pp. 4–15.

[33] S. Gai, C. Li, P. Yang, J. Lin, Chem Rev 114 (2014) 2343–2389.

[34] Luminescence: Phenomena, Materials and Applications & Special Attention to Borate Host Materials, n.d.

[35] D. Chen, Z. Wan, Y. Zhou, X. Zhou, Y. Yu, J. Zhong, M. Ding, Z. Ji, ACS Appl Mater Interfaces 7 (2015) 19484–19493.

[36] C. Feldmann, T. Justel, C.R. Ronda, P.J. Schmidt, Adv Funct Mater 13 (2003) 511–516.

[37] B.R. Judd, J Chem Phys 44 (1966) 839–840.

[38] G.S. Opelt, J Chem Phys 37 (1962) 511–520.

[39] X. Wang, Q. Liu, Y. Bu, C.S. Liu, T. Liu, X. Yan, RSC Adv 5 (2015) 86219–86236.

[40] G.C. Righini, F. Enrichi, L. Zur, M. Ferrari, J Phys Conf Ser 1221 (2019) 012028.

[41] B. Hou, M. Jia, P. Li, G. Liu, Z. Sun, Z. Fu, Inorg Chem 58 (2019) 7939–7946.

[42] V.B. Pawade, H.C. Swart, S.J. Dhoble, Renewable and Sustainable Energy Reviews 52 (2015) 596–612.

[43] N. Yao, J. Huang, K. Fu, X. Deng, M. Ding, X. Xu, RSC Adv 6 (2016) 17546–17559.

[44] T.H. Kim, W. Wang, Q. Li, Front Chem Sci Eng 6 (2012) 13–26.

[45] G. Blasse, Philips Res. Rep. 24 (1969) 131–144.

[46] L.G. Van Uitert, J Electrochem Soc 114 (1967) 1048–1053.

[47] Y. Tian, B. Chen, B. Tian, R. Hua, J. Sun, L. Cheng, H. Zhong, X. Li, J. Zhang, Y. Zheng, T. Yu, L. Huang, Q. Meng, J Alloys Compd 509 (2011) 6096–6101.

[48] J.A. Duffy, M.D. Ingram, J Non Cryst Solids 21 (1976) 373–410.

[49] M. Kumar, A.S. Rao, Opt Mater (Amst) 109 (2020) 110356.

[50] Z. Boruc, B. Fetlinski, M. Kaczkan, S. Turczynski, D. Pawlak, M. Malinowski, J Alloys Compd 532 (2012) 92–97.

[51] B. Tian, B. Chen, Y. Tian, J. Sun, X. Li, J. Zhang, H. Zhong, L. Cheng, R. Hua, Journal of Physics and Chemistry of Solids 73 (2012) 1314–1319.

[52] R.Y. Yang, Y.M. Peng, H.L. Lai, C.J. Chu, B. Chiou, Y.K. Su, Opt Mater (Amst) 35 (2013) 1719–1723.

[53] B. Szpikowska-Sroka, N. Pawlik, T. Goryczka, M. Bańczyk, W.A. Pisarski, J Lumin 188 (2017) 400–408.

[54] L.J. Curtis, H.G. Berry, J. Bromander, Phys Scr 2 (2007) 216–220.

[55] B.C. Jamalaiah, J. Suresh Kumar, A. Mohan Babu, L. Rama Moorthy, K. Jang, H.S. Lee, M. Jayasimhadri, J.H. Jeong, H. Choi, J Lumin 129 (2009) 1023–1028.

[56] D. Haranath, V. Shanker, H. Chander, P. Sharma, Mater Chem Phys 78 (2002) 6–10.

[57] M.K. Sahu, M. Jayasimhadri, J Lumin 227 (2020) 117570.

[58] H. Kaur, M. Jayasimhadri, Ceram Int 45 (2019) 15385–15393.

[59] K. Jha, A.K. Vishwakarma, M. Jayasimhadri, D. Haranath, K. Jang, J Non Cryst Solids 553 (2021) 120516.

[60] N. Deopa, A.S. Rao, Opt Mater (Amst) 72 (2017) 31–39.

[61] A. Kumar, Anu, M.K. Sahu, Ravita, S. Dahiya, N. Deopa, A. Malik, R. Punia, A.S. Rao, J Lumin 244 (2022) 118676.

[62] S. Kaur, A.S. Rao, M. Jayasimhadri, Ceram Int 43 (2017) 7401–7407.

[63] S.B. Mallur, T.C. Khoo, S. Rijal, O.R. Huff, P.K. Babu, Mater Chem Phys 258 (2021) 123886.

[64] R.A. Talewar, S. Mahamuda, A. Vyas, A.S. Rao, S. V. Moharil, J Alloys Compd 775 (2019) 810–817.

[65] R.A. Talewar, S. Mahamuda, K. Swapna, A.S. Rao, J Alloys Compd 771 (2019) 980–986.

[66] Y. Tayal, A.S. Rao, Opt Mater (Amst) 107 (2020) 110070.

[67] A.A. El-Maaref, K.S. Shaaban, M. Abdelawwad, Y.B. Saddeek, Opt Mater (Amst) 72 (2017) 169–176.

[68] C. Zuo, Z. Zhou, L. Zhu, A. Xiao, Y. Chen, Mater Res Bull 83 (2016) 155–159.

[69] J. Zarzycki, Science 267 (1995) 1887.

[70] R.A. Talewar, S. Mahamuda, K. Swapna, M. Venkateswarlu, A.S. Rao, Materials Research Bulletin 105 (2018) 45–54.

[71] B.D. (Bernard D. Cullity, Elements of X-Ray Diffraction, Addison-Wesley Publishing Company, Inc, 1978.

[72] L. Alexander, H.P. Klug, J Appl Phys 21 (1950) 137–142.

[73] B.D. Cullity, Addision-Wesley Publishing COMPANY 2 edition (1978) 0–555.

[74] J.A.D.H. P.R. Griffiths, Fourier Transform Infrared Spectrometry 2nd Ed, WILEY-INTERSCIENCE, 2007.

[75] C.S. Pappas, P.A. Tarantilis, P.C. Harizanis, M.G. Polissiou, Appl Spectrosc 57 (2003) 23–27.

[76] S.K. Sharma, D.S. Verma, L.U. Khan, S. Kumar, S.B. Khan, Handbook of Materials Characterization (2018) 1–613.

[77] J.S. Garcia', L. Bausia', D. Jaque, An Introduction to the Optical Spectroscopy, John Wiley & Sons Ltd, 2005.

[78] M. Gaft, R. Reisfeld, G. Panczer, Modern Luminescence Spectroscopy of Minerals and Materials, 2015.

[79] D. Souri, K. Shomalian, Journal of Non-Crystalline Solids 355 (2009) 1597–1601.

[80] K. Jha, A.K. Vishwakarma, M. Jayasimhadri, D. Haranath, J Alloys Compd 719 (2017) 116–124.

[81] C.R. Ronda, (2008) 260.

[82] Joseph R. Lakowicz, Principles of Fluorescence Spectroscopy, 2006.

[83] a Kumar, S. Tripathi, a D. Deshmukh, D. Haranath, P. Singh, a M. Biradar, J Phys D Appl Phys 46 (2013) 195302.

[84] C.C. Lin, A. Meijerink, R.S. Liu, Journal of Physical Chemistry Letters 7 (2016) 495–503.

[85] A.N. Meza-Rocha, A. Speghini, M. Bettinelli, U. Caldiño, Journal of Luminescence 167 (2015) 305–309.

[86] J. McKittrick, L.E. Shea-Rohwer, Journal of the American Ceramic Society 97 (2014) 1327–1352.

[87] H.K. Yang, J.H. Jeong, Society 12 (2010) 226–230.

[88] H. Yang, G. Zhu, L. Yuan, C. Zhang, F. Li, H. Xu, A. Yu, Journal of American Ceramic Society 51 (2012) 49–51.

[89] J. Li, H. Yan, F. Yan, Optik 127 (2016) 4541–4544.

[90] L. Mishra, A. Sharma, A.K. Vishwakarma, K. Jha, M. Jayasimhadri, B. V. Ratnam, K. Jang, A.S. Rao, R.K. Sinha, Journal of Luminescence 169 (2016) 121–127.

[91] M.K. Sahu, J. Mula, Journal of the American Ceramic Society 102 (2019) 6087–6099.

[92] W. Hordijk, G. Blasse, J Lumin 6 (1973) 137–139.

[93] M. Wilding, Y. Badyal, A. Navrotsky, J Non Cryst Solids 353 (2007) 4792–4800.

[94] C. Liao, R. Cao, W. Wang, W. Hu, G. Zheng, Z. Luo, P. Liu, Materials Research Bulletin 97 (2018) 490–496.

[95] H. Tang, X. Zhang, L. Cheng, L. Jiang, X. Mi, Q. Liu, J. Xie, Y. Wang, Journal of Luminescence 214 (2019) 116532.

[96] K.A. Bashar, W.L. Fong, K.A. Haider, S.O. Baki, M.H.M. Zaid, M.A. Mahdi, J Non Cryst Solids 534 (2020) 119943.

[97] V. Naresh, B.S. Ham, J Alloys Compd 664 (2016) 321–330.

[98] G.S.R. Raju, J.S. Yu, J.Y. Park, H.C. Jung, B.K. Moon, J. Am. Ceram. Soc. 95 (2012) 238–242.

[99] D. Tu, Y. Liang, R. Liu, Z. Cheng, F. Yang, W. Yang, Journal of Alloys and Compounds 509 (2011) 5596–5599.

[100] B. V Ratnam, M. Jayasimhadri, K. Jang, Spectorchimica Acta Part A : Molecular and Biomolecular Spectroscopy 132 (2014) 563–567.

[101] Q. Xu, D. Xu, J. Sun, Optical Materials 42 (2015) 210–214.

[102] S. Al-Waisawy, W.M. Jadwisienczak, J.T. Wright, D. Pendrill, F. Rahman, Journal of Luminescence 169 (2016) 196–203.

[103] B. V Ratnam, M.K. Sahu, A.K. Vishwakarma, K. Jha, H.J. Woo, K. Jang, M. Jayasimhadri, Journal of Luminescence 185 (2017) 99–105.

[104] G. Annadurai, S.M. Moses Kennedy, Journal of Luminescence 169 (2016) 690–694.

[105] A.K. Vishwakarma, K. Jha, M. Jayasimhadri, a. S. Rao, K. Jang, B. Sivaiah, D. Haranath, J Alloys Compd 622 (2015) 97–101.

[106] K. Jha, M. Jayasimhadri, J Lumin 194 (2018) 102–107.

[107] M.K. Sahu, M. Jayasimhadri, K. Jha, B. Sivaiah, A.S. Rao, D. Haranath, J Lumin 202 (2018) 475–483.

[108] X. Min, Z. Huang, M. Fang, Y. Liu, C. Tang, X. Wu, Inorganic Chemistry 53 (2014) 6060–6065.

[109] L. Wang, M. Xu, H. Zhao, D. Jia, New Journal of Chemistry 40 (2016) 3086–3093.

[110] N. Deopa, M.K. Sahu, P.R. Rani, R. Punia, A.S. Rao, J Lumin 222 (2020) 117166.

[111] X. Gu, R. Fu, W. Jiang, P. Zhang, Y. Tang, A. Coşgun, Journal of Rare Earths 33 (2015) 954–960.

[112] A.K. Vishwakarma, M. Jayasimhadri, Journal of Luminescence 176 (2016) 112–117.

[113] G. Swati, S. Chawla, S. Mishra, B. Rajesh, N. Vijayan, B. Sivaiah, a. Dhar, D. Haranath, Appl Surf Sci 333 (2015) 178–185.

[114] P. Kumar, Kanika, S. Singh, R. Lahon, A. Gundimeda, G. Gupta, B.K. Gupta, J Lumin 196 (2018) 207–213.

[115] L. Wang, H.M. Noh, B.K. Moon, S.H. Park, K.H. Kim, J. Shi, J.H. Jeong, Journal of Physical Chemistry C 119 (2015) 15517–15525.

[116] J. Li, L. Chen, Z. Hao, X. Zhang, L. Zhang, Y. Luo, J. Zhang, Inorganic Chemistry 54 (2015) 4806–4810.

[117] G. Annadurai, L. Sun, H. Guo, X. Huang, J Lumin 226 (2020) 117474.

[118] R. Shi, L. Ning, Y. Huang, Y. Tao, L. Zheng, Z. Li, H. Liang, ACS Appl Mater Interfaces 11 (2019) 9691–9695.

[119] A. Okasha, A.M. Abdelghany, S.Y. Marzouk, Journal of Materials Research and Technology 9 (2020) 59–66.

[120] M.K. Sahu, M. Jayasimhadri, Journal of Materials Science: Materials in Electronics 33 (2022) 5201–5213.

[121] Y. Gao, J. Qiu, D. Zhou, Journal of the American Ceramic Society 100 (2017) 2901–2913.

[122] D. Chen, W. Xiang, X. Liang, J. Zhong, H. Yu, M. Ding, H. Lu, Z. Ji, J Eur Ceram Soc 35 (2015) 859–869.

[123] F. Enrichi, C. Armellini, S. Belmokhtar, A. Bouajaj, A. Chiappini, M. Ferrari, A. Quandt, G.C. Righini, A. Vomiero, L. Zur, J. Lumin. 193 (2018) 44–50.

[124] Y. Gao, S. Murai, K. Shinozaki, J. Qiu, K. Tanaka, ACS Appl Electron Mater 1 (2019) 961–971.

[125] K. Jha, M. Jayasimhadri, Journal of the American Ceramic Society 100 (2017) 1402–1411.

[126] C. Madhukar Reddy, B. Deva Prasad Raju, N. John Sushma, N.S. Dhoble, S.J. Dhoble, Renewable and Sustainable Energy Reviews 51 (2015) 566–584.

[127] Y.C. Fang, X.R. Huang, Y. Der Juang, S.Y. Chu, Journal of the American Ceramic Society 95 (2012) 1613–1618.

[128] M. Jayasimhadri, K. Jha, B. V. Ratnam, H.J. Woo, K. Jang, A.S. Rao, D. Haranath, J Alloys Compd 711 (2017) 395–399.

[129] Ravita, A.S. Rao, J Lumin 244 (2022) 118689.

[130] W.T. Carnall, P.R. Fields, K. Rajnak, J Chem Phys 49 (2003) 4447.

[131] K. Jha, M. Jayasimhadri, J Alloys Compd 688 (2016) 833–840.

[132] T.O. Sales, R.J. Amjad, C. Jacinto, M.R. Dousti, J Lumin 205 (2019) 282–286.

[133] N. Deopa, A.S. Rao, J Lumin 194 (2018) 56–63.

[134] K. Swapna, S. Mahamuda, A.S. Rao, M. Jayasimhadri, S. Shakya, G.V. Prakash, J Lumin 156 (2014) 180–187.

[135] S. Kaur, N. Deopa, A. Prasad, R. Bajaj, A.S. Rao, Opt Mater (Amst) 84 (2018) 318–323.

[136] S. Kaur, A.S. Rao, M. Jayasimhadri, V.V. Jaiswal, D. Haranath, J Alloys Compd 826 (2020) 154212.

[137] M. Back, A. Massari, M. Boffelli, F. Gonella, P. Riello, D. Cristofori, R. Riccò, F. Enrichi, Journal of Nanoparticle Research 14 (2012).

[138] M.K. Sahu, S. Bishnoi, G. Swati, M. Jayasimhadri, D. Haranath, Int J Appl Ceram Technol 19 (2022) 488–497.

[139] M. Zhang, M. Jia, T. Sheng, Z. Fu, J Lumin 229 (2021) 117653.

[140] K. Li, X. Liu, Y. Zhang, X. Li, H. Lian, J. Lin, Inorg Chem 54 (2015) 323–333.

[141] S. Zhang, W. Lin, Q. Li, Z. Mu, W. Li, Y. Li, Y. Li, F. Wu, Spectrochim Acta A Mol Biomol Spectrosc 219 (2019) 110–120.

[142] N. Deopa, B. Kumar, M.K. Sahu, P.R. Rani, A.S. Rao, J Non Cryst Solids 513 (2019) 152–158.

[143] Q. Li, S. Zhang, W. Lin, W. Li, Y. Li, Z. Mu, F. Wu, Spectrochim Acta A Mol Biomol Spectrosc 228 (2020) 117755.

[144] R. Jain, R. Sinha, M.K. Sahu, M. Jayasimhadri, Luminescence 36 (2021) 1444–1451.

[145] C.-H. Huang, T.-S. Chan, W.-R. Liu, D.-Y. Wang, Y.-C. Chiu, Y.-T. Yeh, T.-M. Chen, J Mater Chem 22 (2012) 20210.